

MULTI-SCALE FINITE ELEMENT MODELING OF MULTI-PLY WOVEN FABRICS
UNDER BALLISTIC IMPACTS

by

Emre Palta

A dissertation submitted to the faculty of
The University of North Carolina at Charlotte
in partial fulfillment of the requirements
for the degree of Doctor of Philosophy in
Mechanical Engineering

Charlotte

2019

Approved by:

Dr. Howie Fang

Dr. Ronald E. Smelser

Dr. Harish P. Cherukuri

Dr. David C. Weggel

Dr. Matthew Whelan

© 2019
Emre Palta
ALL RIGHTS RESERVED

ABSTRACT

EMRE PALTA. Multi-scale finite element modeling of multi-ply woven fabrics under ballistic impacts. (Under the direction of Dr. HOWIE FANG)

High-strength fiber reinforced woven fabrics are broadly utilized for their high strength-to-weight ratios and good flexibility to provide ballistic protection in security applications such as soft body armor equipment or protective layering of military vehicles. Experimental, numerical and analytical studies have been conducted in literature to understand and improve the ballistic impact response of woven fabrics. Many of the existing studies dealt with the application of single-ply fabrics, though real-world applications of woven fabrics, such as soft body armor equipment, e.g., combat helmets or vests, consist of multi-ply fabrics.

In this dissertation, a state-of-art finite element (FE) modeling technique (i.e., multi-scale FE modeling) is developed to create a FE model of woven fabrics that could be used for investigating ballistic impact responses of multi-ply fabrics. The multi-scale model (i.e., at meso- and macro-scales) created in this study improved the coupling between the interface of meso- and macro-scale regions without using contact definitions, resulting in improved propagation of ballistic shock wave between the two regions of different scales. The multi-scale FE model of a single-ply Kevlar woven fabric was first created and validated with experimental data on out-of-plane displacements of the fabric and residual velocities of the projectiles. The validated single-ply multi-scale model was then used to create a FE model of multi-ply fabrics that were subsequently validated using test data, on the projectile's residual velocities.

To study the effects of the total number of plies on the ballistic impact performance of multi-ply woven fabrics, the multi-scale FE models of three-, five-, seven-, and ten-ply woven fabrics were created. The ballistic limit velocities of the four multi-ply fabrics were first determined under impacts of a NATO specified 1.1 gr fragment simulating projectile. The V_{100} ballistic limit, energy transitions between the projectile and fabrics, displacements of the fabrics, and post-damage patterns of the four multi-ply fabrics were analyzed and discussed in detail.

Finally, the multi-scale FE model of ten-ply woven fabric was used to study the effects of projectile characteristics on its ballistic responses. Six different projectiles, which were in two sizes (.22 and .30 cal.) and three nose shapes (flat, pointed, and spherical), were used to obtain the ballistic responses of the ten-ply woven fabric under impacts at the ballistic limit velocity for each projectile. Energy transitions, out-of-plane displacements, and post-damage patterns of the fabric were then evaluated in detail.

ACKNOWLEDGEMENTS

I should write a whole chapter to express my feeling and appreciation to my advisor, Dr. Howie Fang. It all started in 2013 when he accepted me to join his lab. His support, advice and guidance have never ended since I first joined the lab. Under his supervision, I learned how to define a research problem, find a solution to it, and finally publish the results. His contribution to me was not limited to my academic knowledge, Dr. Fang also inspired me by his wisdom and personality. So, my special thanks go to him for everything that I lived in his lab.

I would like to also thank each and every one of my committee members. The knowledge I gained in the classes I took from Dr. Smelser and Dr. Cherukuri helped me while I was writing this dissertation. I also thank Dr. Weggel for his comments and suggestions to improve my technical writing skills. I do appreciate and thank Dr. Whelan for his insightful comments on my research plan to improve the quality of this study.

Finally, I would like to express my deepest gratefulness to my family. Life is meaningless without them.

TABLE OF CONTENTS

LIST OF TABLES	viii
LIST OF FIGURES	ix
CHAPTER 1: INTRODUCTION	1
1.1 Woven Fabrics	3
1.2 Woven Fabrics Under Transverse Impacts	6
1.2.1 Transverse impact behavior of homogeneous yarn	6
1.2.2 Transverse impact behavior of single-ply woven fabrics	8
1.3 Studies on Woven Fabrics Under Ballistic Impacts	10
1.3.1 Experimental studies	10
1.3.2 Analytical studies	13
1.3.3 Numerical studies	18
1.4 Motivation	28
1.5 Research Objectives	29
1.6 Research Approach	30
1.7 Outline of This Dissertation	31
CHAPTER 2: FINITE ELEMENT MODELING OF WOVEN FABRICS	32
2.1 Micro-scale FE Modeling	33
2.2 Meso-scale FE Modeling	36
2.3 Macro-scale FE Modeling	39
2.4 Multi-scale FE Modeling	41
2.5 FE Model Creation	43
2.5.1 Mesh generation	43
2.5.2 Material modeling	45
CHAPTER 3: VALIDATION OF THE FINITE ELEMENT MODELS	47
3.1 Validation of FE Model of Single-ply Fabric	47
3.1.1 Experimental setup	47
3.1.2 FE models of the experiment	48
3.1.3 Results and discussion	50
3.2 Validation of Multi-scale FE Model of a Multi-ply Fabric	58
CHAPTER 4: THE EFFECT OF TOTAL NUMBER OF PLYS ON BALLISTIC PERFORMANCE OF MULTI-PLY WOVEN FABRICS	61
4.1 Problem Description	61

4.2	Results and Discussion	63
4.2.1	Ballistic limit velocities	63
4.2.2	Fabric responses and energy transitions	65
4.2.3	Out-of-plane displacements	73
4.2.4	Damage patterns	77
CHAPTER 5: THE EFFECT OF PROJECTILE CHARACTERISTICS ON BALLISTIC PERFORMANCE OF MULTI-PLY WOVEN FABRICS		85
5.1	Problem Description	85
5.2	Results and Discussion	87
5.2.1	Ballistic limit velocities	87
5.2.2	Energy transitions	91
5.2.3	Out-of-plane displacements	97
5.2.4	Damage patterns	99
CHAPTER 6: CONCLUSIONS AND FUTURE WORK		107
6.1	Conclusions	107
6.2	Future Work	110
REFERENCES		112

LIST OF TABLES

Table 1.1: High-strength fibers used for ballistic protection.	2
Table 2.1: Dimensions of Kevlar KM2 yarn used in this study.....	44
Table 3.1: Material properties used in the FE models.	50
Table 3.2: Ballistic limit velocities and Recht-Ipson parameters.	60
Table 5.1: Comparison of internal energy of the first and last plies for each projectile...	92
Table 5.2: Total number of broken yarns on the fabric under impacts by the six projectiles at their ballistic limits.....	106

LIST OF FIGURES

Figure 1.1: Hard body armor equipment.....	2
Figure 1.2: An Interceptor Body Amor as an example of soft body armor.	3
Figure 1.3: A schematic of plain-weave woven fabric.	4
Figure 1.4: Three different length scales of a woven fabric. [1].....	5
Figure 1.5: Comparison of strength of various fibers. [2]	6
Figure 1.6: A homogeneous yarn subjected to transverse impact. [6].....	7
Figure 1.7: A schematic of woven fabric under ballistic impact.	8
Figure 1.8: Waves developed in single-ply fabric under ballistic impact.....	9
Figure 1.9: Comparison of the analytical model by Vinson and Zukas to experimental data [20].	15
Figure 1.10: Comparison of the analytical model by Parga-Landa and Hernandez- Olivares to experimental data [22].	16
Figure 1.11: Comparison of Gu’s analytical model to experimental data [24].	17
Figure 1.12: A fabric model using pin-jointed tensile members [28].....	19
Figure 1.13: A sketch of yarn representation in the model by Cunniff et al. [30].....	20
Figure 1.14: An FE model of woven fabric at yarn level [36].....	22
Figure 1.15: A digital element model of woven fabric [41].	24
Figure 1.16: FE model of a woven fabric at yarn level created using shell elements [42].	25
Figure 1.17: Different clamping designs [45].....	26
Figure 1.18: Different weave types used in the FE models by Yang et al. [46].	27
Figure 2.1: Multi-scale FE modeling of woven fabrics.	33
Figure 2.2: Micrographs of yarn and fiber.....	34
Figure 2.3: A micro-scale FE model of a yarn created using beam elements.	35
Figure 2.4: A micro-scale FE model of a woven fabric constructed using beam elements.	35
Figure 2.5: Two meso-scale FE models of a woven fabric.....	37
Figure 2.6: Stress-strain curve of a para-aramid yarn [43].	38
Figure 2.7: The macro-scale FE modeling of woven fabrics [62].	40
Figure 2.8: Repetitive unit cell. [62].....	40

Figure 2.9: A multi-scale FE model of a multi-ply woven fabric [64].	42
Figure 2.10: Cross-sectional view of Kevlar KM2 yarns [58] and the corresponding FE model.	44
Figure 2.11: FE models of the Kevlar S706 fabric.	46
Figure 3.1: The target, fixture and impactor [19].	48
Figure 3.2: A schematic of the impact experiment setup and camera placements [19].	48
Figure 3.3: FE models of the experimental setup.	49
Figure 3.4: Comparison of out-of-plane displacements of the single-ply fabric.	53
Figure 3.5: Transverse wave propagation (in mm) under the impact of 63 m/s at 44, 88, and 138 μ s, respectively.	55
Figure 3.6: Fabric displacements (in mm) at 14.8 μ s in the x - (left) and y - (right) directions under impact of 63 m/s.	56
Figure 3.7: Comparison of the residual velocities and dissipated energies.	58
Figure 3.8: The FSP and its corresponding FE model.	59
Figure 3.9: Residual velocities of the multi-ply fabrics.	60
Figure 4.1: Multi-scale FE model of the four multi-ply Kevlar woven fabric targets.	62
Figure 4.2: FE model of the impact setup.	63
Figure 4.3: Ballistic limit plots of multi-ply Kevlar woven fabrics.	64
Figure 4.4: Comparison of the V_{100} ballistic limits and efficiencies of the four multi-ply fabrics.	65
Figure 4.5: Fabric response and energy transitions of the three-ply fabric at V_{100} .	69
Figure 4.6: Fabric response and energy transitions of the five-ply fabric at V_{100} .	70
Figure 4.7: Fabric response and energy transitions of the seven-ply fabric at V_{100} .	71
Figure 4.8: Fabric response and energy transitions of the ten-ply fabric at V_{100} .	72
Figure 4.9: Dynamic out-of-plane displacements of the four multi-ply fabrics.	73
Figure 4.10: Sequential cross-sectional displacement profiles of the warp (left) and weft directions (right) in the impact point.	76
Figure 4.11: Post-impact damage patterns of the first and the last ply of the three-ply fabric.	79
Figure 4.12: Post-impact damage patterns of the first and the last ply of the five-ply fabric.	80

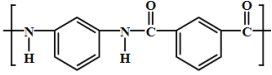
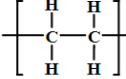
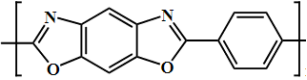
Figure 4.13: Post-impact damage patterns of the first and the last ply of the seven-ply fabric.	81
Figure 4.14: Post-impact damage patterns of the first and the last ply of the ten-ply fabric.	82
Figure 4.15: Schematic classification of damage patterns of the last plies of multi-ply fabrics under V_{100} impacts.	84
Figure 4.16: Failure time representation of the multiply fabrics.	84
Figure 5.1: FE models of the six projectiles: RCC, conical and spherical (from left to right).	87
Figure 5.2: Residual velocities of the projectiles.	88
Figure 5.3: Comparison of the ballistic limits for the projectiles.	89
Figure 5.4: Comparison of the projectiles.	91
Figure 5.5: Energy absorption of the fabric for conical projectiles at ballistic limits.	93
Figure 5.6: Energy absorption of the fabric for spherical projectiles at ballistic limits.	94
Figure 5.7: Energy absorption of the fabric for RCC projectiles at ballistic limits.	95
Figure 5.8: Cross-sectional views of out-of-plane displacements of the warp and weft yarns at the impact point for impacts by the .22 cal. projectile.	98
Figure 5.9: Cross-sectional views of out-of-plane displacements of the warp and weft yarns at the impact point for impacts by the .30 cal. projectile.	98
Figure 5.10: Post-impact damage patterns of the fabric impacted by a .22 cal. conical projectile at ballistic limit velocity.	103
Figure 5.11: Post-impact damage patterns of the fabric impacted by a .30 cal. conical projectile at ballistic limit velocity.	103
Figure 5.12: Post-impact damage patterns of the fabric impacted by a .22 cal. spherical projectile at ballistic limit velocity.	104
Figure 5.13: Post-impact damage patterns of the fabric impacted by a .30 cal. spherical projectile at ballistic limit velocity.	104
Figure 5.14: Post-impact damage patterns of the fabric impacted by a .22 cal. RCC projectile at ballistic limit velocity.	105
Figure 5.15: Post-impact damage patterns of the fabric impacted by a .30 cal. RCC projectile at ballistic limit velocity.	105

Figure 5.16: The primary yarns underneath the projectiles. 106

CHAPTER 1: INTRODUCTION

Armor equipment in various forms has been used since rudimentary humankind, from leather used as body armors at the very early ages to metals and composite materials used in modern advanced armors. The most significant changes in armor technology occurred during World War I (WWI) and World War II (WWII). Body armors made of steels were broadly utilized as either vests or helmets in these two wars, and the steel body armors provided good protection for that time. Although steel body armors could provide adequate protections during WWI and WWII, they became inadequate with the development of the gun technology. New armor materials were needed to construct lighter, stronger and flexible body armor equipment, which would provide adequate ballistic protection while maintaining mobility. Thanks to the innovation of high-strength fibers in the 1960s, the need of new armor materials has been met. High-strength fibers are synthetic high-performance fibers, with molecules characterized by relatively rigid polymer chains. Aramid (i.e., Kevlar and Twaron), high performance polyethylene (HPPE) (i.e., Spectra and Dyneema), poly (p-phenylene-2,6-benzobisoxazole) (PBO) (i.e., Zylon) are the high-strength fibers commonly used for ballistic protections. Table 1 summarizes the features along with chemical structures of these fibers. Although a few non-woven fabrics with high-strength fiber reinforcements are available in the market, high-strength fibers are mostly used in woven fabrics to construct ballistic body armor equipment.

Table 1.1: High-strength fibers used for ballistic protection.

Name	Type	Chemical Structure
Kevlar and Twaron	Para-aramid	
Spectra and Dyneema	HPPE	
Zylon	PBO	

Ballistic body armor equipment is divided into two main categories: hard and soft body armors. Hard body armor equipment is typically made of rigid materials such as steel plates, ceramic tiles and boron carbide plates. Hard body armor equipment is usually thick and mainly used for protections under impact of rifle bullets. There also exists hard body armor equipment which is the combination of the rigid materials and flexible materials (e.g., woven fabrics). In addition, composite laminates made of Kevlar/epoxy materials are also used in hard body armor equipment, e.g., the new generation combat helmet made of woven fabric reinforced composite laminates. Figure 1.1 shows examples of hard body armor equipment.



Figure 1.1: Hard body armor equipment.

Since the innovation of high-strength fibers, aramid reinforced woven fabrics have been extensively used to create soft body armors. Soft body armor equipment is generally flexible and lightweight and is designed for low-level threats. Soft body armor equipment consists of multi-ply woven fabrics, which are manufactured by stacking single-ply woven fabrics on top of each other until the desired protection level is reached. Soft body armor equipment may have 10 to 50 plies with weight ranging from 3 to 10 kg. The Interceptor Body Armor (see Fig. 1.2), which is used by the U.S. military forces, is a well-known soft body armor equipment that consists of an outer vest, deltoid protectors, side protectors, and a groin protector, which are all constructed from aramid reinforced woven fabrics or Kevlar KM2 fabrics.



Figure 1.2: An Interceptor Body Amor as an example of soft body armor.

1.1 Woven Fabrics

Woven fabrics are made of interlaced yarns, named weft and warp yarns, that consist of thousands of organic or synthetic fibers. Woven fabrics may contain one or more different materials woven together. Although several interwoven patterns, called weaves,

exist such as twill, basket and harness satin, many woven fabrics utilized as armor have a two-dimensional plain weave, which has two engaged yarn sets perpendicular to each other. Figure 1.3 shows a schematic of a plain-weave woven fabric used in soft body armor equipment.

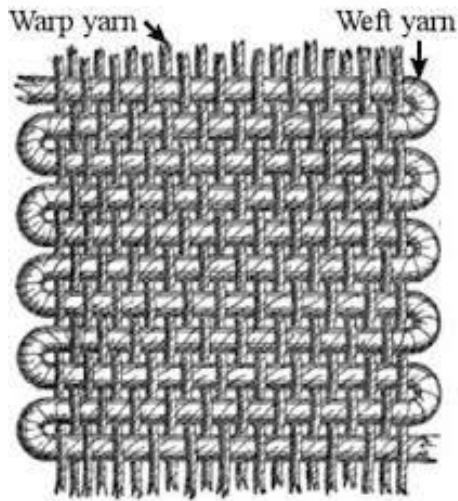


Figure 1.3: A schematic of plain-weave woven fabric.

By nature of their compositions, woven fabric materials can be hierarchically characterized at three length scales: 1) micro-scale for the fibers ($\sim 10^{-3}$ mm), 2) meso-scale for the yarn ($\sim 10^{-1}$ mm), and 3) macro-scale for the fabric ($\sim 10^2$ mm). In other words, woven fabrics consist of yarns, each of which is made of hundreds of fibers. Figure 1.4 shows a woven fabric at different length scales. This multi-scale internal structure allows relative motions between fibers and between yarns, making woven fabrics highly flexible with very specific mechanical behavior. Since fibers or yarns in woven fabrics can easily displace, extend, and slide relative to each other, woven fabrics can undergo large deformations. The mechanical behavior and impact response of woven fabrics are mainly

affected by the material properties of fibers. For ballistic protections, fibers are required to have low density, high strength, and high energy absorption capability. Figure 1.5 shows fiber strength in textile units (N/tex) and in engineering units (GPa). Textile units relate the strength to the weight of the fiber while engineering units refer to the cross-section and volume of a fiber. It can be seen that the combination of low density and high strength makes HPPE and aramid fibers the best options for ballistic impact protections [2].

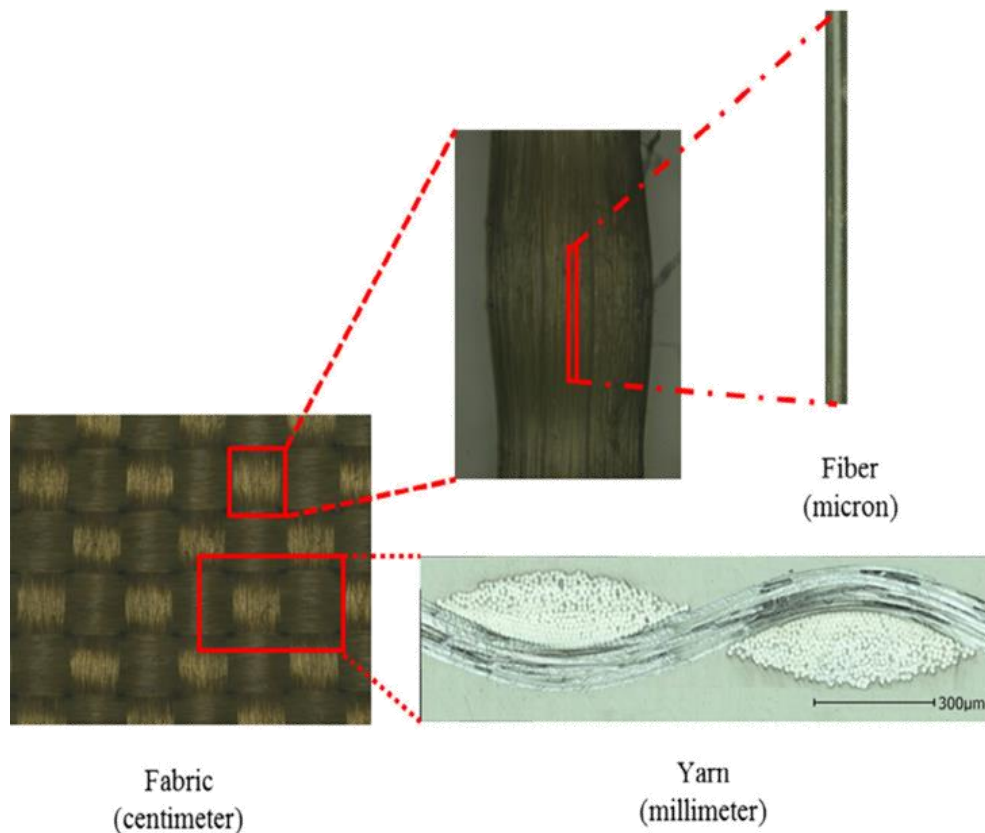


Figure 1.4: Three different length scales of a woven fabric. [1]

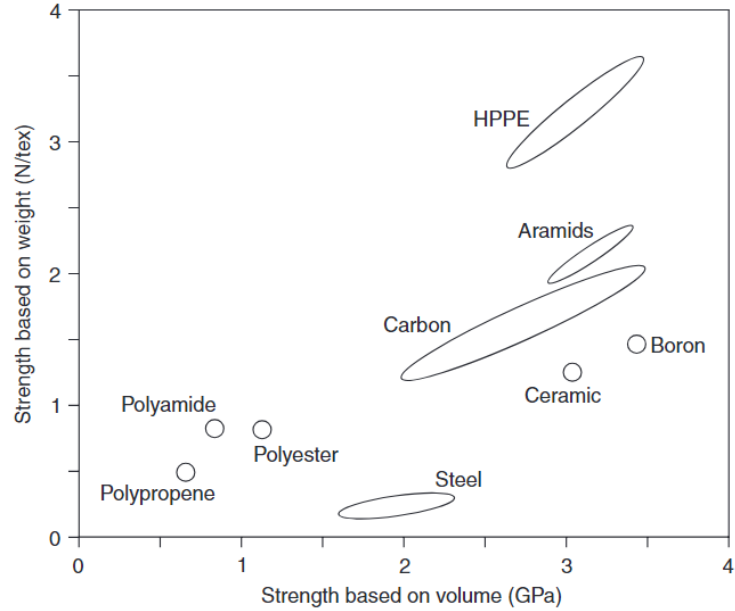


Figure 1.5: Comparison of strength of various fibers. [2]

1.2 Woven Fabrics Under Transverse Impacts

1.2.1 Transverse impact behavior of homogeneous yarn

Smith et al. [3-5] developed analytical formulations for the behavior of homogeneous yarn under transverse impacts. In Smith's theory, it was assumed that the homogeneous yarn was linear elastic and the impact velocity was constant at the impact point. Additionally, the projectile geometry and the deformation through the thickness of the yarn were not considered. According to the formulation, after a homogeneous yarn is impacted transversely by a projectile, as shown in Figure 1.6, the two waves propagate both longitudinally and transversely from the point of impact. The longitudinal strain wave propagates along the longitudinal axis of the yarns at sound speed and is given by

$$c = \sqrt{\frac{E}{\rho}} \quad (1)$$

where E and ρ are the Young's modulus and density of the yarn, respectively. The transverse displacement wave travels away from the impact point at a speed which is an order of magnitude lower than the longitudinal wave speed (i.e., the sound speed of material).

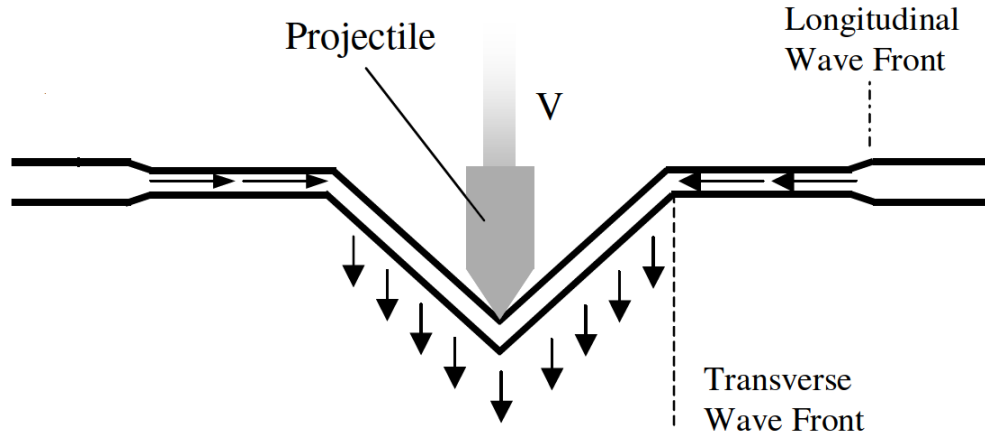


Figure 1.6: A homogeneous yarn subjected to transverse impact. [6]

The strain in the yarn is zero ahead of the longitudinal wave front, and a constant tensile strain is developed behind the wave front. The tensile strain (ε) is formulated as follows:

$$2\varepsilon\sqrt{\varepsilon(1+\varepsilon)} - \varepsilon^2 = \rho \frac{V^2}{E} \quad (2)$$

where V is the impact velocity in addition to Young's modulus (E) and density (ρ) of the yarn. The transverse displacement wave velocity, u , is given by

$$u = c \sqrt{\frac{\varepsilon}{1+\varepsilon}} \quad (3)$$

The strain in the yarn does not change ahead of the transverse wave front, but the motion of the yarn shows a rapid change. Ahead of the transverse wave front but behind the

longitudinal wave front, the yarn moves longitudinally toward the impact point. Behind the transverse wave front, the yarn moves transversely in the impact direction [7].

1.2.2 Transverse impact behavior of single-ply woven fabrics

The transverse impact behavior of single-ply woven fabrics possesses similarities with the behavior of a single yarn under transverse impact. When an impactor hits a single-ply woven fabric, the impactor, depending on its diameter, directly engages with some yarns which are called primary (or principal) yarns, while the yarns away from the impact zone are referred to as secondary yarns, as shown schematically in Figure 1.7.

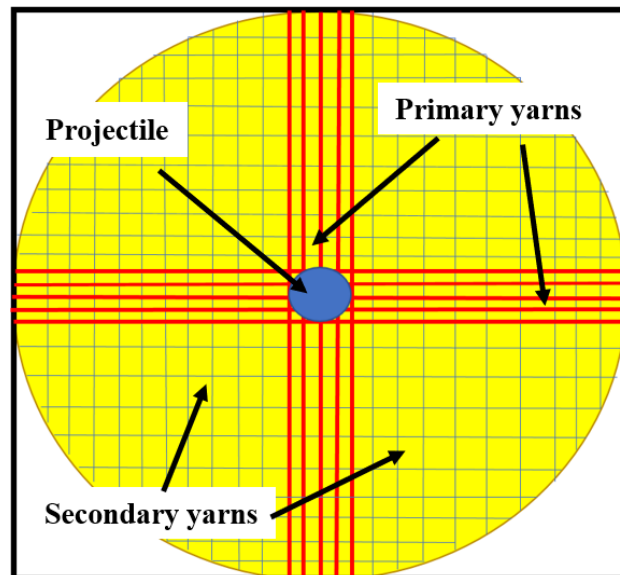


Figure 1.7: A schematic of woven fabric under ballistic impact.

After the impactor hits the fabric, longitudinal strain waves are generated and propagate at the sound speed along the longitudinal axis of the primary yarns, which also deflects in the transverse the direction (i.e., out-of-plane) due to transverse waves, as shown in Figure 1.8. The secondary yarns at the crossover points are then pulled out of the initial

fabric plane by the primary yarns. The secondary yarns undergo an elastic deformation and develop a strain wave similar to those observed in the primary yarns. The waves in secondary yarns are spread through the crossover point in which the yarns engaged with each other. These yarn-to-yarn interactions create bowing and subsequent misalignment of the secondary yarns toward the impact point. The transverse deflection proceeds until the strain at the impact point reaches the breaking strain. The majority of the kinetic energy of the projectile is absorbed by the primary yarns as strain energy and kinetic energy in the yarns. Since secondary yarns undergo elastic deformation, the amount of energy absorbed by secondary yarns are very small compared to that absorbed by the primary yarns. Roylance [8] found that due to the crossover points on the fabric, the wave velocity in a fabric, c' , is smaller than the wave velocity in a single yarn, c , by a factor of $\sqrt{2}$.

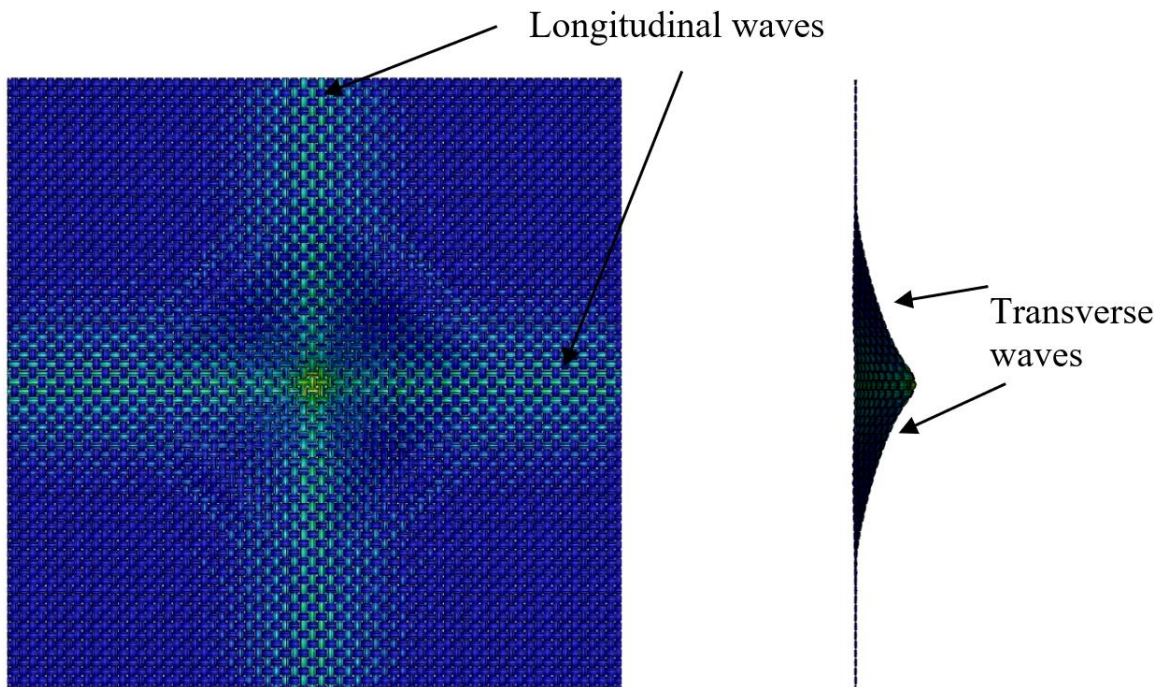


Figure 1.8: Waves developed in single-ply fabric under ballistic impact.

1.3 Studies on Woven Fabrics Under Ballistic Impacts

Because para-aramid fiber reinforced woven fabrics have been extensively utilized in body armor equipment since 1960, several studies have been conducted in literature to fully understand the responses and mechanism of ballistic impacts on woven fabrics. The studies available in literature are divided into three major categories, i.e., experimental, analytical and numerical. A compressive review of these studies is provided in the following subsections.

1.3.1 Experimental studies

In experimental studies of woven fabrics, real ballistic impacts were conducted, and the test data were captured thorough photography, microscopy, or scanning. Although experimental studies are necessary to have benchmark data to validate analytical or numerical studies, only a small number of experimental studies are available in literature because conducting the ballistic impact experiments is expensive and time-consuming.

In one of the earliest experimental studies, Wilde et al. [9] investigated the ballistic impact resistance behavior of a single-ply nylon fabric under impacts of cylindrical steel projectile with a 0.55-cm diameter and at velocities ranging from 116 to 537 m/s. The responses of the fabric and projectile were examined using the high-speed photography. It was shown that the fabric deformation exhibited a pyramidal shape before penetration and more conical shape after penetration. The authors also found that the broken yarns within the deformation cone could account for up to 100% of the absorbed impact energy. This study further demonstrated that the high-speed photography techniques could provide insight into the responses of woven fabrics under ballistic impacts.

Laible et al. [10] conducted experiments on Kevlar 29 and fiberglass laminates under impacts of a 9-mm projectile at speeds ranging from 335 to 396 m/s. They recorded post impact damages of the test samples for comparison and they concluded that the Kevlar laminates exhibited some advantage over the fiber glass laminates. Kevlar laminates provided complete protection against a 9-mm projectile up to 395 m/s while the fiber glass laminates were perforated under the impacts of the same projectile at 350 m/s.

The effects of projectile geometry on performance of fabrics was experimentally examined by Montgomery et al. [11] in which one-, two- and three-ply Kevlar 49 woven fabrics were impacted by .22 cal. flat, round, soft-point and spherical-nose projectiles at velocities ranging from 200 to 600 m/s. Based on the residual velocities of the projectiles measured across all impact cases. The authors concluded that a more pointed projectile does not decelerate as fast as a blunt projectile at high impact velocities. It was also found that at low velocities, pointed projectiles were decelerated faster than blunt projectiles.

In the study by Taylor and Vinson [12], multi-ply fabrics composed of one- to five-Kevlar 29 plies were tested under impacts of .22 cal. round nose, 9 mm diameter semi-wad cutter and flat nose projectiles at velocities of 240, 310 and 380 m/s. The main conclusion drawn from the study was that the average failure strain for a given impact velocity was independent of the number of layers (or plies) in the target.

A high-speed photographic technique was also used by Field and Sun [13] in an experimental study of the behavior of para-aramid fibers (i.e., Kevlar 29 and Spectra 1000) under impacts of a 2-mm diameter steel ball at a velocity of 1000 m/s. Using the high-speed photography, they were able to observe the transverse waves and determine the wave speeds in single fibers impacted by the projectile. Ultimately, they found that fibers with

high dynamic modulus, which affects both the strength and stress wave speeds, were able to reach large strains before failure.

The effects of friction between the yarns on the ballistic performance of woven fabrics were experimentally studied by Briscoe and Motamedi [14] on single-ply Kevlar 29 and Kevlar 49 fabrics. In their study, the fabrics were impacted by a 6.35-mm diameter steel ball at velocities ranging from 50 to 250 m/s. The residual velocities of the projectiles were recorded using high-speed photography and the results indicated that the fabric with the largest inter-yarn friction dissipated the largest amount of energy during the impact.

The ballistic performance of a single-ply Twaron fabric was experimentally examined by Shim et al. [15]. The target was clamped at the vertical sides and impacted by a 9-mm spherical steel projectile at speeds ranging from 140 to 420 m/s. It was observed that fabric deformation was localized to the impact points and only yarns near the impact point were broken after the perforation.

Tan et al. [16] conducted an experimental study on a single-ply Twaron fabric impacted by projectiles of different shapes with flat, hemispherical, ogival and conical heads. The target was clamped along two sides and impacted by the projectiles at speeds ranging from 50 to 650 m/s. The experimental results showed that, while the amounts of energy absorbed by the fabrics were quantitatively different for the four projectiles, they showed similar trends: energy absorption was increased with the increase of the impact speed up to a critical value before it started to decrease. The study also showed that the fabric exhibited the largest ballistic limit when impacted by the flat-head projectile and the smallest ballistic limit under impact of the conical-head projectile. In a subsequent study by Lim et al. [17], they extended their initial work (Tan et al. [16]) to investigate the

ballistic performance of two-ply Twaron fabrics under the same impact conditions as those in the previous work [16]. The main conclusion from the subsequent study was that the increase in energy absorption was not linearly proportional to the total number of plies. In other words, the absorbed energy by the double-ply fabric was not twice as much as that by the single-ply fabric. They also found that the failure mechanism of the two-ply fabric was similar to that of the single-ply fabric. However, the damage severity of the impact and distal plies differed.

Rabb [18] investigated the effect of shear thickening fluid on ballistic performance of two- and four-ply Kevlar KM2 fabrics using a set of experiments in which dry and impregnated fabrics were impacted by a 1.1 fragment simulating projectile (FSP). Details of Rabb's work are given in Chapter 3 of this dissertation in which the experimental results were used to validate the numerical models used in this research.

More recently, Yu et al. [19] conducted an experimental study to investigate the ballistic behavior of a single-ply Kevlar KM2 fabric impacted by different projectiles. The experimental data from Yu's study were also used to validate the numerical models for this research (see Chapter 3 for details of the experimental study).

1.3.2 Analytical studies

Well-established equations and laws such as conservation of energy and momentum of continuum mechanics were used in analytical studies to predict behaviors of woven fabric under ballistic impacts. The governing equations used in analytical studies were established using several parameters involved in ballistic impact processes. Although analytical models are useful to estimate impact phenomena with reasonable efficiency, due

to the complexity of the nature of woven fabrics, there is no single, agreed-upon analytical model that can be generally applied to a wide range of fabric materials.

Wilde et al. [9] established a simplified analytical model, which was one of the earliest analytical models in the 1970's. The main purpose of the analytical model was to predict the energy loss of the projectile. To this end, Wilde et al. [9] assumed that the loss of kinetic energy on the projectile occurred only in the forms of strain and kinetic energy of the fabric and that the loss of strain energy was only caused by the broken yarns. In addition, they assumed that the loss of kinetic energy was caused by the out-of-plane motion of the fabrics. Using this analytical model, which required the deformation size and the impact velocity as the inputs, they found that broken yarns in the deformation cone could account for up to 100% of the total observed energy loss of the projectile. Although the analytical model was capable of predicting the loss of kinetic energy on the projectile with reasonable accuracy, the model was rather basic due to the above-mentioned assumptions.

Vinson and Zukas [20] developed an analytical model in which woven fabric were assumed to be homogeneous, flexible and lacking adequate geometry of yarn. A stepwise calculation procedure was utilized in the model to determine the fabric strains, projectile positions and accelerations for impacts on both nylon and Kevlar woven fabrics. The geometry, modulus, and ultimate strain of the projectile and target were the inputs for the analytical model. Since the model assumed that the failure strain of the fibers in the fabric was independent of the total number of plies in the target, the model was also used to predict the ballistic responses of multi-ply fabric targets. Despite the above-mentioned

assumptions, this analytical model could predict the residual velocity with relatively good accuracy, as shown in Figure 1.9.

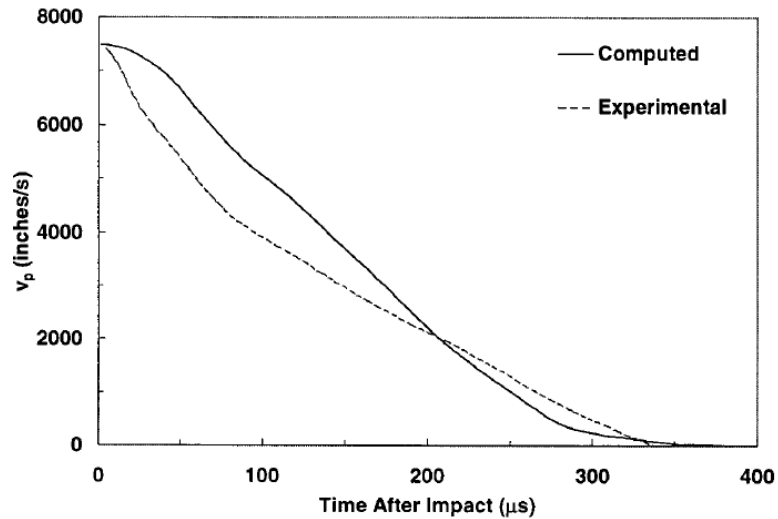


Figure 1.9: Comparison of the analytical model by Vinson and Zukas to experimental data [20].

To approximate the arrest of a projectile in both a linear (small deformation) and non-linear system (large deformation), Leech et al. [21] developed a mathematical model based on Hamilton's principle and Fourier representation. In this mathematical model, the fabric was assumed as linear-elastic material. The solution of the model involved an ordinary differential equation that was capable of predicting the velocity history of a projectile captured by the fabric. Although the model correlated well with experimental data for the impacts where full penetration did not occur, the model was not capable of predicting the impact cases in which full penetration (i.e., perforation) occurred.

Although the above-mentioned analytical models provided insight into ballistic impacts of woven fabrics for the time, more complex and capable analytical models were developed in the 1990's, e.g., the analytical model developed by Parga-Landa and Hernandez-Olivares [22] based on the principle of conservation of momentum. It was

assumed that the projectile was rigid and the fibers were linear-elastic until failure. The geometry of the yarn's cross-section was taken into account in the model, which was capable of calculating the impact forces, stresses and strains in the fabric as well as the velocity and displacement of the projectile. Predictions based on the model were shown to agree well with experimental data shown in Figure 1.10.

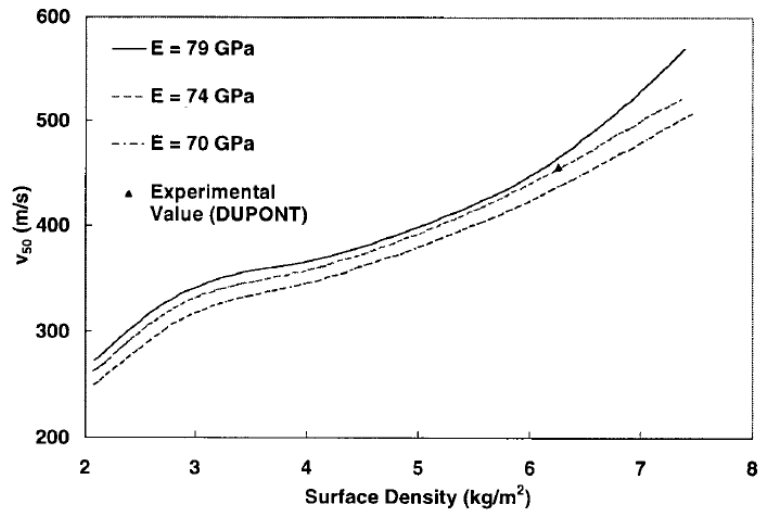


Figure 1.10: Comparison of the analytical model by Parga-Landa and Hernandez-Olivares to experimental data [22].

The analytical model developed by Billon and Robinson [23] was used to predict the velocity history of a projectile impacting single- and multi-ply woven fabric armor plates. The model assumed that the kinetic energy loss was a linear function of projectile penetration depth. Although the analytical model was capable of predicting the ballistic limits for single-ply fabrics, the prediction on the ballistic limits for multi-ply fabrics were quite different from experimental data since the inter-ply friction was not considered in the model.

Gu [24] developed an analytical model based on the law of energy conservation and used the model to predict the loss of kinetic energy and residual velocity of the projectile penetrating multi-ply plain weave woven fabrics. Although the analytical model considered strain-rate effects on the fiber, the model did not consider the shape of the projectile and the projectile was simplified as a particle in the analysis. Gu [24] validated the analytical model using experimental data of 5- to 35-ply Twaron fabrics subjected to impacts by a cylindrical steel projectile with a 7.62-mm diameter. Since the geometry of the projectile and yarn cross-sections were not considered in the analytical model, there was considerable error between the experimental data and analytical results for fabrics of ten or more plies, as shown in Figure 1.11.

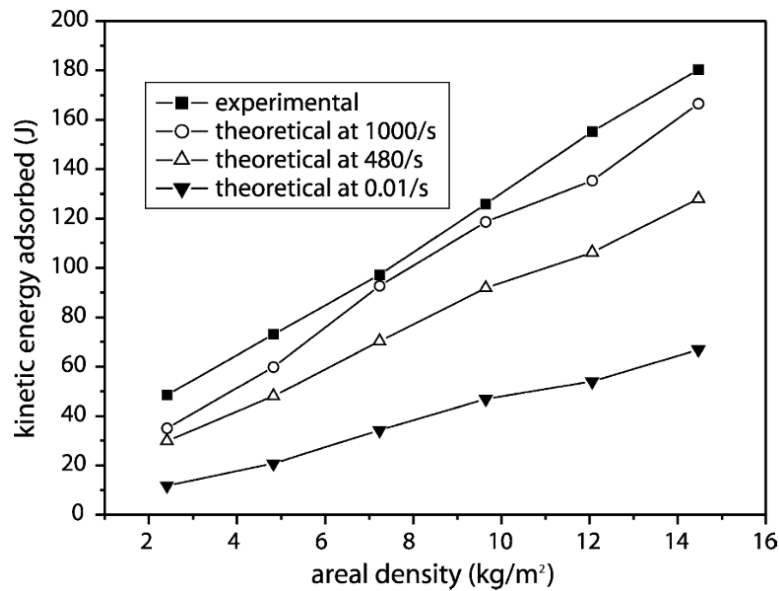


Figure 1.11: Comparison of Gu’s analytical model to experimental data [24].

Mamivand and Liaghat [25] developed an analytical model to predict the ballistic limits of multi-ply woven fabrics. The target in this model was assumed to be a square with

a side length L and made of n -ply fabrics with no bonding between the plies and was fully constrained along all edges. The fabric was assumed to be linear-elastic and conservation of momentum and wave theory were used to predict the perforation process of multi-ply fabrics impacted by flat-head cylindrical projectiles. The ballistic limit, shape of back-face deformation of the fabric, and velocity change of the projectile were predicted by the analytical model and compared to a semi-empirical study from literature. Good correlation was found between the analytical model and the semi-empirical study.

More recently, Ha-Minh et al. [26] conducted an analytical study in which both energy conservation and strain wave theory were used to investigate the ballistic response of 2D plain-weave woven fabrics. The analytical model considered reflections of deformation waves and was capable of predicting the evolution of parameters during the impact event continuously in terms of time and the limit velocity of fabric deformation. The results from the analytical model was compared and found to agree well to experimental data of a ten-ply woven fabric impacted by a 7.62-mm FSP at 375 m/s.

1.3.3 Numerical studies

Numerical methods, particularly the finite element methods, has been widely used to understand ballistic impact behavior of woven fabrics. Because all components of a fabric can be modeled explicitly, numerical models can capture particular phenomena such as yarn cross-over interactions and crimping that are difficult for analytical methods. With the ever-increasing computational power, numerical models have seen more and more extensive development.

Early efforts in the major development of numerical models for woven fabrics under ballistic impacts began in the 1970s. Roylance [27] developed a numerical model

that could predict the response of a single yarn under ballistic impacts. Viscoelastic material behavior has been employed in the model, and the model was solved using a direct analysis technique. Based on the previous work on single fibers, Roylance et al. [28] developed a pin-joint model in which yarns were modeled as segments of orthogonal pins connected by nodes, with a mass of m , at the cross-over points to create an entire sheet of woven nylon fabric as shown in Figure 1.12. Like the previous work on a single yarn, the sheet model utilized direct analysis for computation. In a subsequent study by Roylance and Wang [29], they improved their initial models to capture non-linear viscoelastic behaviors of the fabric. This model was capable of predicting the deformed shape and wave propagations of the fabric.

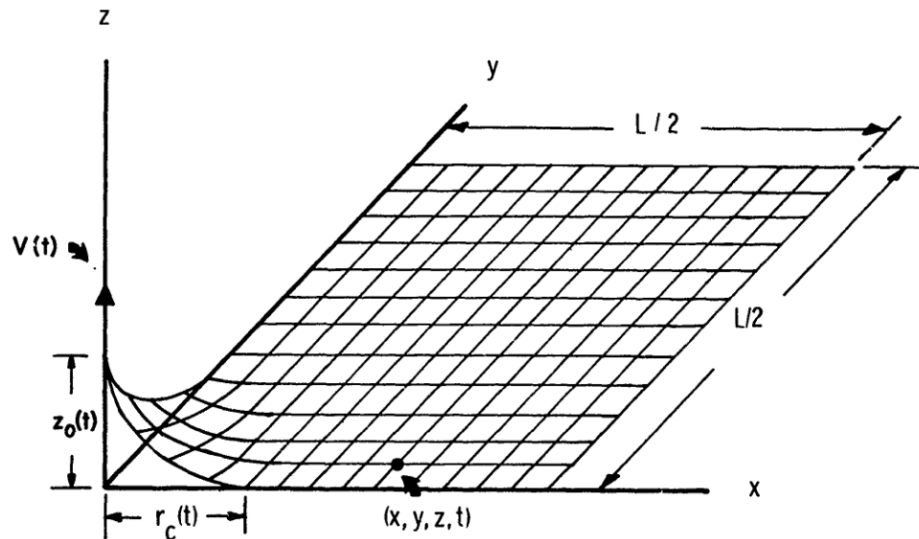


Figure 1.12: A fabric model using pin-jointed tensile members [28].

In 1998, Cunniff et al. [30] established a new model to overcome the shortcomings of the previous models. The new model stepped away from their previous work to include out-of-plane yarn undulations with elastic inter-yarn coupling at crossovers as well as

subdivision of yarn segments between crossovers to increase resolution near the impact zone. Figure 1.13 shows a sketch of yarn representation in the new model. A transverse spring was inserted between the warp and weft yarns at crossover points to allow detailed analysis of the cooperative nature of wave propagation in fabrics. The spring stiffness was determined by stress-strain relations of the fabric in the transverse direction.

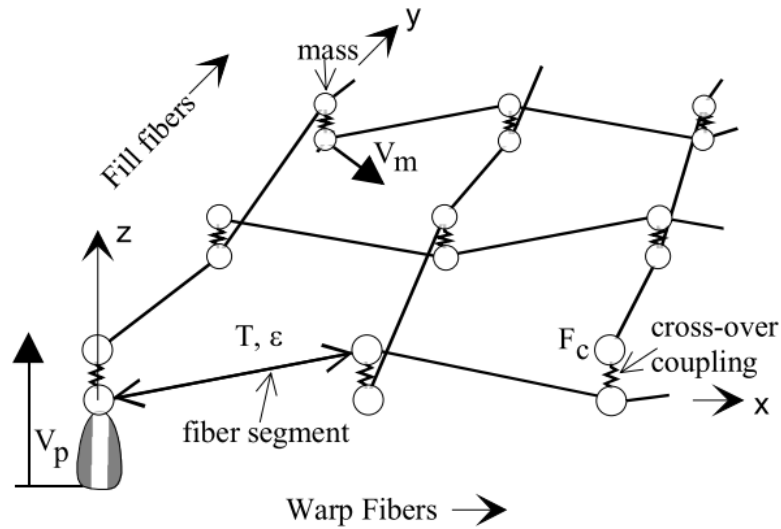


Figure 1.13: A sketch of yarn representation in the model by Cunniff et al. [30].

The above-mentioned models aimed to capture the ballistic responses of woven fabrics with considerable amount of details, but they were not capable of accurately representing the complex geometry of the fabric due to some assumptions on the weave geometry and yarn interactions. With the rapid growth of computing technology, non-linear finite element (FE) modeling techniques implemented in commercial FE codes such as LS-DYNA and ABAQUS were extensively used to simulate ballistic impacts and to study resistance mechanism of woven fabrics. In the studies by Shockey et al. [31-33], they modelled the yarns of fabric using three-dimensional brick elements, resulting in a model

with large number of elements and interactions. Despite its high computational cost, this model could generate realistic responses without making any major assumptions. The results were shown to agree well with experimental data of perforation tests.

Lim et al. [34] conducted a numerical study in which a single-ply woven fabric was modelled using homogeneous membrane elements in LS-DYNA. A strain-rate dependent, isotropic elastic-plastic material model was used in the FE model, which was validated against the perforation tests of a single sheet impacted by a spherical projectile. Although the model did not account for yarn slippage and unraveling, the numerical results were in close agreement with experimental data.

Ivanov and Tabiei [35] developed a computational micro-mechanical material model for woven fabrics under ballistic impacts. A single-ply woven fabric was modelled using membrane elements and the entire fabric was assumed homogeneous and viscoelastic with strain-rate dependent failure. The numerical model was validated against experimental data and was shown to have reasonably good accuracy. Although the numerical models by Lim et al. [34] and Ivanov and Tabiei [35] were computationally efficient, they were not capable of simulating yarn sliding with friction and yarn pullouts, which could affect the behavior of woven fabrics under ballistic impacts. Although the models could predict the residual velocities with acceptable accuracy, they were not adequate for predicting out-of-plane displacements and damage patterns of the fabrics.

The effects of friction on the ballistic performance of woven fabrics were studied by Duan et al. [36] on a plain-weave single-ply woven fabric modeled at yarn level. The yarns were assumed as homogeneous and created using brick element in LS-DYNA, as shown in Figure 1.14. Three types of boundary conditions, four edges clamped, two edges

clamped, and four edges free, were applied to the fabric impacted by a spherical projectile. The simulation results showed that friction played a role in yarn failures and that boundary conditions played a larger role than previously thought in terms of influencing the friction. It was found that the fabric absorbed more energy when two edges remained free than the other cases.

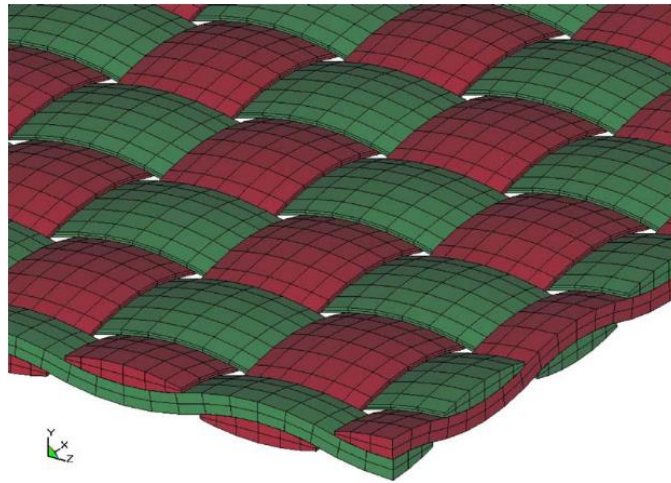


Figure 1.14: An FE model of woven fabric at yarn level [36].

In a later work by Duan et al. [37], they took a similar approach to their previous study and found that yarn strain and kinetic energy both increased proportionally with the increase of yarn friction, which also accounted for the high energy absorption observed on the fabric. However, it was noted that the overall influence of friction could not be simply determined by summing the projectile-to-fabric and yarn-to-yarn frictions [38].

Rao et al. [39] created a 3D FE model at yarn level of a single-ply Kevlar KM2 fabric under impacts of a rigid spherical projectile to study the effect of material properties of the yarn on the ballistic impact performance of woven fabrics. The yarns were assumed as homogeneous and modelled using brick elements. Simulation results showed that the

ballistic performance of woven fabrics depended on yarn-to-yarn friction, elastic modulus and strength of the yarns. While the friction between the yarns affected the ballistic performance, material properties of the yarns had a significant influence on the effect of friction.

The effects of projectile nose angle on the ballistic performance of woven fabrics has been numerically studied by Talebi et al. [40]. Ausing a 3D FE model of single-ply fabric created at yarn level using brick elements in LS-DYNA. In the FE model, the yarns were assumed homogeneous with orthotropic elastic material properties. The nose angle of the projectile was adjusted from 180° (i.e., a flat nose) to 30° (i.e., a tip nose) at a 15° increment. The main conclusion drawn from the study was that at a nose angle of 60° , the projectile had the largest damage to the fabric.

A micro-scale (i.e., at the fiber level) model based on an explicit digital element method was developed by Wang et al. [41] to study the ballistic performance of woven fabrics. In this micro-scale model, each yarn was digitized as an assembly of digital fibers. Each digital fiber is further digitized into a short digital rod element chain connected by frictionless pins (i.e., nodes). Figure 1.15 shows concept of digital element simulation. The digital element model was validated against experimental data and found to have a good correlation with the experimental data.

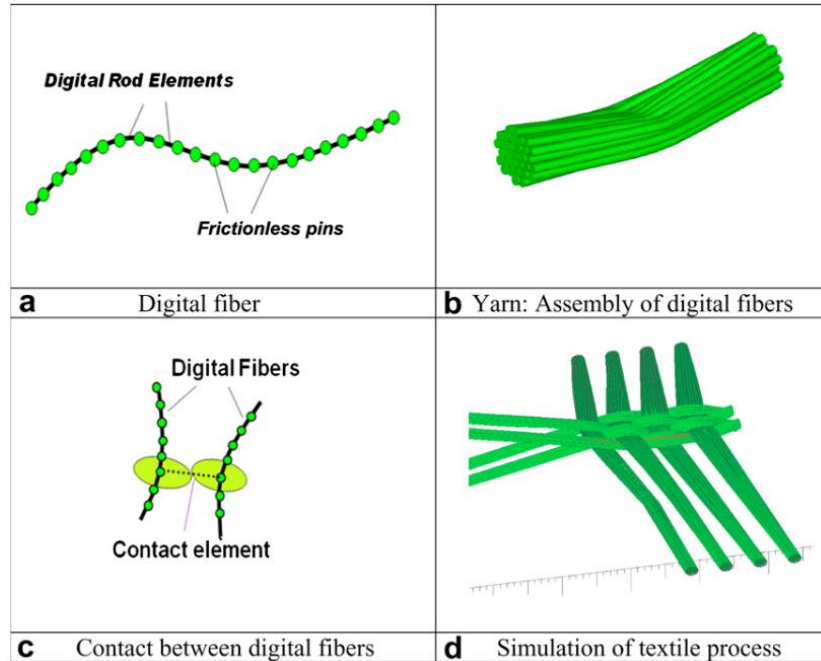


Figure 1.15: A digital element model of woven fabric [41].

Ha-Minh et al. [42] studied the effect of transverse mechanical properties of the yarn on the ballistic responses of a single-ply plain-weave (i.e., Kevlar KM2) woven fabric. Unlike the previously-mentioned numerical studies, Ha-Minh et al. used shell elements to create the woven fabric at yarn level (i.e., meso-scale), as shown in Figure 1.16. The numerical model was validated against experimental data and it was found that the effect of Poisson's ratio of the yarn was negligible. Ha-Minh et al. also found that the shear modulus of a yarn was an important material parameter that mainly influenced the ballistic performance of the single-ply plain-weave woven fabric. They found that using a higher shear modulus for the yarn caused early failure in the pure shearing mode.

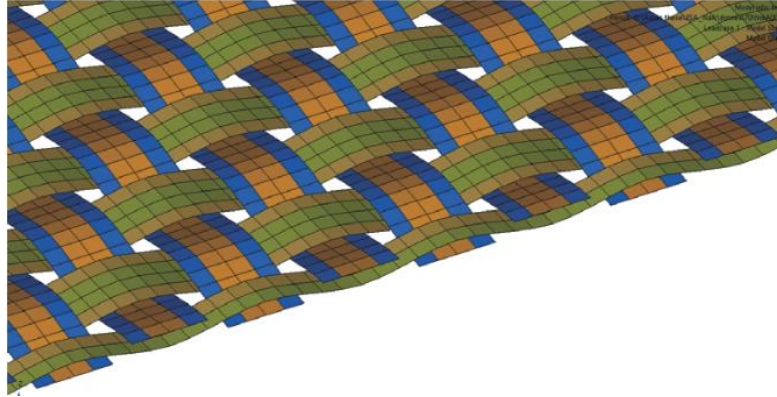


Figure 1.16: FE model of a woven fabric at yarn level created using shell elements [42].

In a later study by Ha-Minh et al. [43], they created an FE model of a woven fabric at the macro-scale to compare with their initial yarn-level model [42]. The entire fabric was assumed homogeneous and modelled using membrane elements. They found that the macro-scale model could reduce the computational cost but could not provide details of the impact mechanism of woven fabrics due to geometric and mechanical simplifications.

Nilakantan et al. [44] studied the effects of projectile size and shape on the ballistic responses of a single-ply, fully clamped woven fabric using a validated FE model that was created at yarn-level by using brick elements in LS-DYNA. Six different projectiles of various shapes (i.e., spherical, cylindrical and conical) with varying sizes but the same mass was considered. They found that the conical projectiles had the slowest decelerations by the target. It was also found that the conical projectiles caused gradual yarn failures, and the cylindrical projectiles caused abrupt yarn failures. In a subsequent numerical study by Nilakantan and Nutt [45], the effect of clamping designs on the ballistic performance of woven fabrics was investigated using the same FE model created in the previous study [44]. They created six different clamping designs as shown in Figure 1.17, four-side, two-side, circular, diamond, and two corner-clamped constraints. The V_{50} velocities were

calculated for each clamping design. The main conclusion drawn from the study was that the circular frame design resulted in the highest V_{50} velocity. This study gives an important indication of how boundary conditions may change the ballistic performance of woven fabrics.

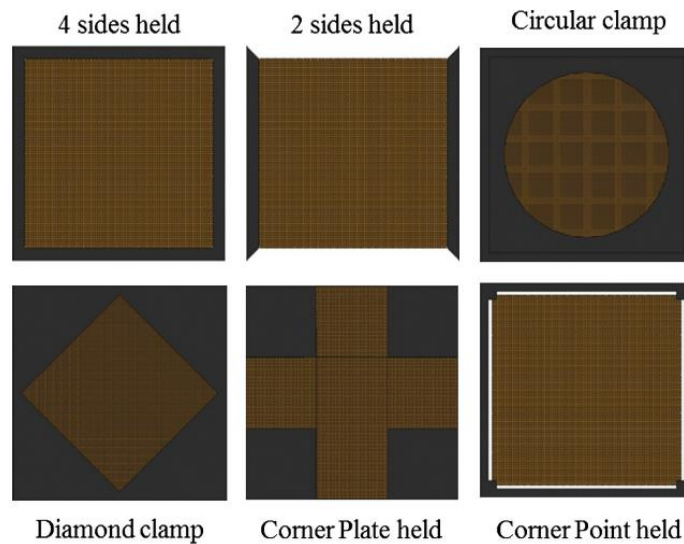


Figure 1.17: Different clamping designs [45].

The previously-mentioned numerical studies dealt with the ballistic impact performance of plain-weave single-ply woven fabrics. In the work by Yang et al. [46], they conducted a numerical study of the effect of weaving architectures on the ballistic responses of a single- and a five-ply woven fabric. The FE models of the woven fabrics were created at yarn-level using the brick elements for four weave patterns: plain, 2/2 basket, 4-harness satin, and 2/2 twill, as shown in Figure 1.18. It was found that the weaving architecture has less influence on the ballistic performance of multi-ply fabrics than on that of single-ply fabrics.

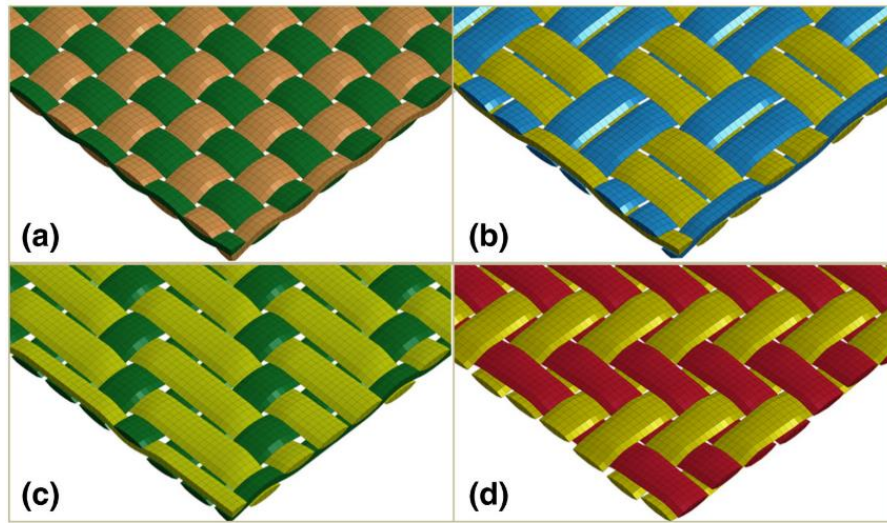


Figure 1.18: Different weave types used in the FE models by Yang et al. [46].

a. plain; b. 2/2 basket; c. 4-harness stain; and d. 2/2 twill.

Recently, Zhou and Chen [47] conducted a numerical study on how fabric construction parameters, such as crimp and thread density, affected the ballistic performance of woven fabrics. Using FE model of a single-ply woven fabric created with brick elements, they found that the energy absorption capacity of the fabric decreased as the increase of number of yarns per inch in the fabric. It was also found that there was an inverse correlation between the crimp (or undulation) of yarns and the tensile modulus of the fabric. Based on these research findings, they claimed that fabrics with low yarn density and high tightness were desirable for ballistic impact protection.

More recently, the effect of inter-yarn friction on the ballistic performance of woven fabrics were revisited in a numerical study by Chu and Chen [48]. They created the FE model of a single-ply woven fabric using brick elements in ABAQUS under impact of a cylindrical-nosed projectile. They defined different coefficients of friction between the yarns and assessed how inter-yarn friction affected the behavior of single-ply fabric in

terms of deformations, energy absorption capacity and forms of energy absorption. They concluded that increasing the inter-yarn friction could decrease the transverse deflections of the fabric (i.e., reduce the back-face deformation). While strain energy was the dominate form of energy absorption for impact cases with near-zero inter-yarn friction, kinetic energy became the dominate one for impact cases with high inter-yarn frictions.

1.4 Motivation

Real-world applications of woven fabrics such as soft body armor equipment consist of multi-ply fabrics, e.g., combat helmets [49,50] or vests [51]; however, most of the aforementioned studies on ballistic impacts in literature focused on single-ply woven fabrics. The energy absorption/dissipation mechanism of a multi-ply fabric takes a different form from that of a single-ply fabric due to interactions between adjacent plies of the fabric and between the projectile and the entire fabric [52]. Although there exist some experimental works on multi-ply woven fabrics under ballistic impacts, these experimental studies could not provide insight into detailed physical events happening during the ballistic impacts since the ballistic impacts occurred in very short period ($\sim 10^1 \mu\text{s}$). For example, experimental studies could not provide details on the interactions between yarns, plies, and the projectile and yarns as well as the energy dissipations of individual yarns and plies, which were very important impact phenomena to understand the impact mechanism of woven fabrics. Moreover, other factors such as the exact impact location, velocity and angle were very difficult to control precisely. Multi-ply woven fabrics under ballistic impacts were mostly studies in the analytical literature. Due to the complexity of these problems, several assumptions must be made in the analytical methods, which limited the outcomes of the studies. There are also a few numerical studies [35, 53-55] in literature on

ballistic impacts of multi-ply fabrics. Due to the high computational cost, some simplifications were made in these studies. For example, in the macro-scale models [35, 53], the entire fabric was assumed homogeneous; hence the models lacked the capability of providing important impact phenomena such as the effects of friction between the yarns, yarn pull-out behavior and yarn-to-projectile interactions. In meso-scale models, [54, 55], only a quarter of the fabric was modelled to reduce the computational cost. Although quarter models might be accurate for single-ply fabrics, but they are not desirable for multi-ply fabrics due to the use of symmetric boundary conditions [52]. To this end, there is a need to develop a full-size numerical model, which is accurate and computationally efficient so as to study the resistance mechanisms of multi-ply woven fabrics under ballistic impacts.

1.5 Research Objectives

The main objectives of this research were:

- I. To develop a validated FE model of full-size woven fabrics with good accuracy and computational efficiency for the first time in literature so that it could be used to investigate the resistance mechanism of multi-ply woven fabrics under ballistic impacts.
- II. To have a full understanding of ballistic impact phenomena of multi-ply woven fabric such as energy dissipations, damage patterns and displacements of individual yarns that occur during ballistic impacts.
- III. To study the effect of number of plies on the ballistic performance of multi-ply woven fabrics.

- IV. To investigate how the characteristics of a projectile (i.e., size, nose shape and impact velocity) affect the ballistic responses of multi-ply woven fabrics.
- V. To identify important parameters for designing lighter and stronger ballistic body armor equipment.

1.6 Research Approach

To achieve the objectives of this research, a state-of-art numerical modeling technique was used to create a cost-efficient FE model that can be used to study multi-ply fabrics under ballistic impacts. In light of the transverse responses of single-ply fabrics, a multi-scale (i.e., combining macro- and meso-scale) FE model of a single-ply woven fabric was created. A meso-scale FE model of the single-ply woven fabric was also created to compare with the multi-scale model for both solution accuracy and computational efficiency. The two FE models were validated against experimental data and the results showed that the multi-scale model significantly reduced the computational cost while maintaining the accuracy. The multi-scale FE model of the single-ply woven fabric was then used to construct the FE model of a multi-ply woven fabric, which was also validated to ensure accurate ply-to-ply interactions.

Four different multi-ply fabrics with three, five, seven and ten plies, were created using the validated multi-scale FE model to investigate the effect of the number of plies on the ballistic impact resistance of multi-ply woven fabrics. The simulation results were analyzed to provide guidance and suggestions towards building lighter and stronger ballistic body armor. Finally, the ten-ply woven fabric was used to investigate the ballistic impact performance under ballistic impacts of six different projectiles, which were in two

sizes (i.e., .22 and .30 cal.) and three shapes (i.e., conical, spherical and cylindrical). The findings provided insight into ballistic responses of multi-ply woven fabrics under different impact conditions.

1.7 Outline of This Dissertation

In Chapter 2, FE modeling techniques (i.e., micro-, meso- and macro-scale modeling) for woven fabrics under ballistic impacts are first introduced. In addition, the FE models created in this study are explained in detail. Model validations of the single- and multi-ply FE models of woven fabrics for this study are given in Chapter 3. The effect of total number of plies on the ballistic performance of woven fabric is presented in Chapter 4 in which the simulation results are evaluated in all possible aspects of ballistic impacts. Finally, the ballistic responses of multi-ply woven fabrics under ballistic impacts of different projectiles are discussed in detail in Chapter 5 followed by some concluding remarks and future work in Chapter 6.

CHAPTER 2: FINITE ELEMENT MODELING OF WOVEN FABRICS

Thanks to the development of high-performance computing technologies, finite element (FE) modeling has become the most commonly used numerical modeling and simulation tool to investigate the ballistic performance of woven fabrics. Since woven fabrics are multi-scale in nature (see Chapter 1), they can be modeled at three different length scales, micro-scale (i.e., at fiber level), meso-scale (i.e., at yarn level), and macro-scale (i.e., at fabric level). Figure 2.1 shows the modeling procedure used for FE modeling of woven fabrics at different length scales. The most detailed FE model of a woven fabric can be created at fiber level (i.e., micro-scale) while the most simplified model can be created at the fabric level (i.e., macro-scale). Macro-scale FE modeling is the most cost-efficient technique and the computational expense dramatically increases from macro- to micro-scale modeling. In micro- and meso-scale modeling techniques, localization methodology is employed to predict the global and local responses of woven fabrics. In meso- and macro-scale FE modeling techniques, homogenization methodology is used to mimic the behavior of fabrics under ballistic impacts.

In the micro-scale modeling, the fibers of a fabric are explicitly modeled so that fiber interactions can be observed during a ballistic impact. In meso-scale modeling, the woven fabric is represented by homogenized yarns; hence, only yarn interactions can be represented. In macro-scale modeling, the fabric is modeled as a homogeneous continuum

in which fiber interactions and yarn interactions are not explicitly represented in the constitutive laws.

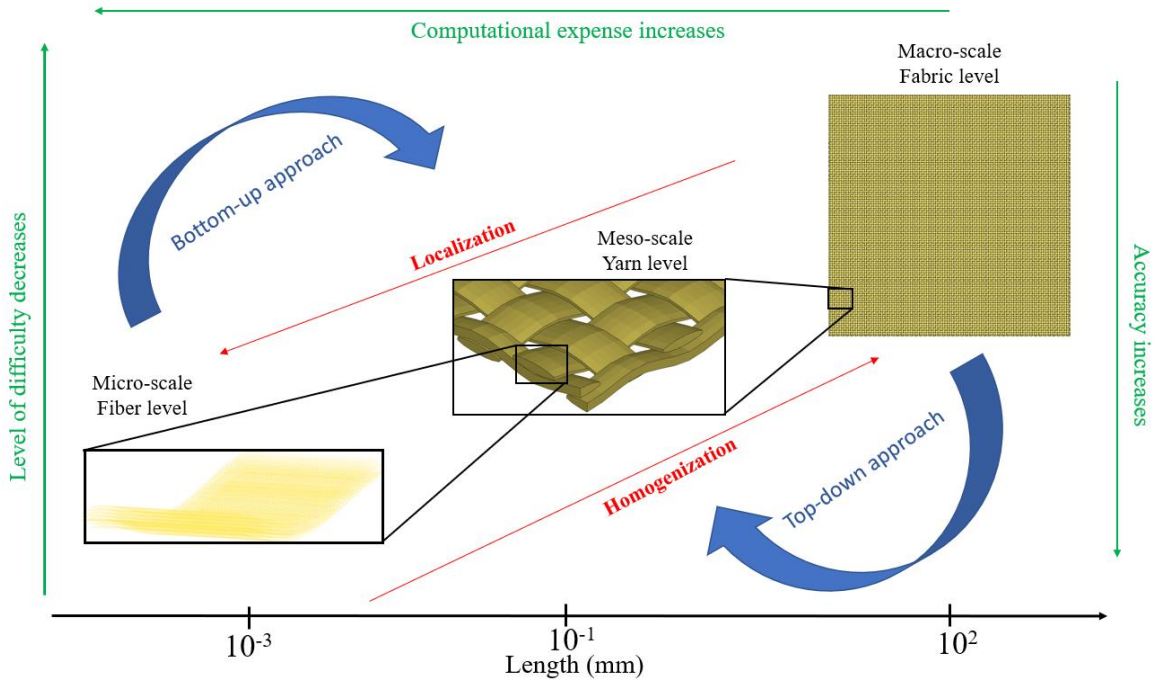
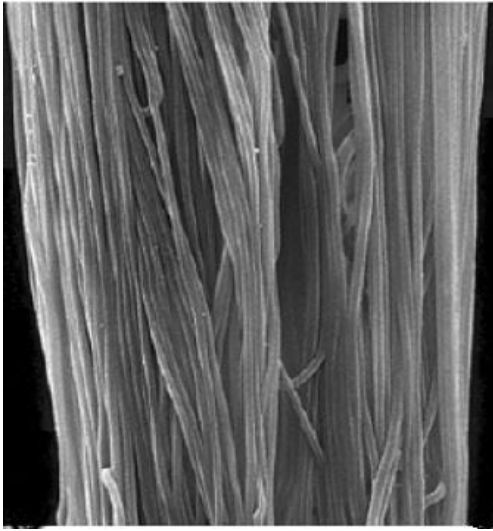


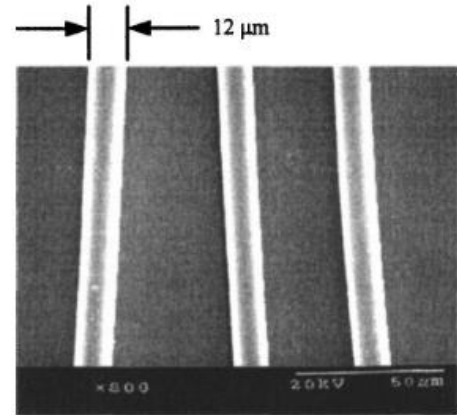
Figure 2.1: Multi-scale FE modeling of woven fabrics.

2.1 Micro-scale FE Modeling

Woven fabrics are constructed of interlacing yarns each of which consists of a bundle of fibers, as shown in Figure 2.2a. High-strength aramid (i.e., Kevlar KM2) fibers have circular cross-sections with 10-12 μm diameters (see Figure 2.2b). In micro-scale modeling, individual fibers within the yarns are explicitly modeled to study the important impact phenomena for woven fabrics such as fiber failures, fiber energy dissipation, fiber-to-fiber interactions, yarn-to-fiber interactions and fiber-to-projectile interactions. Since the fibers are explicitly modeled, the micro-scale FE modeling provides the most accurate and realistic yarn deformations and failures.



a. A yarn consisting of a bundle of fibers. [56]



b. A single Kevlar KM2 fiber. [57]

Figure 2.2: Micrographs of yarn and fiber.

Both continuous and discrete models have been created to model woven fabrics at the fiber level (i.e., micro-scale). 1D rods [41], 3D beams [58] and solid elements [59] can be used to model a fiber under ballistic impact. Figure 2.3 shows a micro-scale FE model of a yarn created using the beam elements in LS-DYNA. Since the micro-scale FE modeling of woven fabrics has extremely high computational cost with current computing technology, only 19 to 30 fibers can be modelled so far for each yarn to reduce the computational expenses, even though a yarn consists of hundreds of fibers,. The micro-scale FE model of a woven fabric can be created by assembling multiple yarns as shown in Figure 2.4.

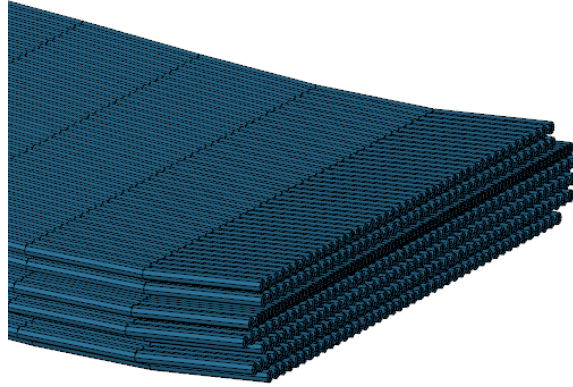


Figure 2.3: A micro-scale FE model of a yarn created using beam elements.

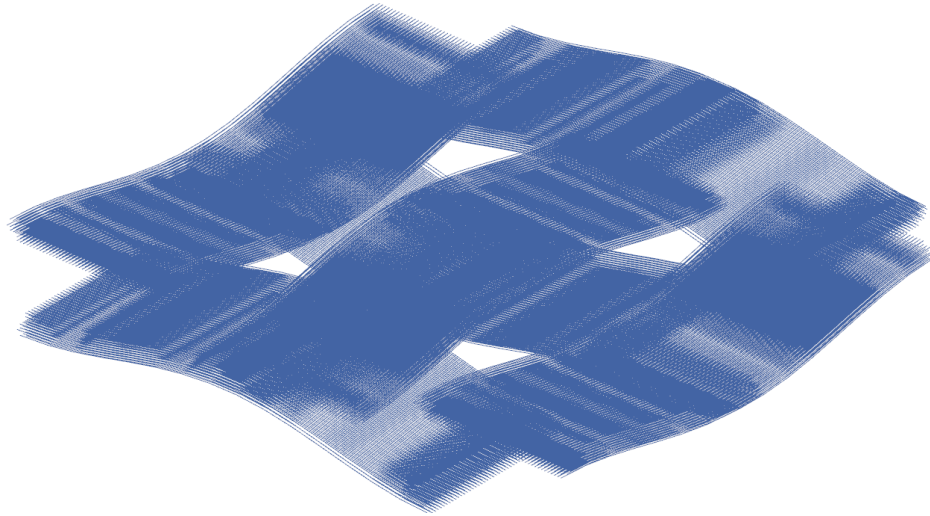
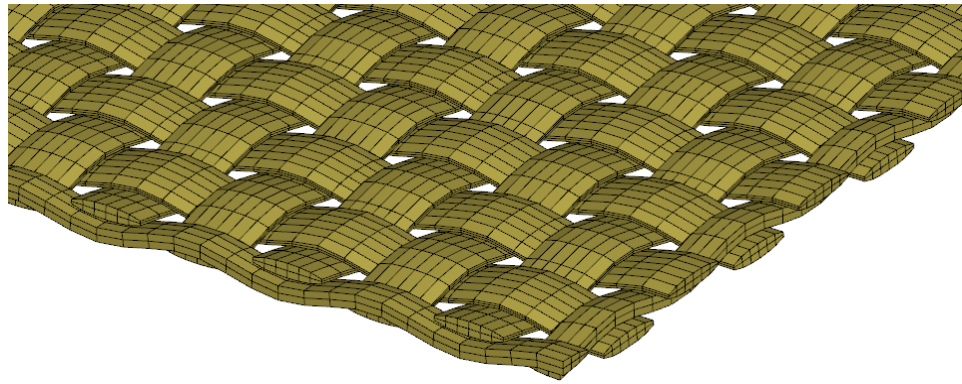


Figure 2.4: A micro-scale FE model of a woven fabric constructed using beam elements.

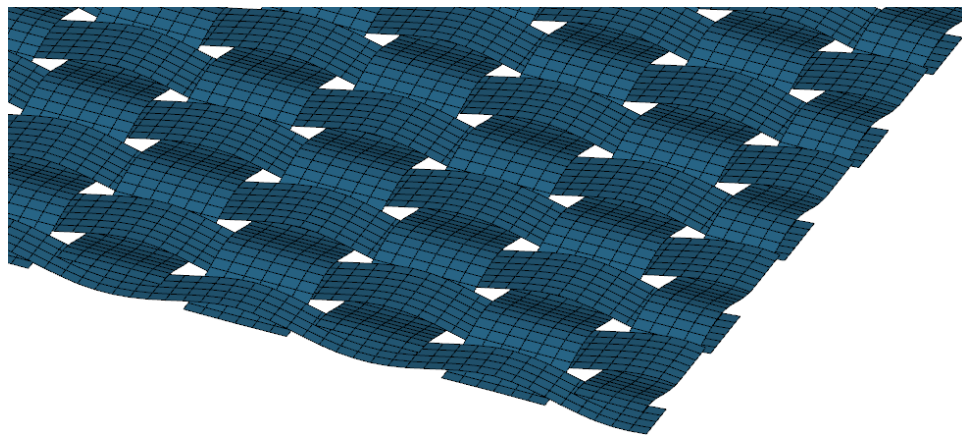
The high-strength fibers show transverse isotropy with linear elastic behavior in longitudinal tension and nonlinear inelastic behavior in transverse compression [57]. For a linear elastic and transversely isotropic material, five material constants are needed to describe the fibers' stress-strain responses. The mechanical properties of high-strength fibers were determined via a set of experiments (i.e., quasi-static and dynamic tests) in Reference [57].

2.2 Meso-scale FE Modeling

The meso-scale (i.e., yarn level) FE modeling is the most commonly used numerical modeling technique in literature since it has relatively low computational cost while it maintains reasonable accuracy [52]. In contrast to the micro-scale FE modeling, the woven fabrics in a meso-scale models are represented by homogenized yarns, which are considered as a homogeneous continuum and modeled using either hexahedron (i.e., solid element) or shell elements. The meso-scale FE models of woven fabrics could represent explicitly the yarn cross-sections and undulation (i.e., crimp). The meso-scale FE modeling also allows for simulating yarn-to-yarn friction and yarn-to-projectile friction; hence, yarn-to-yarn and yarn-to-projectile interactions in a ballistic impact can be considered. The effect of projectile characteristics and fabric architecture can also be investigated by utilizing the meso-scale FE modeling technique. Figure 2.5 shows two meso-scale FE models of a woven fabric consisting of homogeneous yarn with undulation created by using solid and shell elements, respectively. The cross-section of the yarns can be accurately modeled using solid elements; however, solid elements, due to their natures, are generally overly stiff in bending, and using solid elements to construct the entire fabric is very expensive. For this reason, using shell elements with different nodal thickness has become more popular in recent literature [52]. Depending on the width of the yarn, several elements with different nodal thicknesses through the width of the yarn are used to accurately represent the cross-sections of the yarns.



a.



b.

Figure 2.5: Two meso-scale FE models of a woven fabric.

a. Using solid elements; and b. using shell elements.

Depending on the applications, different material models can be used for yarns made of high-strength fibers. For ballistic impact applications, the homogeneous yarns are generally assumed to be linearly elastic (until failure occurs in the axial direction) with transversely isotropic material properties [52]. Figure 2.6 shows the stress-strain curve of an aramid yarn (i.e., one made of a bundle of high-strength fibers). In the meso-scale FE modeling technique, the transverse compressive response of the yarn is not considered. Moreover, fiber interactions within the yarn were assumed to have no effect on the behavior of the homogenized yarn model; hence, fiber compression, progressive fiber failure, fiber-

to-fiber contact and friction, and fiber spreading within in a yarn are neglected [60]. Since the transverse yarn strength data is not available in literature, only tensile failure of the yarn is considered in meso-scale FE modeling.

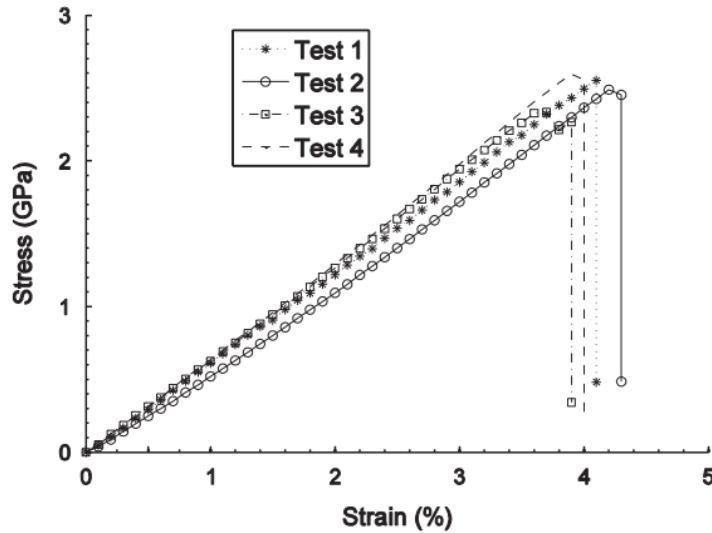


Figure 2.6: Stress-strain curve of a para-aramid yarn [43].

A transversely isotropic material is a special class of orthotropic materials which has the same properties in one plane and different properties in the direction normal to this plane. Transversely isotropic materials can be described by five independent elastic constants. The constitutive relationship for a transversely isotropic yarn with a 1-2 isotropic plane is given in Eq. (5), where 1 and 2 lies in thickness and width of the yarn, respectively, while 3 represents the axial or longitudinal direction of the yarn can be given by

$$E_{ij} = \begin{bmatrix} E_{11} & E_{12} & E_{13} & 0 & 0 & 0 \\ & E_{22} & E_{23} & 0 & 0 & 0 \\ & & E_{33} & 0 & 0 & 0 \\ & & & E_{44} & 0 & 0 \\ & & & & E_{55} & 0 \\ & & & & & E_{66} \end{bmatrix} \quad (5)$$

The longitudinal Young's modulus is given by $E_L = E_{33}$, similarly the transverse Young's modulus is $E_T = E_{22} = E_{33}$. The shear modulus is $G = E_{44} = E_{55}$ and the in-plane shear modulus is given by $G_{12} = E_{66} = 2 \frac{E_T}{(1+\nu_{21})}$, where ν is the Poisson's ratio. Moreover, with $\nu_{23} = \nu_{13}$, $E_{12} = -\nu_{21}E_T$, and $E_{13} = E_{23} = -\nu_{31}E_T$, Eq. (5) can be written with the five independent material constants as follows [61].

$$E_{ij} = \begin{bmatrix} E_T & -\nu_{21}E_T & -\nu_{31}E_T & 0 & 0 & 0 \\ & E_T & -\nu_{31}E_T & 0 & 0 & 0 \\ & & E_L & 0 & 0 & 0 \\ & & & G & 0 & 0 \\ & & & & G & 0 \\ & & & & & 2 \frac{E_T}{(1+\nu_{21})} \end{bmatrix} \quad (6)$$

2.3 Macro-scale FE Modeling

In the macro-scale (i.e., fabric level) FE modeling technique, the global responses of the fabric are intended to be captured without considering fiber-to-fiber /or yarn-to-yarn interactions that are captured in micro- and meso-scale models. Although woven fabrics consist of yarns, which in turn consist of hundreds of fibers, woven fabrics under ballistic impacts resemble thin, homogeneous plates. Therefore, woven fabrics are assumed to be homogeneous plates in macro-scale FE models, as shown in Figure 2.7. Most of the macro-scale FE models of woven fabrics are created using shell or membrane elements since the thickness of the fabric is small compared to other in-plane dimensions and stays almost constant during deformation [60].

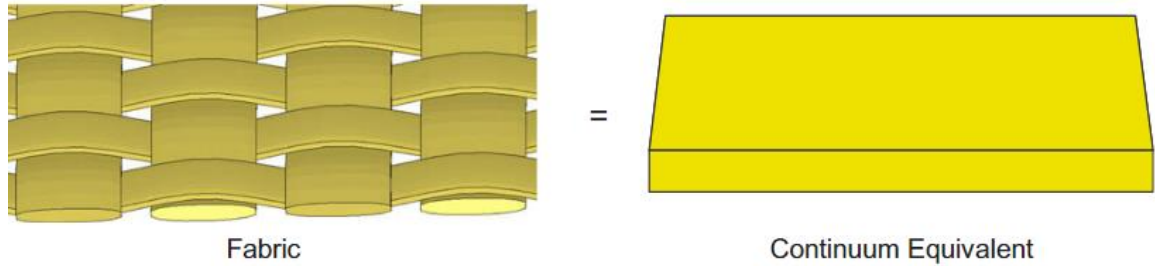


Figure 2.7: The macro-scale FE modeling of woven fabrics [62].

Nonlinear orthogonal material models are used to simulate the responses of woven fabrics at the macro-scale. To determine the material properties of the fabric as an equivalent continuum using shell elements, two main approaches are mainly used. In the first approach, representative unit cells (RUCs) or representative volume elements (RVEs) are used since the woven fabric has a repetitive pattern. An example of a repetitive unit cell for a plain weave fabric is shown in Figure 2.8. In this approach, a fabric is modelled as at the continuum scale accounting for the yarn interactions through contact forces computed from equilibrium at the cross-overs with no through thickness stresses and strains [63]. The second approach is similar to the first one, except that the constitutive relations are obtained by fabric-level experiments [63].

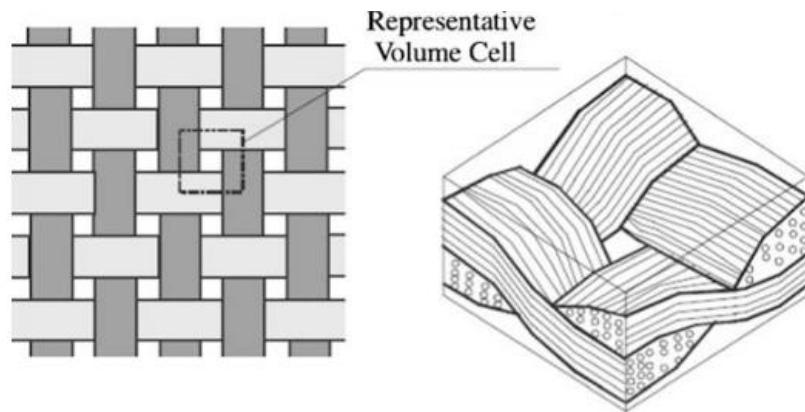


Figure 2.8: Repetitive unit cell. [62]

The macro-scale FE modeling is the most computationally efficient one among the three FE modeling techniques. However, the macro-scale models are not capable of simulating yarn sliding with friction and yarn pullouts, which affect the behavior of woven fabrics under ballistic impacts. Although the macro-scale FE models can predict the residual velocities with reasonable accuracy, they are not adequate for predicting out-of-plane displacements and damage patterns of the fabrics.

2.4 Multi-scale FE Modeling

Each of the aforementioned modeling approaches has its own advantages and limitations. For numerical modeling, the challenge lies in reducing the computational cost while obtaining accurate results. To this end, a multi-scale modeling technique, which combines models at two or more different length scales to construct a single FE model of the fabric, is needed to obtain accurate results at affordable computational costs. In recent years, multi-scale modeling was developed by combining meso- with macro-scale models [64-68]. In these models, the region at close proximity to the impact point was modelled at meso-scale, and the surrounding region was modeled at macro-scale, as shown in Figure 2.9.

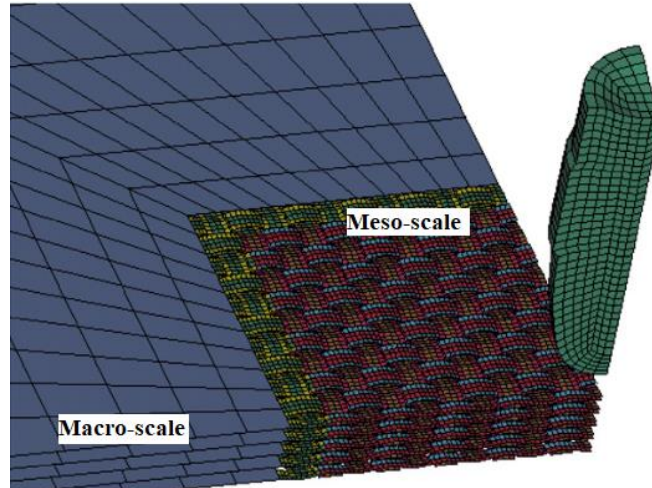


Figure 2.9: A multi-scale FE model of a multi-ply woven fabric [64].

When utilizing a multi-scale FE modeling technique for modelling woven fabrics, the most challenging task is to ensure accurate wave propagation from the meso-scale region to macro-scale region. The wave propagation must be transmitted accurately from the meso- to the macro-scale to obtain accurate dynamics of the fabric. However, in the aforementioned multi-scale FE models [64-68], tied contacts were used between the meso- and macro-scale regions and created artificial contact stiffness and contact forces that consequently ruined the nature of wave propagation. In addition, the tied contact definition lacked rotational degrees of freedom for the nodes along the edges of the interface regions, which artificially increased the rigidity of the yarns along the interface. Another drawback of these multi-scale FE models was that surface-to-surface contacts were used between yarns and caused inter-penetration of parallel yarns due to the inability of the contact algorithm to detect and handle self-penetrations [69]. It should be noted that the above-mentioned multi-scale models [65-67] have not been validated using experimental data, and they were limited to single-ply fabrics impacted by a single velocity. The multi-scale

FE model of woven fabrics created in this research overcame the above shortcomings and was used to investigate the ballistic performance of multi-ply woven fabrics.

2.5 FE Model Creation

A plain weave Kevlar S706 fabric, which had 34 Kevlar KM2 fiber 600 denier yarns per inch in both the warp and weft directions and had an areal density of 180 g/cm², was modelled in this study. Two FE models were created for this Kevlar fabric sheet, one being a full meso-scale model and the other a multi-scale model combining meso- and macro-scale models.

2.5.1 Mesh generation

Fully integrated shell elements in LS-DYNA with variable nodal thickness were used to create the yarns in both the meso- and multi-scale FE models. Six elements were used across the yarn width to represent the yarn cross-section. The crimp of the yarn was assumed to be trigonometric and modeled using a centerline equation given by:

$$\left(\frac{t}{2}\right)\left(\cos\frac{\pi x}{s}\right) \quad (7)$$

where t and s correspond to the maximum thickness of the yarn cross-section and the span of the yarn, respectively. The warp and weft yarns were assumed to be identical and were assigned the parameters given in Table 2.1. Figure 2.10 shows a comparison of the cross-section with undulation of the yarn and its corresponding FE model.

Table 2.1: Dimensions of Kevlar KM2 yarn used in this study.

Yarn parameter	Dimension (mm)
Span	0.747
Width	0.536
Thickness	0.115

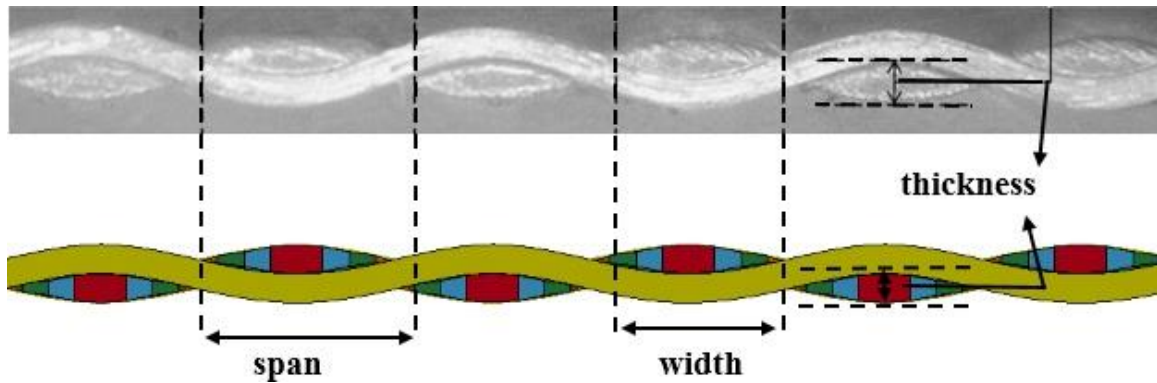


Figure 2.10: Cross-sectional view of Kevlar KM2 yarns [58] and the corresponding FE model.

Stiffness-based membrane elements in LS-DYNA were used to create the macro-scale mesh of the multi-scale model. Since the cross-sections of warp and weft yarns were the same and parallel yarns were located side by side in the fabric, the size of the membrane elements was equal to the gap between the yarns (i.e., ~ 0.2 mm). This choice gives the most realistic ballistic impact response of the woven fabric at the macro-scale [43]. The thickness of the macro-scale region was 0.23 mm, the same as the actual thickness at the crossover point of the fabric.

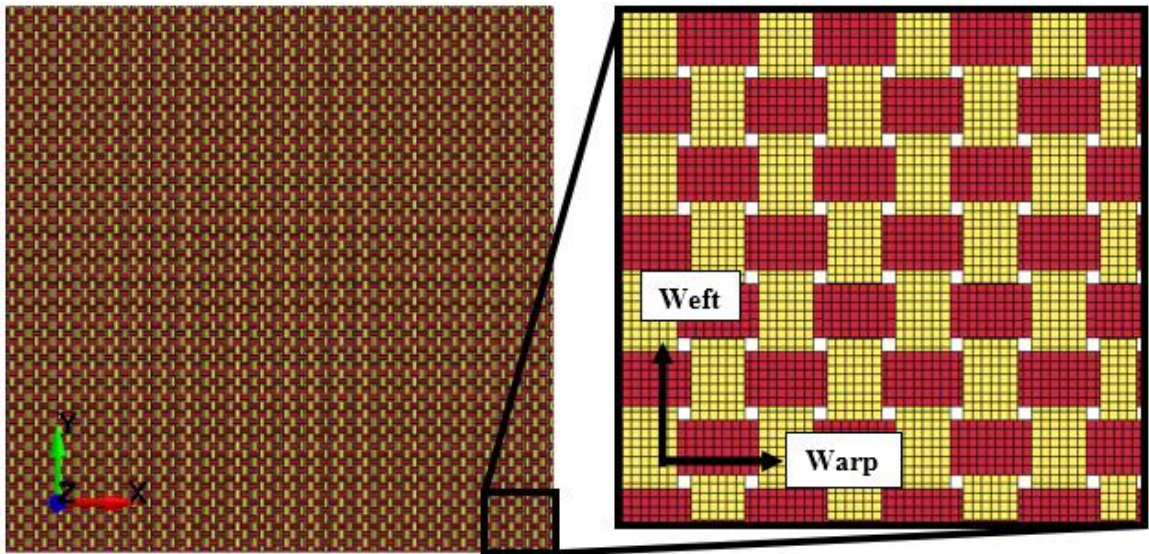
The multi-scale FE model was structured as a “center-cross”, with the primary yarns (i.e., those carrying most of the transmitted energy from the projectile and undergoing large permanent deformations) modelled at the meso-scale. The secondary yarns, which might have out-of-plane dynamic deflections but remain elastic with no

perforations, were modelled at the macro-scale (i.e., the woven fabric modeled as homogeneous plate). Unlike existing multi-scale models in literature, the meso- and macro-scale meshes are connected by sharing nodes along the edge of the interface rather than by tied contacts. This modeling technique allowed for wave propagation to be accurately transmitted from the meso-scale to the macro-scale region. In the multi-scale model, the meso-scale region was created larger than the diameter of the projectiles to ensure no perforation occurring outside the region of the primary yarns.

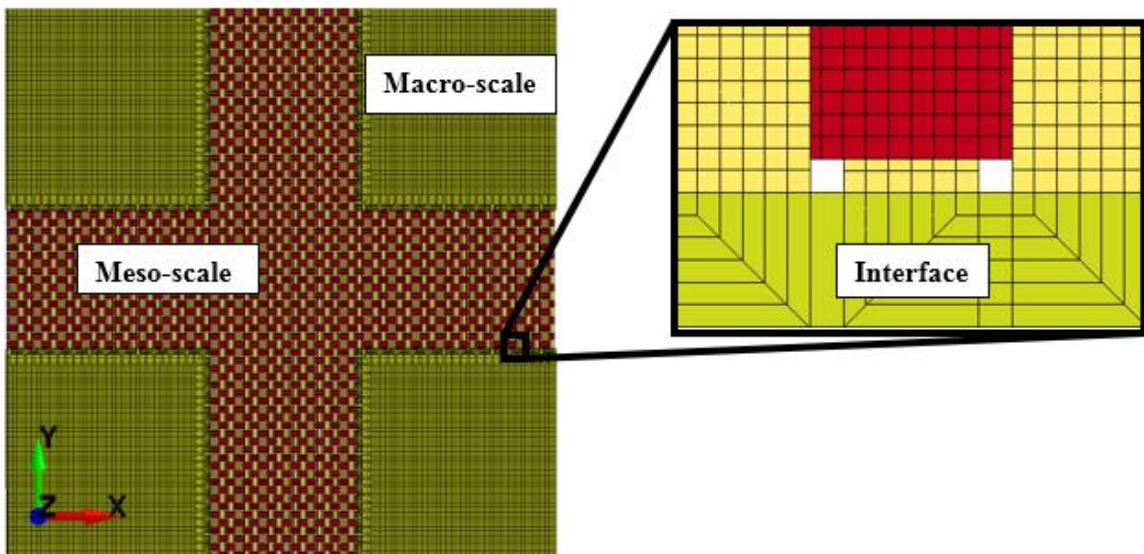
Finally, the full meso-scale fabric model, which was 52 x 52 mm in size, had a total of 413,816 elements, while the multi-scale model had a total of 227,003 elements, with 187,272 and 39,731 elements for the meso- and macro-scale models, respectively. Figure 2.11 shows the two FE models of the woven fabric created in this study.

2.5.2 Material modeling

Woven fabrics at different length scales (i.e., macro-, meso-, and micro-scales) possess elastic, orthotropic constitutive behavior [52]. The orthotropic material model requires the following nine elastic constants: E_{11} , E_{22} , E_{33} , G_{11} , G_{22} , G_{33} , ν_{11} , ν_{22} , and ν_{33} , where E , G , and ν are Young's moduli, shear moduli, and Poisson's ratio, respectively. Material directions 11 and 22 denote the longitudinal direction and width of the fabric, respectively, whereas 33 represents the out-of-plane direction of the fabric. In literature, it was shown that Poisson's ratios were close to zero, and the shear moduli were equal (i.e., $G_{11} = G_{22} = G_{33}$) and small compared to the longitudinal elastic modulus, E_{11} [52]. Hence, a linear elastic orthotropic material model was used for both the meso- and macro-scale models of this study. The material model used in this research along with the material properties are given in Chapter 4.



(a)



(b)

Figure 2.11: FE models of the Kevlar S706 fabric.

(a) the meso-scale; and (b) the multi-scale.

CHAPTER 3: VALIDATION OF THE FINITE ELEMENT MODELS

In this chapter, the FE models created in Chapter 2 are validated. Details of the experimental setup and the corresponding FE models are first discussed in detail and simulation results were compared to experimental data obtained from literature.

3.1 Validation of FE Model of Single-ply Fabric

3.1.1 Experimental setup

Yu et al. [19] conducted a comprehensive experimental study on a 177.8×177.8 mm single-ply, plain weave Kevlar S706 fabric under impacts of a spherical stainless-steel projectile with a diameter of 5.56 mm and a mass of 0.692 g (see Figure 3.1) at impact velocities ranging from 38 to 447 m/s. The fabric was clamped to a steel frame that had a circular aperture with a diameter of 50.8 mm. To reduce slippage, the surfaces of the steel frame contacting the fabric were covered with a coarse anti-slip tape. The frame and the fabric were fixed by eight peripheral bolts tightened to a 3-GPa total pressure, as shown in Figure 3.1. Residual velocities of the projectile and out-plane-displacements of the fabric were measured and recorded. To track dynamic deflection of the fabric, the digital image correlation technique was utilized for the targeted area. The targeted area on the fabric was painted with a random pattern of black dots for displacement tracking. Two high-speed cameras were installed behind the fixture to generate stereo images of the impact event. Figure 3.2 shows the schematic of the experimental test setup.

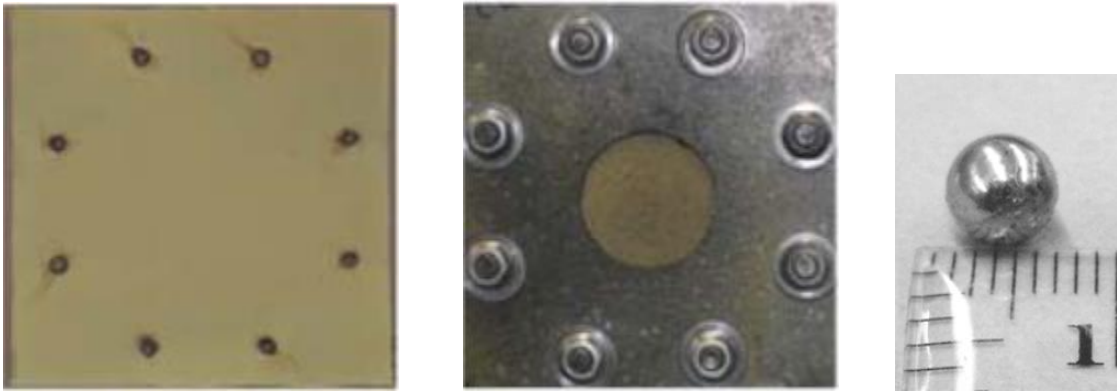


Figure 3.1: The target, fixture and impactor [19].

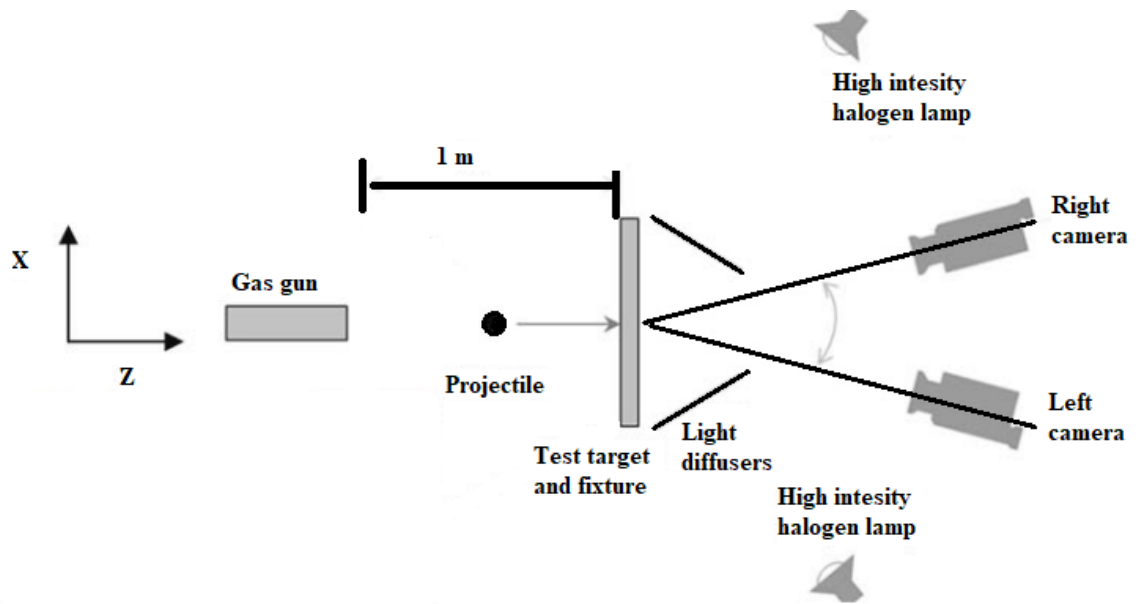


Figure 3.2: A schematic of the impact experiment setup and camera placements [19].

3.1.2 FE models of the experiment

In the FE model of the 50.8-mm diameter fabric shown in Figure 3.3, the nodes along the circular boundary were constrained for all the nodal degrees of freedom, resembling the clamped boundary used in the experiment. The material properties used for

the macro-scale fabric model of this study were taken from Reference [53] in which a representative unit cell method was utilized along with some empirically obtained values. In literature, many researchers [36-52] assumed that homogenized yarn models had the same material properties as the fibers had. Hence, the material properties obtained for KM2 fibers through dynamic experimental tests [57] were used for the meso-scale fabric models of this study. The Poisson's ratio of the yarn was set to zero since fiber interaction was neglected in the homogenized yarn model [60]. An elastic orthotropic material model (i.e., MAT #2 MAT_ORTHOTROPIC_ELASTIC in LS-DYNA) was used for both the meso- and multi-scale models with the material parameters given in Table 3.1.

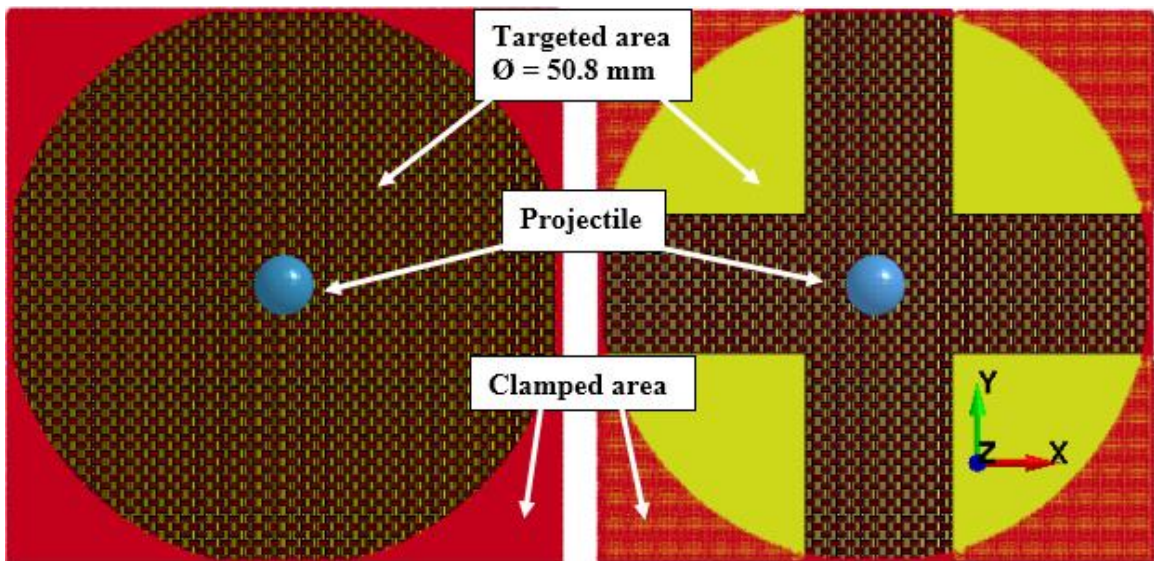


Figure 3.3: FE models of the experimental setup.

In general, the ultimate strength of the yarns follow a probabilistic distribution, which cannot be fully represented in a single deterministic simulation. For this reason, the experimentally obtained mean value of yarn strength (i.e., 3.225 GPa) [58] was used in both numerical models. Yarn failure was implemented using an element deletion algorithm

based on the maximum principal stress failure criterion. Since no fabric failure was anticipated in the macro-scale region, no failure criterion was defined for this area. A static coefficient of friction, 0.2, was used between the yarns and the projectile and the fabric [52]. Since no permanent deformation was observed in the projectile in the experiments, the projectile was modeled as an elastic material. In the numerical simulations, a total of 14 different velocities ranging from 38 to 447 m/s were assigned to the projectile. The residual velocities of the projectile and out-of-plane displacements of the fabric were obtained from simulation results and compared to experimental data. To handle the potential contacts between yarns and between the projectile and the fabric, the segment-based eroding single-surface contact algorithm was employed for the entire model. Nonlinear FE software, LS-DYNA, was used to carry out all the simulations.

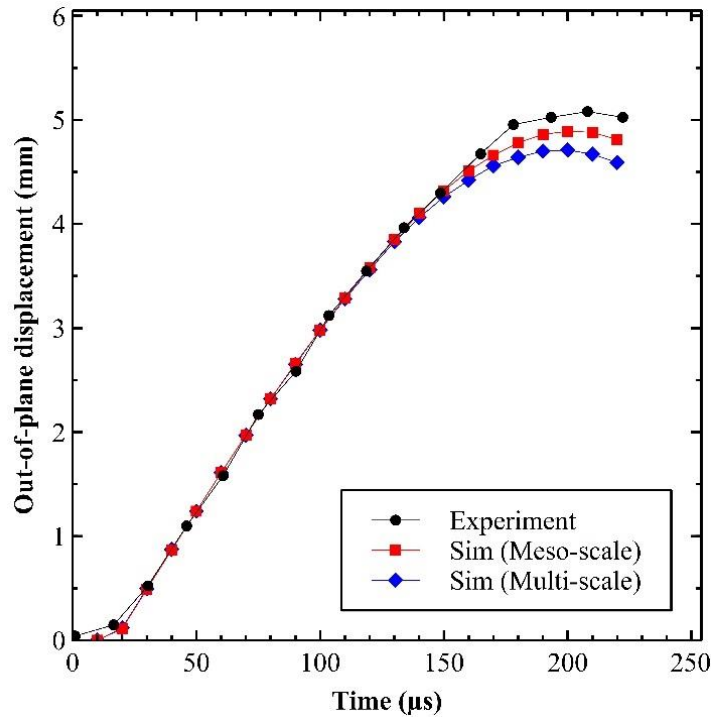
Table 3.1: Material properties used in the FE models.

	Meso-scale region [57]		Macro-scale region [53]
	<i>Warp</i>	<i>Weft</i>	
ρ (kg/m ³)	1440	1440	1310
E_{11} (GPa)	84.6	1.34	70
E_{22} (GPa)	1.34	84.6	7.4
G (GPa)	24.4	24.4	3.3
σ_f (GPa)	3.225	3.225	

3.1.3 Results and discussion

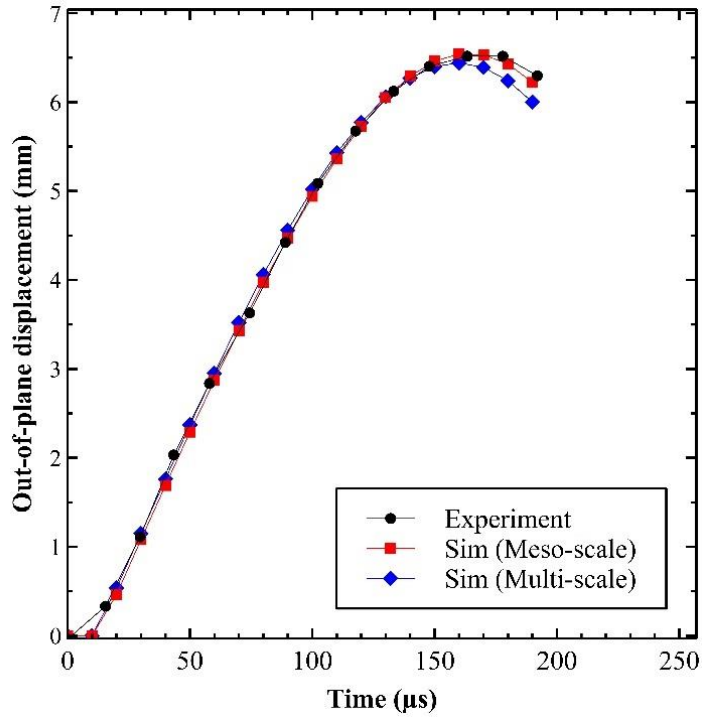
Figure 3.4 shows a comparison of out-of-plane dynamic deflections from the simulation results of the meso- and multi-scale models and from the experimental data. For the non-penetrated cases shown in Figs. 4a-c, the results were compared to the point of

maximum fabric displacement where the projectile started to bounce back. For penetrated cases, the dynamic deflection of the fabric was tracked until perforation occurred. It is observed from Figure 3.4 that the simulation results matched well to the experimental data. For the non-penetrated cases, both the meso- and multi-scale models produced slightly smaller peak displacements than those from the experiments. These discrepancies were found to be diminished in the penetrated cases. For both non-penetrated and penetrated cases, the numerical models were capable of capturing the rates of fabric deflections. It was also observed that the multi-scale models produced smaller peak displacements than the meso-scale models on the same impact cases and that the differences reduced to negligible when the impact velocity was increased.

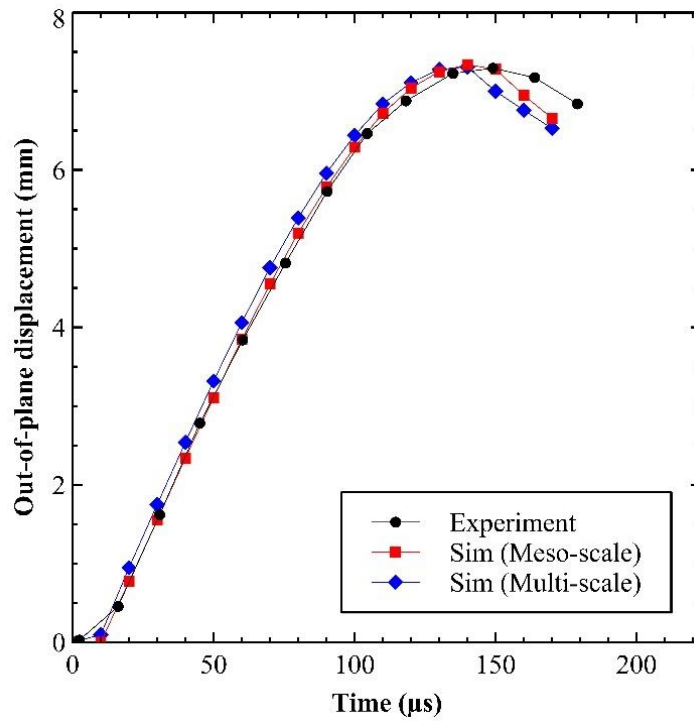


a. 38 m/s

Figure cont'd

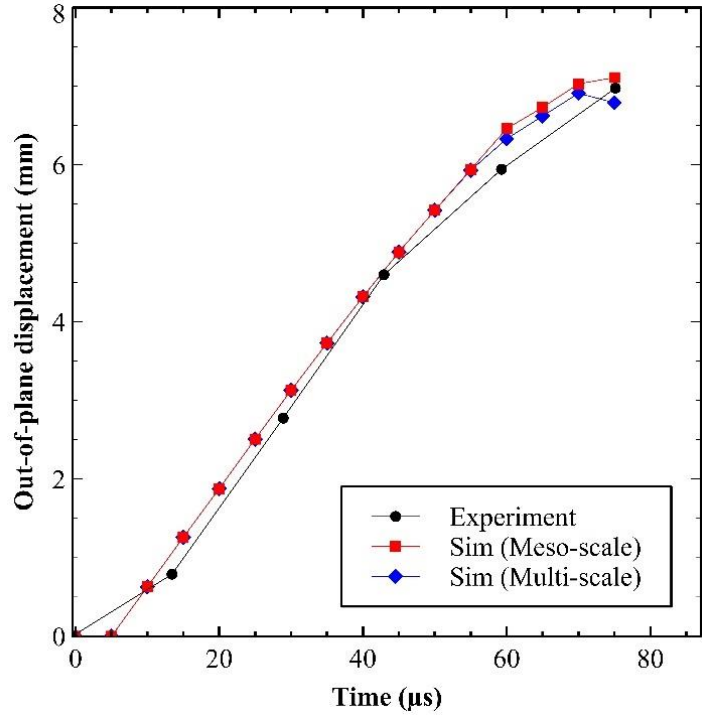


b. 63 m/s

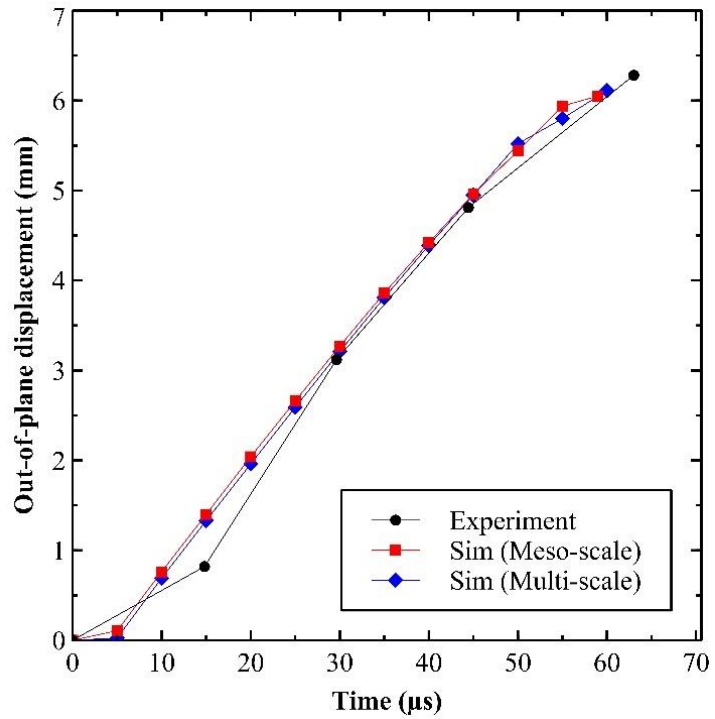


c. 83 m/s

Figure cont'd



d. 142 m/s



e. 157 m/s

Figure 3.4: Comparison of out-of-plane displacements of the single-ply fabric.

(a-c) non-penetrated cases; and (d-e) penetrated cases.

Besides dynamic deflections, the two numerical models also predicted well on wave propagation in the fabric. Figure 3.5 shows the experimental data and the simulation results of wave propagation of the fabric under the impact at 63 m/s. The back-face deformation, an important dynamic response of woven fabric during an impact, was observed from the simulation results to form a shape resembling a “square pyramid,” which was the same as seen in the experiment. The transverse waves in the primary yarns were found to travel away from the impact point faster than in other yarns. These transverse wave propagations caused the primary yarns to deflect in the out-of-plane directions, which transmitted the waves to secondary yarns at cross-over points. Due to friction at the cross-over points of the fabric, the secondary yarns “resisted” deflecting and consequently caused the out-of-plane displacements of the fabric to form a square-pyramid shape. This impact phenomenon was predicted well by both numerical models.

The simulation results were also compared to experimental data on fabric displacements in the x - and y - directions. As shown in Figure 3.6, the principal yarns bowed toward the impact location in the experiment. Although the displacements by both numerical models differed slightly from those of the experiments, similar displacement patterns were observed in both numerical models.

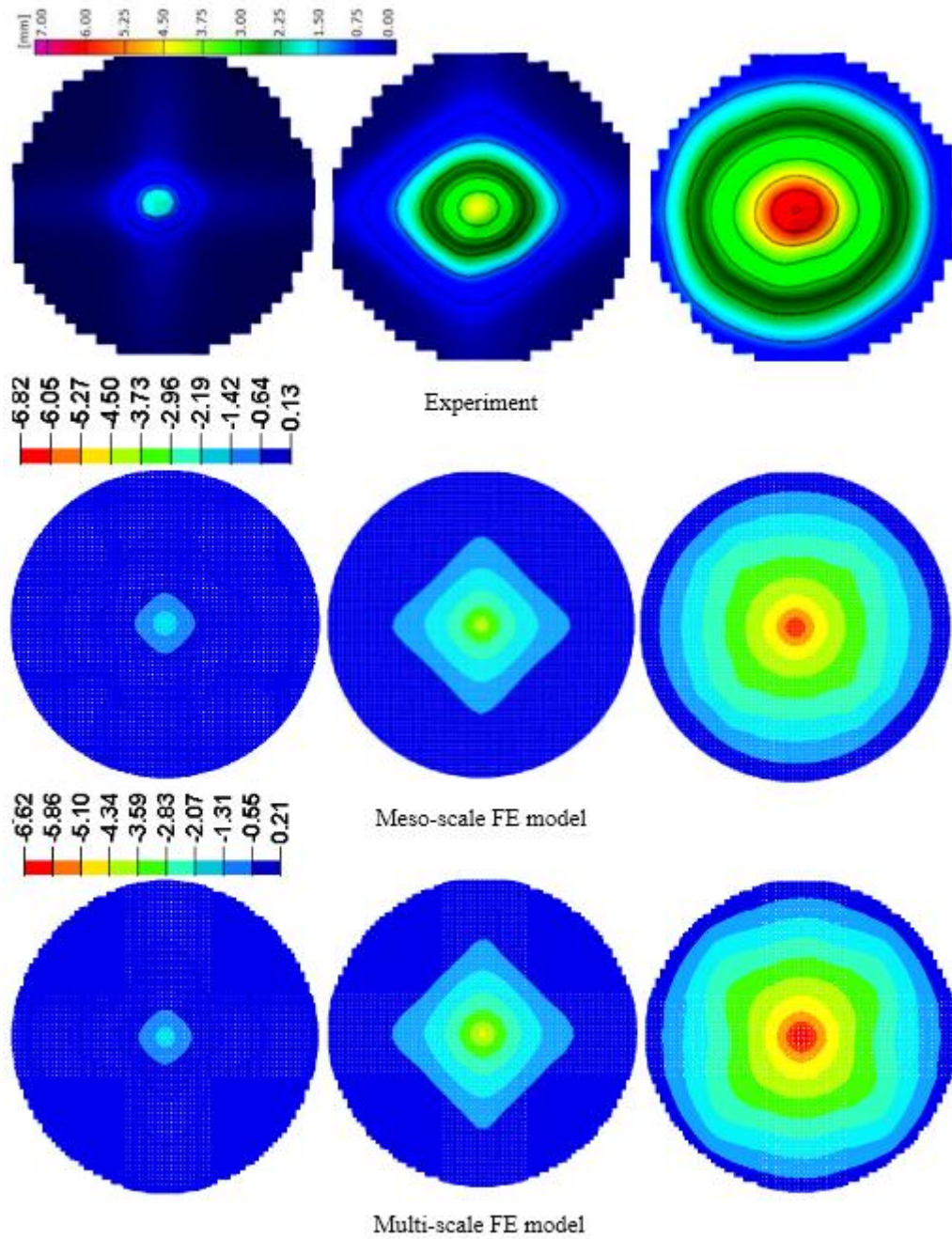


Figure 3.5: Transverse wave propagation (in mm) under the impact of 63 m/s at 44, 88, and 138 μs , respectively.

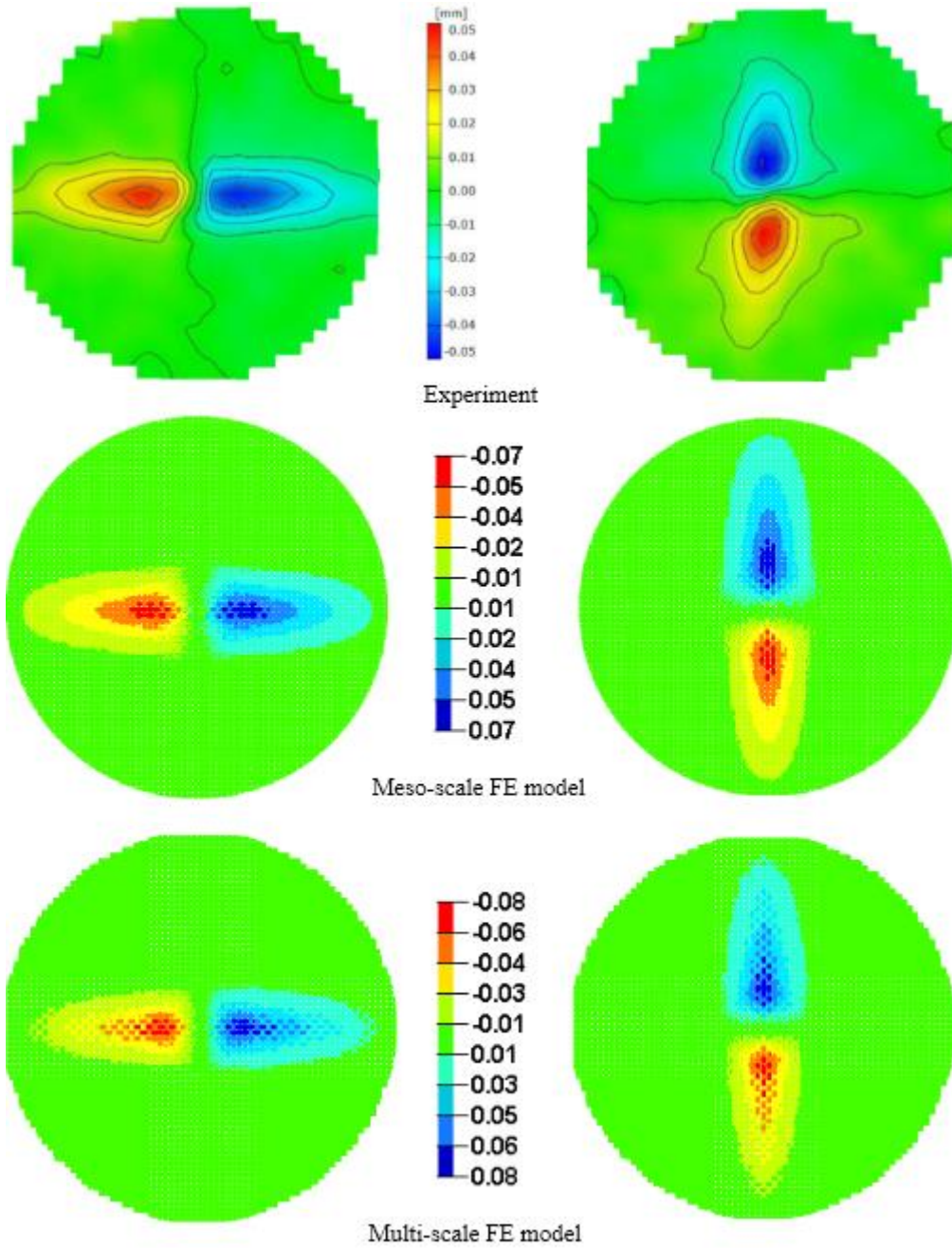


Figure 3.6: Fabric displacements (in mm) at $14.8 \mu\text{s}$ in the x - (left) and y - (right) directions under impact of 63 m/s .

Figure 3.7 shows the comparison of simulation results with experimental data on residual velocities and dissipated energies. The dissipated energy (ΔE) can be calculated as:

$$\Delta E = \frac{1}{2}mv_i^2 - \frac{1}{2}mv_r^2 \quad (8)$$

where m , v_i and v_r are the mass, initial velocity and residual velocity, respectively, of the projectile. Figure 3.7 shows three different regions of the projectile's initial velocities based on the corresponding residual velocities: 1) low velocities (i.e., below 83 m/s) with no penetration; 2) intermediate velocities (i.e., from 83 to 147 m/s) with energy dissipation reaching the highest level; and 3) high velocities (i.e., from 147 to 447 m/s) with reduced energy absorption due to perforation. These three regions predicted by the numerical models were in overall good agreement with the experimental data, as shown in Figure 3.7, with the largest difference in residual velocity occurred in the region of intermediate velocities.

Overall, both the meso- and multi-scale models were capable of predicting important responses of woven fabrics under dynamic loadings such as fabric deformations and residual velocities. Regarding the computational cost of the two numerical models, the multi-scale model was more efficient than the meso-scale model, because the multi-scale model had approximately half the number of elements of the meso-scale model. Considering its numerical accuracy and computational efficiency, the validated multi-scale model was adopted for modeling multi-ply fabrics in the subsequent sections.

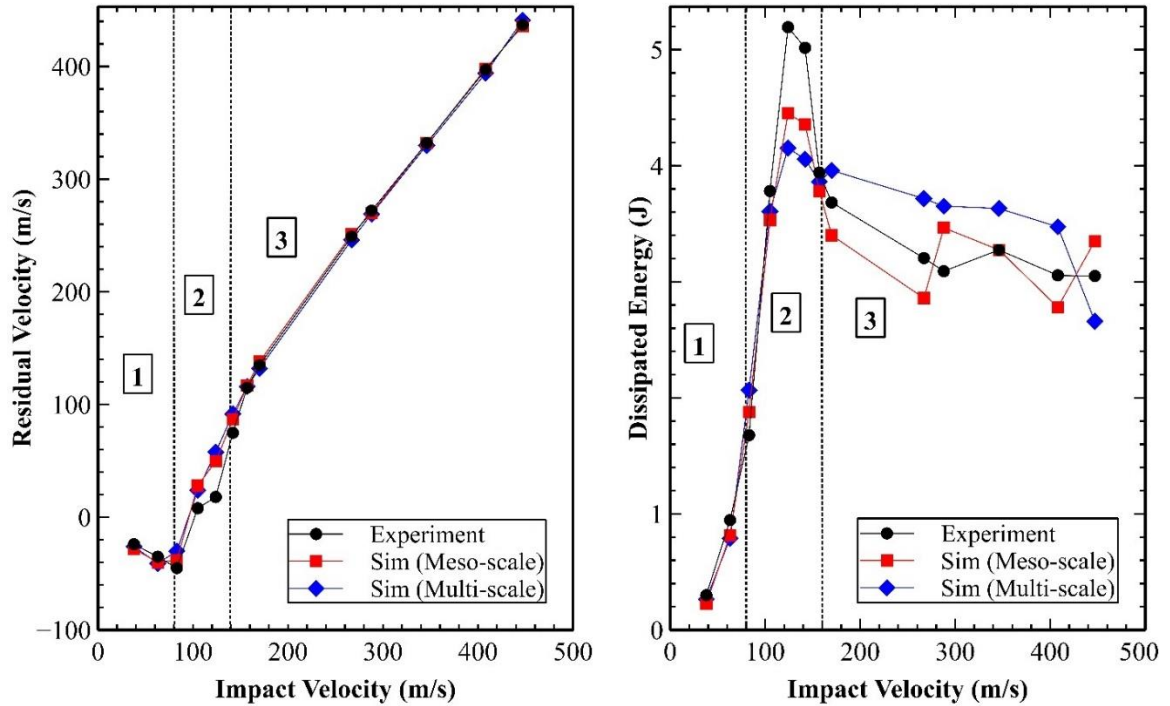


Figure 3.7: Comparison of the residual velocities and dissipated energies.

3.2 Validation of Multi-scale FE Model of a Multi-ply Fabric

Although the single-ply fabric models could predict fabric responses well compared to the experimental data, the effect of ply interactions should be validated before using the model for a multi-ply fabric. Rabb [18] evaluated the ballistic limits of two- and four-ply Kevlar S706 fabrics under impacts of a 1.1-gr. fragment simulating projectile (FSP) as shown in Figure 3.8 at different impact velocities ranging from 190 to 430 m/s. The target shape and boundary conditions in the multi-ply experiments was the same as those in the single-ply experiments in Section 2.2, except that the radius of the multi-ply target doubled that of the single-ply fabric specimen.

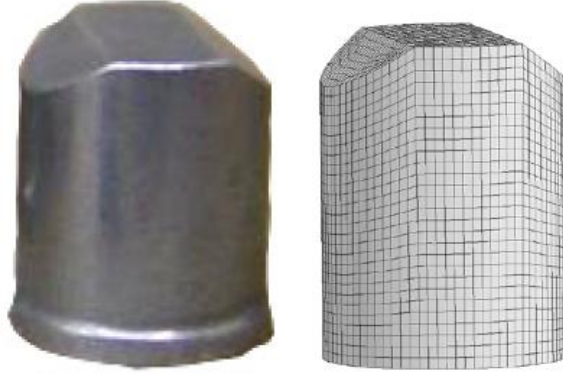


Figure 3.8: The FSP and its corresponding FE model.

To create the multi-ply fabric model, the single-ply multi-scale mesh was duplicated and stacked on top each other without bonding. The friction coefficient between plies was set to be the same as that between yarns. The impact velocities used in the experiments were assigned to the projectile in the FE model, and the residual velocities were obtained from simulation results. The Recht-Ipson analytical model [70] was employed to predict the ballistic limit, i.e., the lowest impact velocity causing a full perforation. The following equation is used in the Recht-Ipson model to create the best fit of the impact velocities and corresponding residual velocities using the least square method.

$$v_r = a(v_i^p - v_{bl}^p)^{\frac{1}{p}} \quad (9)$$

where v_r is the residual velocity, v_i is the initial velocity, v_{bl} is the ballistic limit, and a and p are empirical constants to best fit the data. In this study, the parameter, a , was assigned a value of one since there was no plugging on the projectile [52].

Figure 3.9 shows the comparison of residual velocities from simulation results with experimental data for a two- and four-ply fabric. In Figure 3.9, the solid and dashed lines represent the best fits by the Recht-Ipson models for experimental data and simulation

results, respectively. Table 3.2 summarizes the ballistic limits (V_{bl}) and the parameters of the Recht-Ipson model for the experimental data and simulation results shown in Figure 3.9. For both the two- and four-ply fabric targets, the simulation results had less than 2.3% errors compared to the experimental data of the ballistic limits. The residual velocities from the simulations were in good agreement with the experimental data, especially with the case of the four-ply fabric. Overall, the multi-scale FE model was shown to be capable of predicting the ballistic behavior of multi-ply woven fabric for a range of impact velocities; hence, the multi-scale model was used in the subsequent numerical simulations.

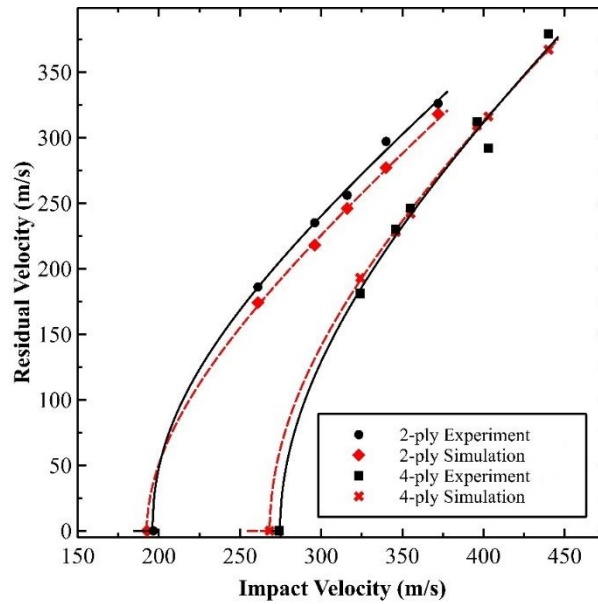


Figure 3.9: Residual velocities of the multi-ply fabrics.

Table 3.2: Ballistic limit velocities and Recht-Ipson parameters.

Fabric	Experiment [18]		Simulation	
	p	V_{bl} (m/s)	p	V_{bl} (m/s)
Two-ply	2.21	196.3	1.93	192.6
Four-ply	2.02	274.7	2.01	268.3

CHAPTER 4: THE EFFECT OF TOTAL NUMBER OF PLYS ON BALLISTIC PERFORMANCE OF MULTI-PLY WOVEN FABRICS

4.1 Problem Description

In this Chapter, the multi-scale FE models were used to evaluate the ballistic performance of four different multi-ply Kevlar woven fabric targets with three, five, seven, and ten plies, as shown in Figure 4.1. Kevlar woven fabrics can be utilized as either a composite such as hard body armors and protective layers of armored vehicle [50], or dry, flexible fabrics such as soft body armors [52]. To construct multi-ply fabric composites, epoxy/resin is used between adjacent plies; however, for multi-ply soft armors, individual plies are placed on top each other without any means of bonding. In this study, the ballistic impact resistance mechanisms of dry, flexible multi-ply woven fabrics were investigated; hence, no bonding was applied and modelled between the plies. To assist the discussion, each ply was assigned a number in ascending order starting from the one on the impact side, i.e., the side closest to the projectile. In the multi-ply FE models as shown in Figure 4.2, all the targets were constrained at four edges and impacted at the center of the target by an FSP, the same bullet as that used in the model validation of multi-ply fabrics. The multi-ply woven fabric targets were assumed dry and their ballistic performance was investigated at ten different impact velocities. Ballistic limit velocities were first determined, followed by a detailed analysis of the mechanism of ballistic impact resistance.

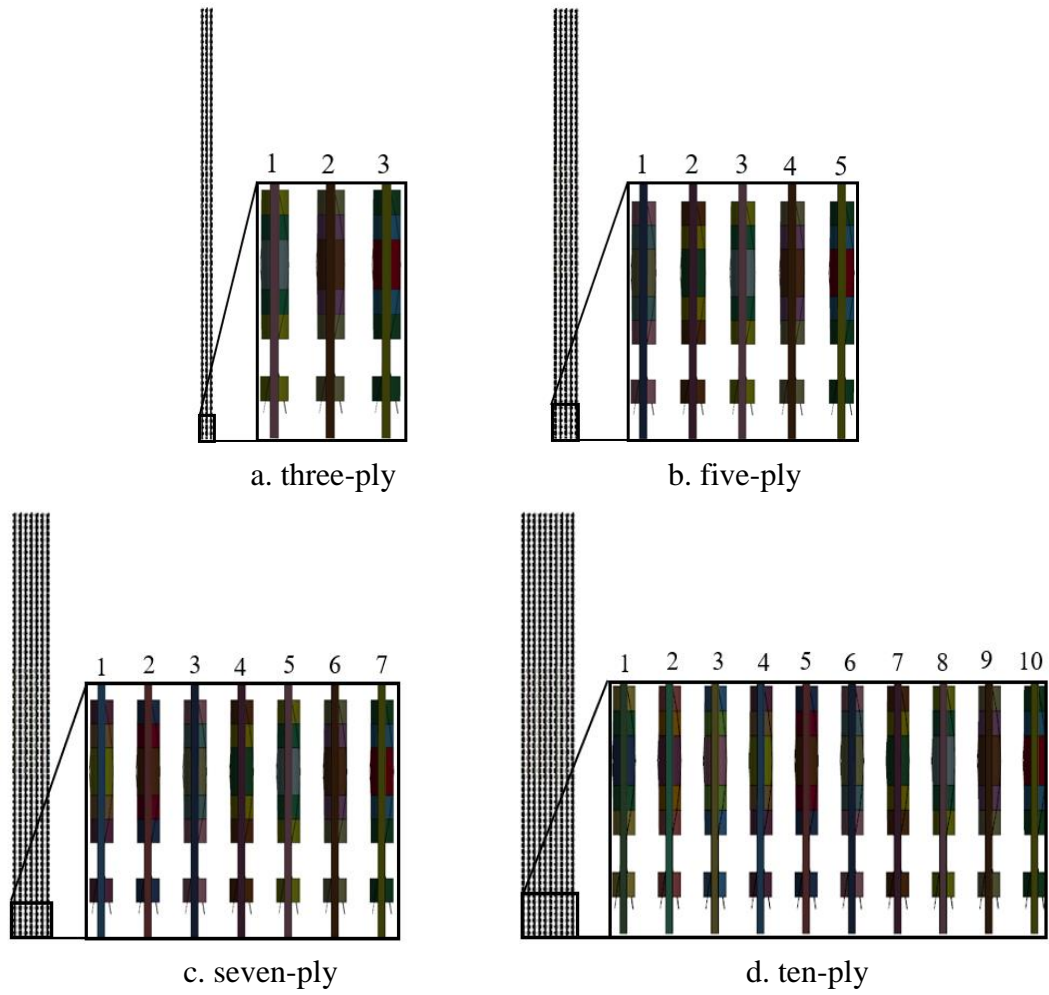


Figure 4.1: Multi-scale FE model of the four multi-ply Kevlar woven fabric targets.

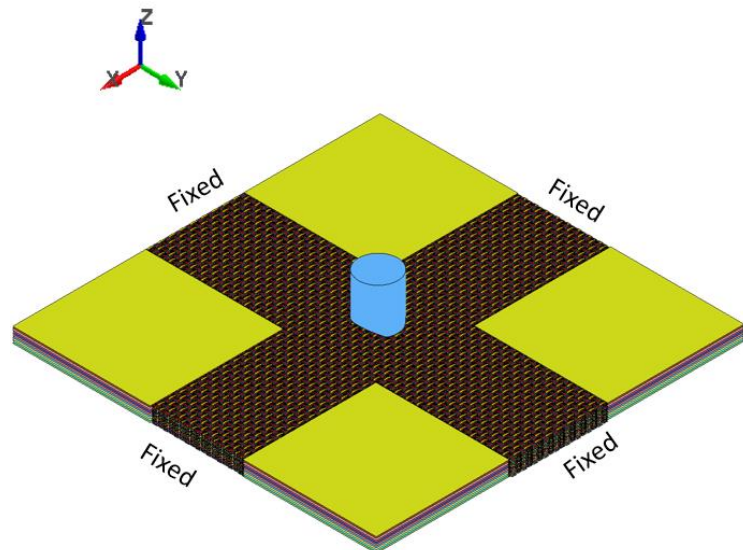
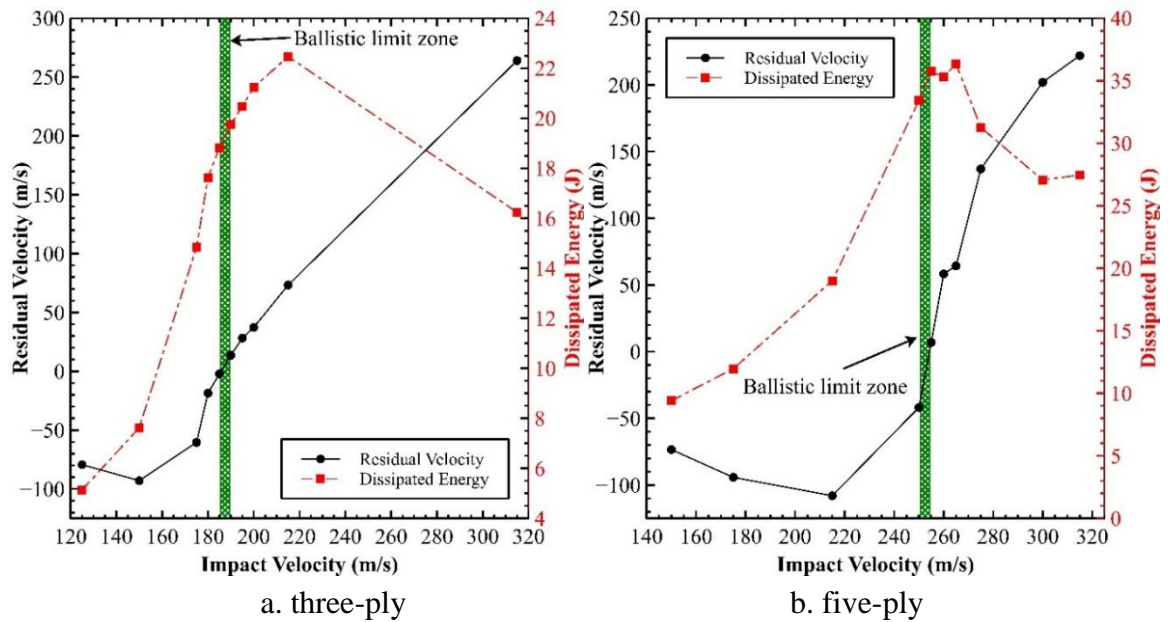


Figure 4.2: FE model of the impact setup.

4.2 Results and Discussion

4.2.1 Ballistic limit velocities

There are three types of ballistic limits in literature, V_0 , V_{50} , and V_{100} . The ballistic limit, V_0 , is defined as the maximum velocity at which the projectile does not make a full penetration. The ballistic limit, V_{50} , is defined as the velocity at which the projectile has a 50% probability of making a full penetration. The ballistic limit, V_{100} , is defined as the minimum velocity at which the projectile makes a full penetration. The ballistic limits of multi-ply fabric targets were obtained from simulation results and are shown on the plots of residual velocities and dissipated energies with respect to the impact velocities (see Figure 4.3). In these plots, the green areas show the “ballistic limit zone” with the left side as the impact velocity for V_0 and the right side as the impact velocity for V_{100} . The V_{50} ballistic limits were calculated as the average of V_0 and V_{100} .



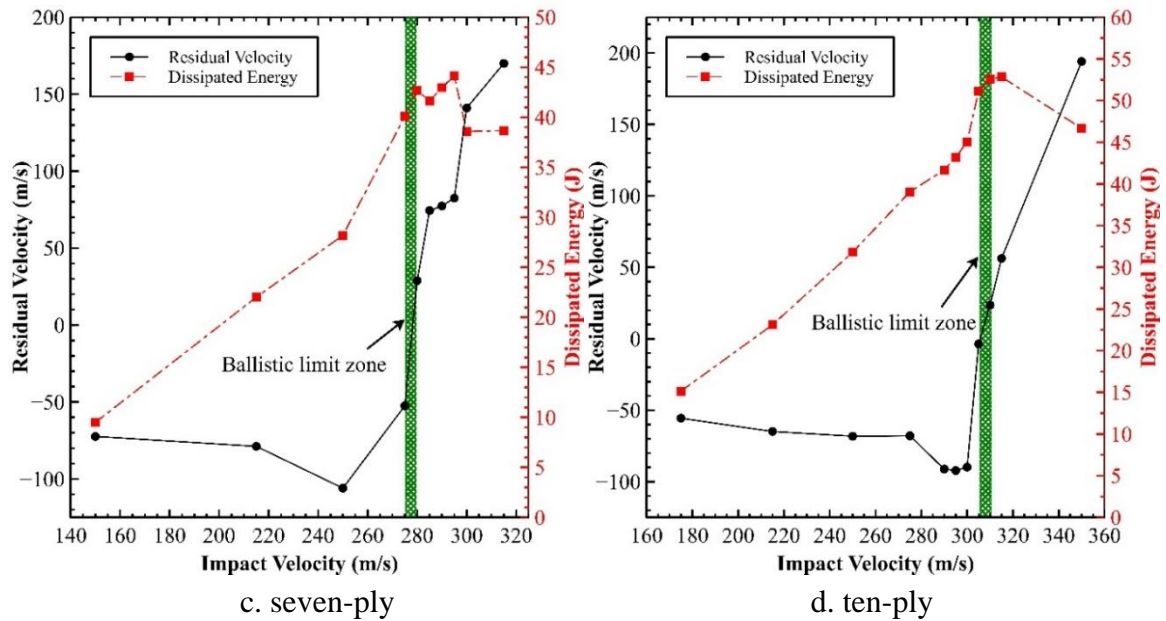


Figure 4.3: Ballistic limit plots of multi-ply Kevlar woven fabrics.

As expected, the ten-ply fabric had the highest ballistic limits while the three-ply fabric had the lowest ones. For all the multi-ply fabric targets, the energy dissipations followed the same trend before reaching the first ballistic limit, V_0 : the kinetic energy was rapidly dissipated until the projectile started to penetrate the fabric. For impact velocities greater than the V_{100} limit, the dissipated energy increased until the impact velocity reached 3 to 15% of the V_{100} limit, after which the dissipated energy declined sharply in the high-velocity region.

Figure 4.4 shows the V_{100} ballistic limits and the ratios of V_{100} to the total number of plies for the four multi-ply fabric targets. The V_{100} -to-ply ratios were used to assess the relative efficiency of a target, i.e., a target with a high ratio was considered more efficient than one with a low ratio. It was found that the V_{100} -to-ply ratio was the highest for the three-ply fabric (63.3), followed by the five-ply fabric (51) and the seven-ply fabric (40),

and was the lowest for the ten-ply fabric (31). This decreasing trend of V_{100} -to-ply ratios indicated that the efficiency of the target was decreased as the total number of plies was increased. This suggested that adding more plies might not bring as much benefit when the number of plies in the fabric reached a certain limit.

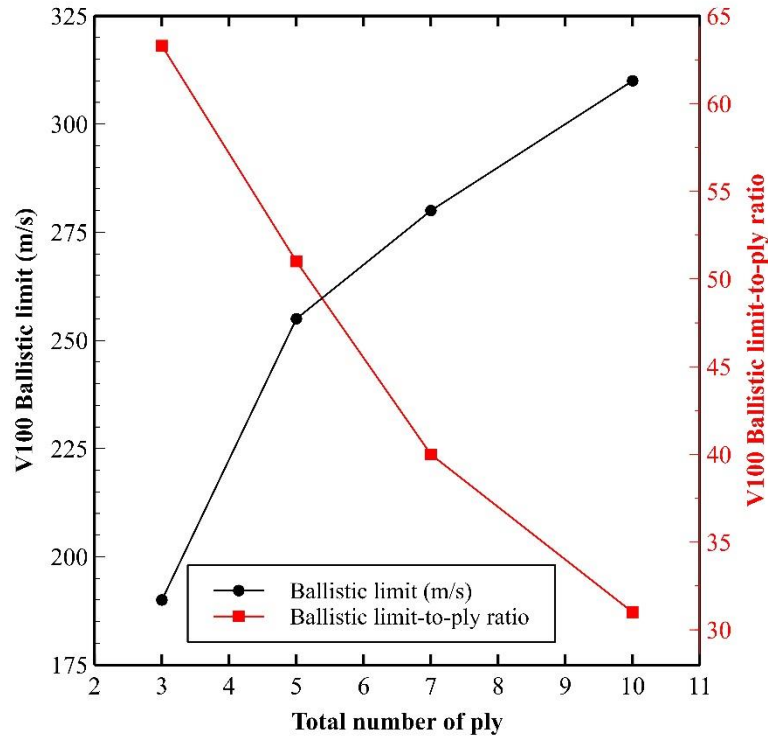


Figure 4.4: Comparison of the V_{100} ballistic limits and efficiencies of the four multi-ply fabrics.

4.2.2 Fabric responses and energy transitions

Fabric responses and energy transitions of the multi-ply fabric targets were studied in detail for impacts at velocities corresponding to the V_{100} ballistic limits so as to observe the full perforations of the multi-ply woven fabric. During an impact, part of the initial kinetic energy of the projectile transformed to different forms and thus the total energy

included: a) the remaining kinetic energy of the projectile; b) the internal energy of projectile due to deformation; c) the kinetic energy of the fabric; d) the internal energy of the fabric; and e) the frictional energy on the projectile-fabric, yarn-yarn, and fiber-fiber interfaces. The FSP was modeled as elastic rather than rigid material to capture the realistic energy transition between the projectile and the fabric. The internal energy of the fabric contained the energy absorbed by the primary yarns due to tensile failures and by the secondary yarns due to elastic deformations. The kinetic energy of the fabric was from the back-face deformations of the fabric, which resumed a “square pyramid” shape. The frictional energy was negligible compared to all other forms of energy during the impact process. For the case chosen in this work, the internal and kinetic energies of the projectile were much less than those of the fabric. Because there was no permanent deformation occurred in the projectile and the residual velocity was close to zero which both lead inconsiderable amounts of the internal and kinetic energy of the projectile, respectively. Therefore, only the internal and kinetic energy of the fabric were presented in detail.

Figures 4.5 to 4.8 show the energy transitions and fabric responses for the four multi-ply woven fabric targets under impacts of a 1.1-gr. FSP at impact velocities corresponding to their respective V_{100} ballistic limits. As seen in Figures 4.5a to 4.8a, all the four multi-ply fabric targets exhibited the same type of response that can be divided into two stages: pre-perforation and full-penetration stages. At the pre-perforation stage, the projectile lost 90-95% of its kinetic energy while the fabric reached the largest transverse displacement. It was also observed that targets with more plies took less time to reach the maximum reduction of kinetic energy in this stage than those with fewer plies. For example, the FSP lost approximately 95% of its kinetic energy within 40 μ s on the ten-

ply fabric target, while it took 70 μ s on the three-ply fabric target. During the full-penetration stage, only 2 to 3% of the initial kinetic energy of the FSP was absorbed by the fabric. Since the yarns of the last plies were already in high tensile stresses, they failed quickly upon reaching the failure stress value, resulting in full penetrations. It was also observed that the projectile rotated more in the later stage than in the early stage of the impact. After losing contact with the fabric, the kinetic energy of the FSP became negligible.

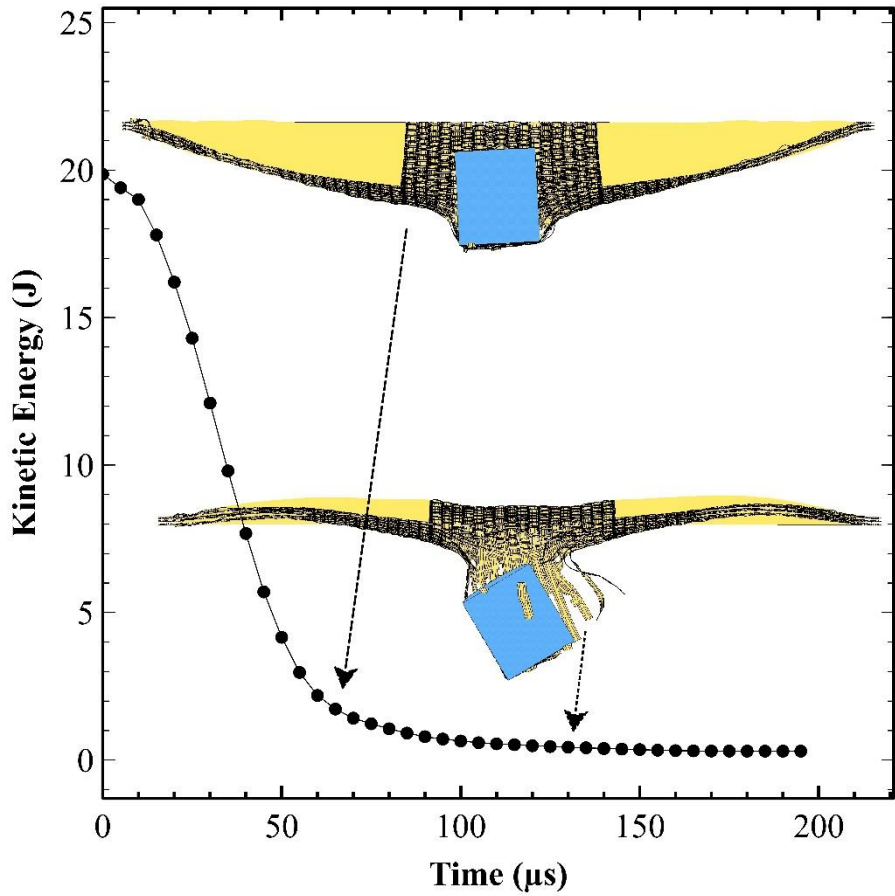
Although the overall responses of the multi-ply fabric targets were similar to each other, the individual plies in each of the four targets behaved differently and had their own distinguishing responses. For ease of discussion, the plies of the multi-ply fabric targets were assigned names using a ply's location as well as the target it belonged to. For example, the second ply of the five-ply fabric target was named as "2P5T", the sixth ply of the seven-ply target was named as "6P7T", and the tenth ply of the ten-ply target was named as "10P10T".

Among all the first plies in the four targets, the 1P3T was found to have the largest internal energy, and the amount of internal energy of the first ply decreased as the increase of the total number of plies. The reason behind this observation was that the first ply supported by more back plies had higher bending stiffness and thus smaller transverse deflections than one backed by fewer plies. Consequently, the first ply backed by more plies broke sooner than one backed by fewer plies, resulting in less energy dissipation to the secondary yarns.

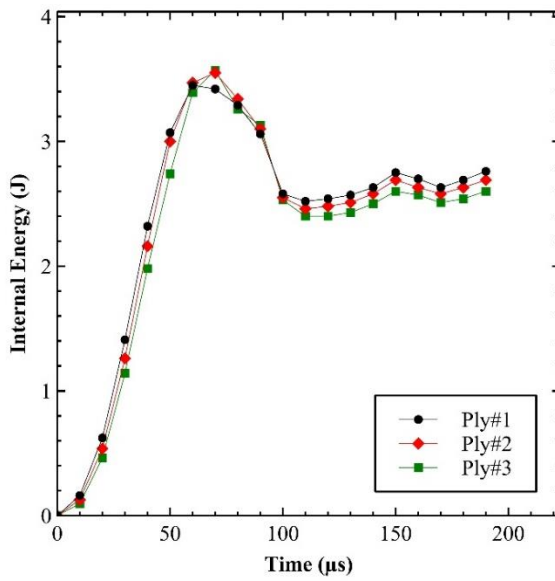
The three- and five-ply fabrics had similar trend in their internal energy absorptions as shown in Figures 4.5b to 4.8b: the magnitudes of the plies within the same multi-ply

fabric were very close to each other. Two main observations were obtained from the internal energy of the seven- and ten-ply fabrics as shown in Figures 4.6b and 4.7b. First, although the magnitudes of the internal energy of the individual plies of the seven- and ten-ply fabrics were different, they had similar trends in their internal energies, i.e., plies with high numbers having larger internal energy than those with a low number. Second, the internal energies of the last two plies of both targets (i.e., 6P7T-7P7T and 9P10T-10P10T) were very close to each other. These two findings indicated that perforations in the plies generally occurred in the sequence from lower ply number to higher ply number. When the projectile reached the last two plies, it stretched these two plies to a point where the last ply broke immediately following the breakage of the one before the second-to-last ply. Additionally, the first three plies of the ten-ply fabric had similar amount of internal energy, which indicated that there was no considerable difference in the time of perforation between these plies. Figures 4.5c to 4.8c show the kinetic energies of each individual plies of the fabrics. The trends in the KE graphs of the five-, seven- and ten- ply were similar to their internal energy graphs; hence, the same conclusions extracted previously hold true for their kinetic energy graphs as well.

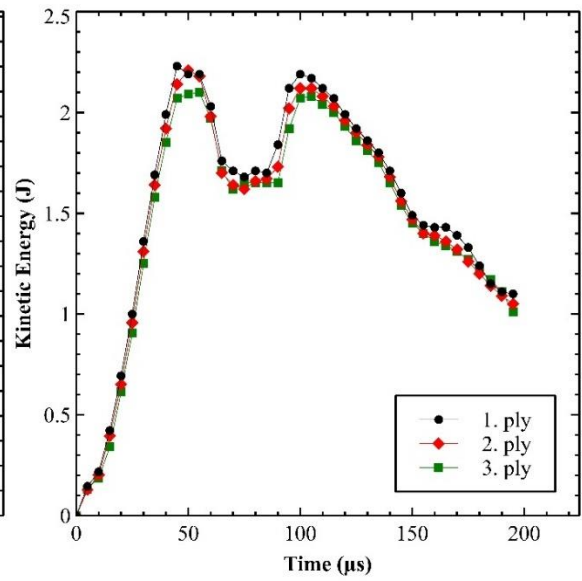
Overall, for the chosen case, the kinetic energy of the projectile mainly transformed to the internal and kinetic energies of the fabrics. The total magnitude of the internal energy of the fabrics was larger than that of the kinetic energy regardless of total ply number. However, the magnitude and trend of energy on each individual ply varied among fabrics with different number of plies.



a.

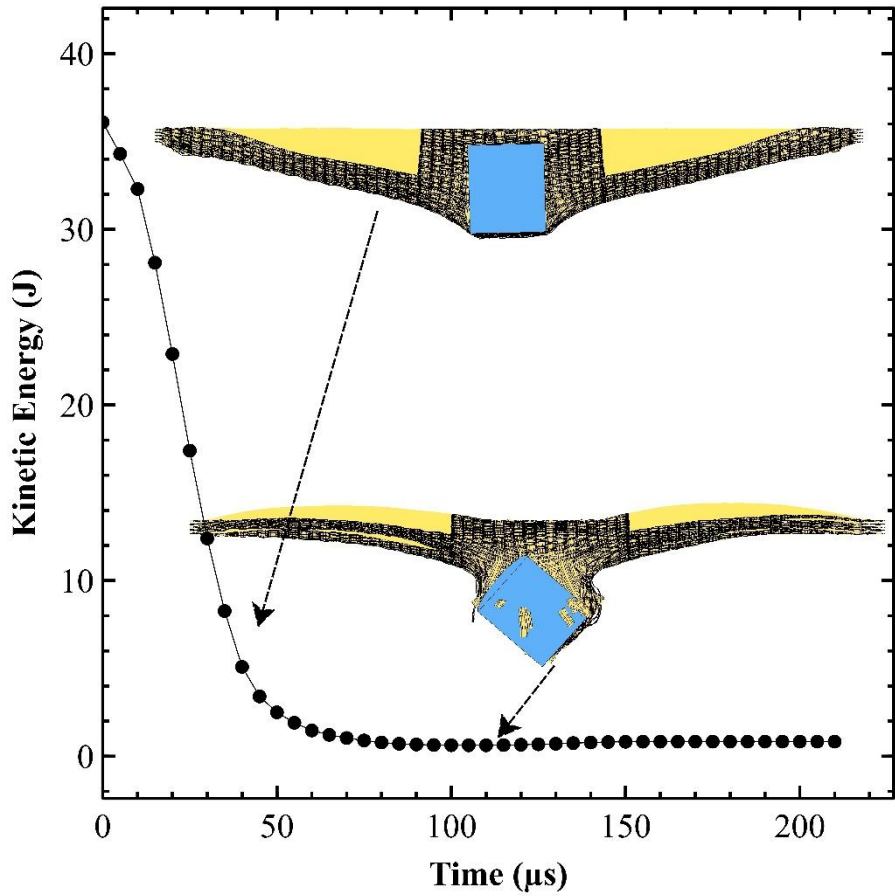


b.

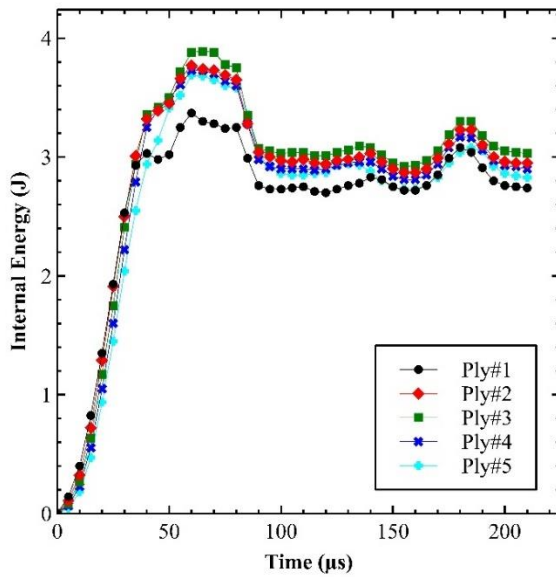


c.

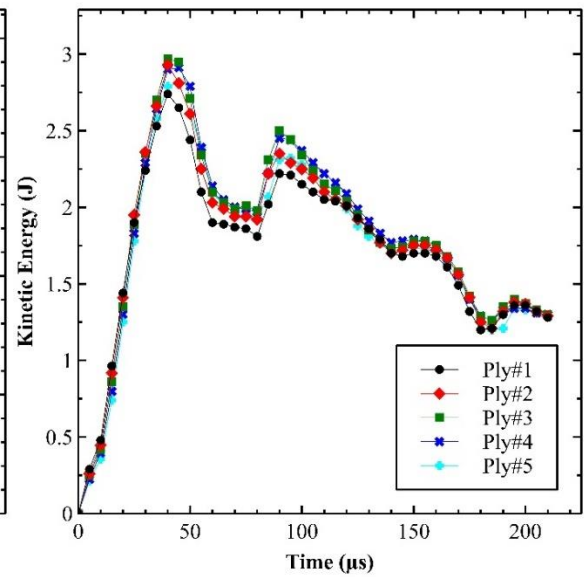
Figure 4.5: Fabric response and energy transitions of the three-ply fabric at V_{100} .
a. kinetic energy -projectile; b. internal energy - fabric; and c. kinetic energy – fabric.



a.



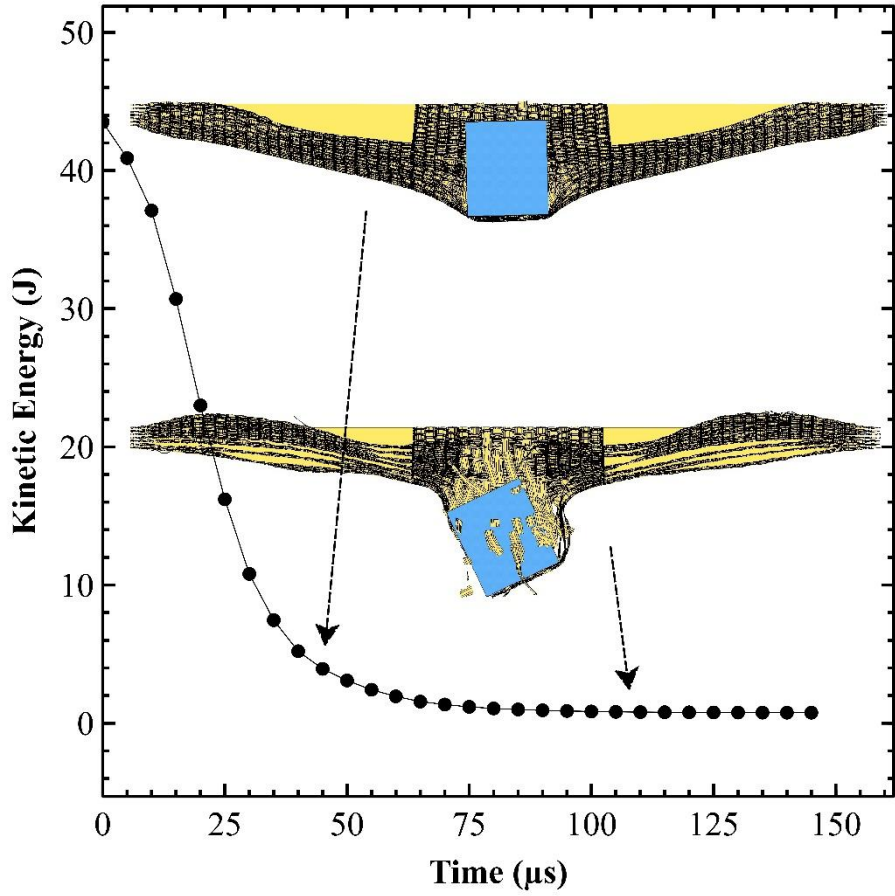
b.



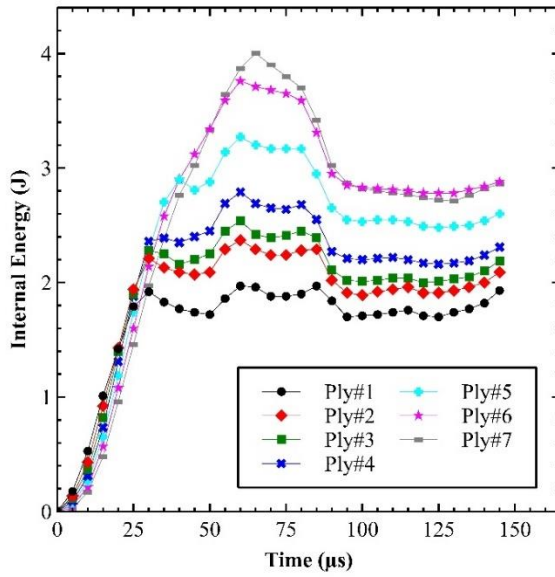
c.

Figure 4.6: Fabric response and energy transitions of the five-ply fabric at V_{100} .

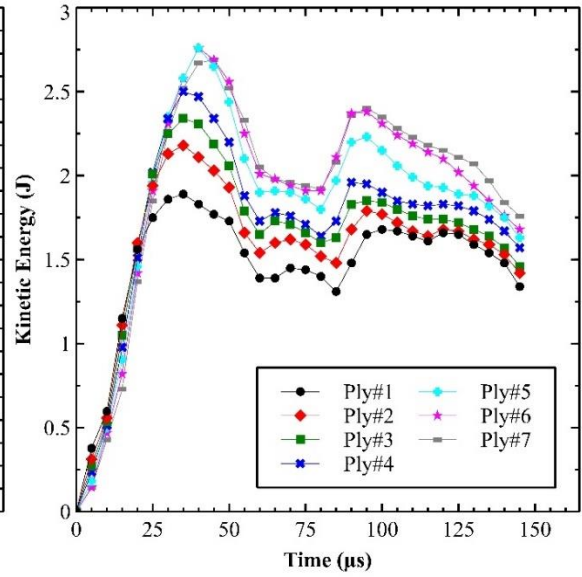
a. kinetic energy -projectile; b. internal energy - fabric; and c. kinetic energy – fabric.



a.

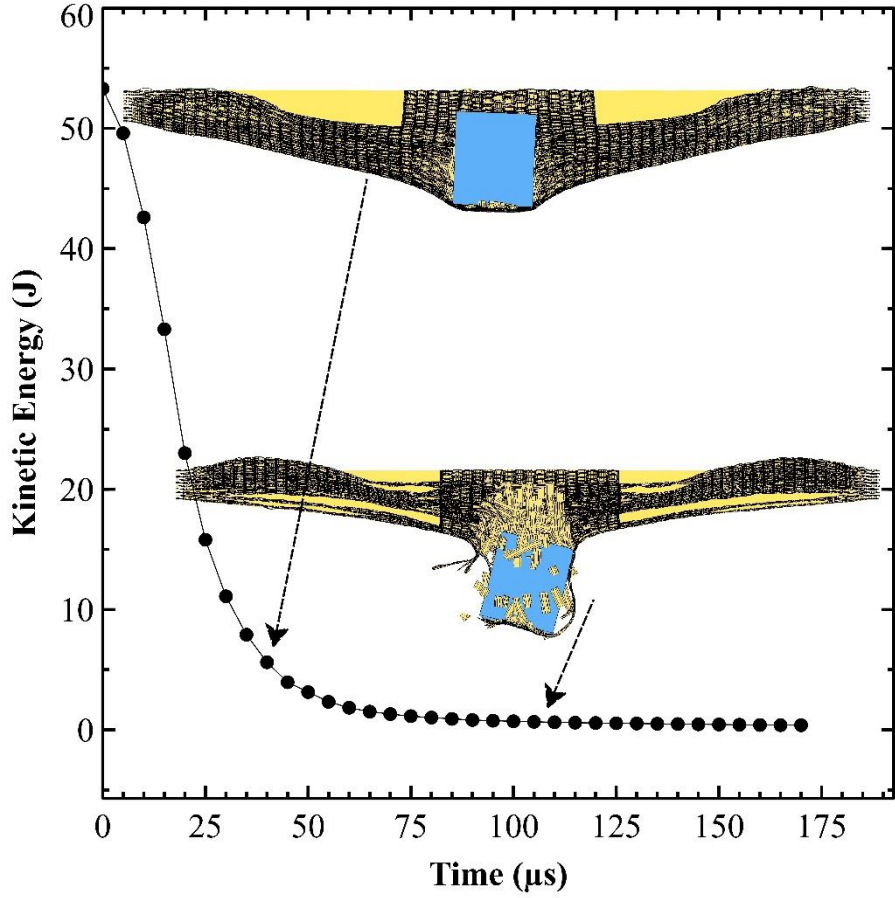


b.

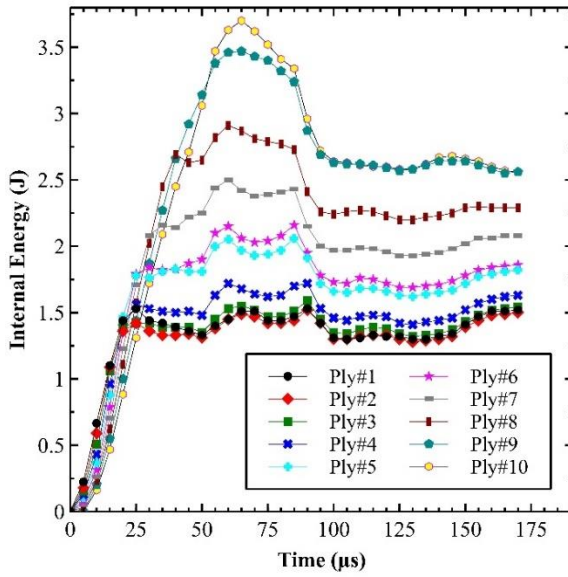


c.

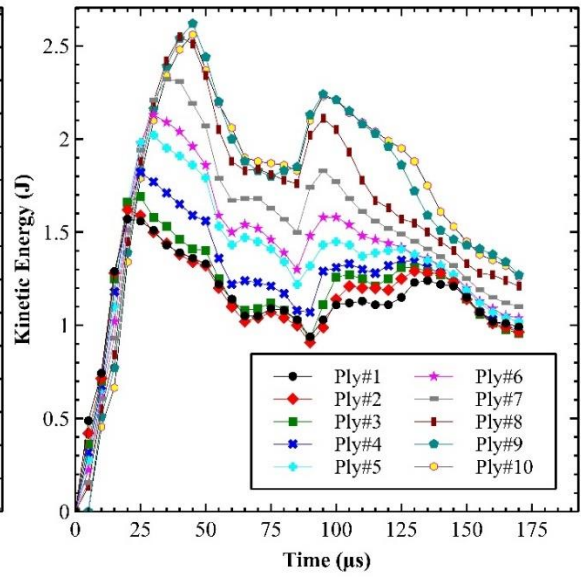
Figure 4.7: Fabric response and energy transitions of the seven-ply fabric at V_{100} . a. kinetic energy - projectile; b. internal energy - fabric; and c. kinetic energy - fabric.



a.



b.



c.

Figure 4.8: Fabric response and energy transitions of the ten-ply fabric at V_{100} .

a. kinetic energy - projectile; b. internal energy - fabric; and c. kinetic energy - fabric.

4.2.3 Out-of-plane displacements

Figure 4.9 shows the comparison of the dynamic out-of-plane displacements of the four multi-ply fabric targets. In this comparison, the dynamic out-of-plane displacement of the last ply was considered as the representative displacement of the entire multi-ply fabric target. For a consistent comparison, the out-of-plane displacements were compared till the instant when the yarns on the last plies started to break. Therefore, the last instant of time of each target in 4.9 represented the instant when the first yarn in the last ply of the fabric broke. In other words, the final instant of time in Figure 4.9 did not represent the time when the full penetrations occurred. Figure 4.9 also illustrates the rate of dynamic deflection of the four targets, the three-ply fabric had the smallest rate of dynamic deflection, which indicated that the deceleration of the projectile was smaller for the three-ply fabric than those of other fabrics (i.e., five-, seven-, and ten-ply fabrics).

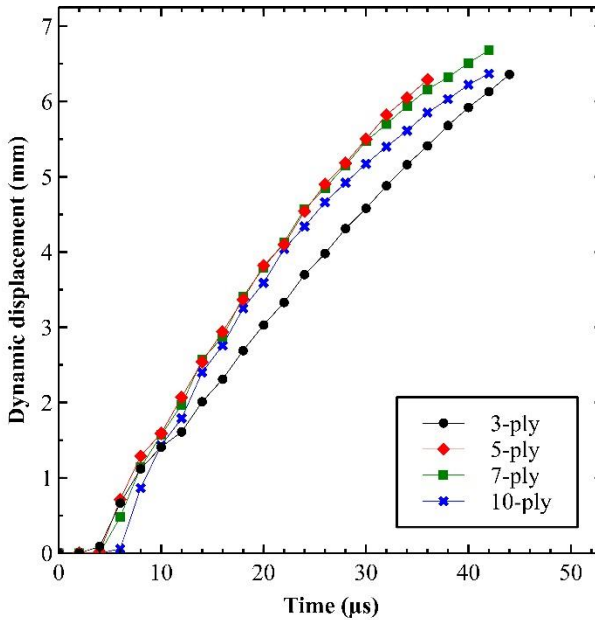
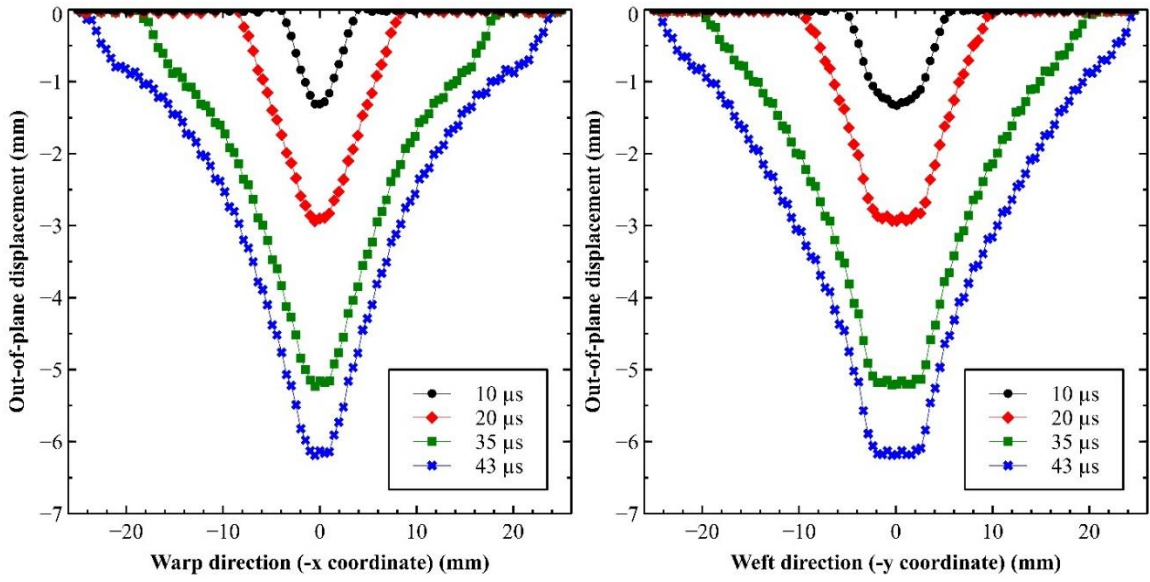
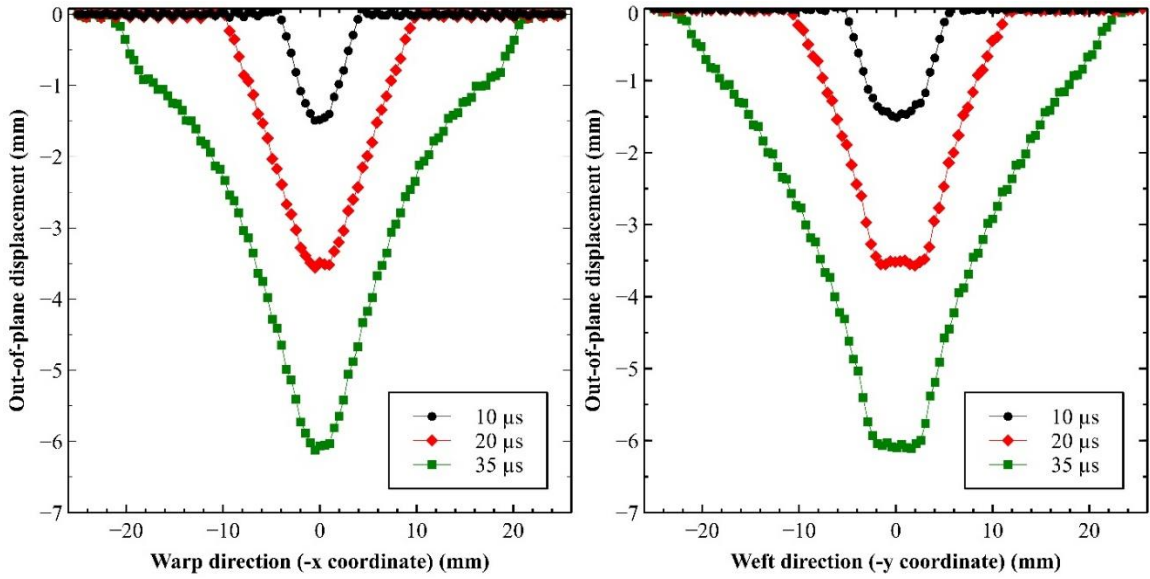


Figure 4.9: Dynamic out-of-plane displacements of the four multi-ply fabrics.

Figure 4.10 shows the sequential cross-sectional displacement profiles at the impact point of the warp and weft yarns in the last ply of four multi-ply fabric targets. The furthest displacement profiles in Figure 4.10 corresponded to the respective maximum displacements of the four multi-ply fabric targets at their final instants in Figure 4.9. The displacement profiles showed the wave propagation of the primary warp and weft yarns in the fabric at the impact location. Figure 4.10 showed that back-face deformation phenomenon (i.e., shape of square pyramid) was also captured for multi-ply fabrics. It was observed from all the multi-ply fabrics that wave propagations occurred faster in the weft direction than those in the warp direction, resulting in dissimilar warp and weft displacement profiles. As can be seen in Figure 3.8, the FSP had two chamfered edges on the impact face that made the flat region a near-elliptical shape. In the numerical model, the long axis of the flat region of the FSP face was oriented along the weft (y -) direction and perpendicular to the warp (x -) direction. Therefore, the initial interaction between the FSP and the target occurred on the yarns in the weft direction, followed by the interaction between the chamfered edges and the warp yarns. The aforementioned initial orientation of the FSP resulted in the variation between the out-of-plane displacements of the warp and weft yarns. This finding showed that a roll angle on the impactor could affect the ballistic response of the fabric.

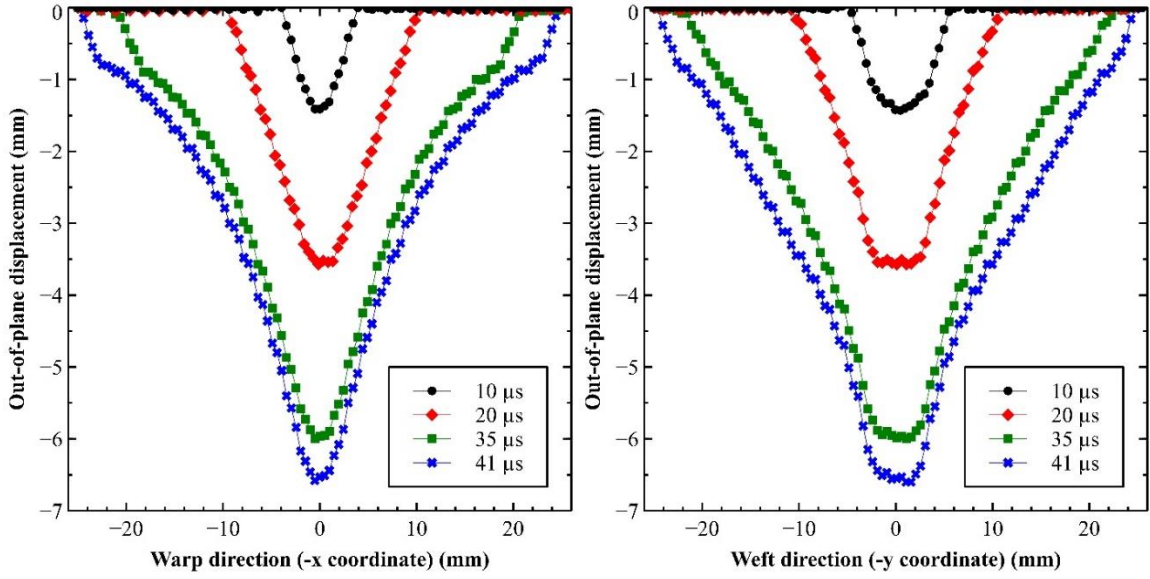


a. three-ply

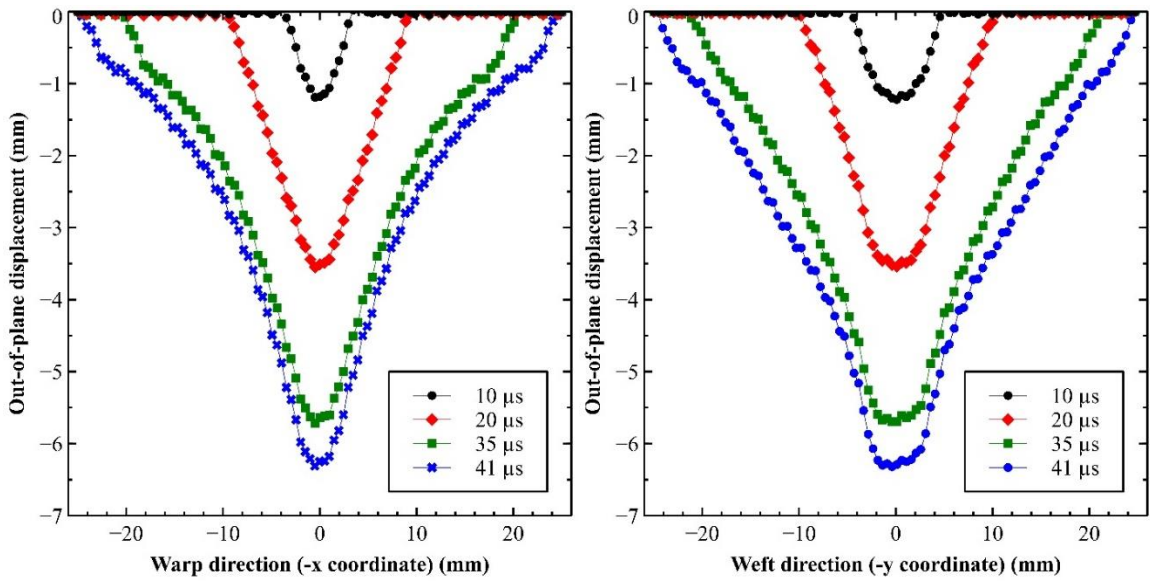


b. five-ply

Figure cont'd



c. seven-ply



d. ten-ply

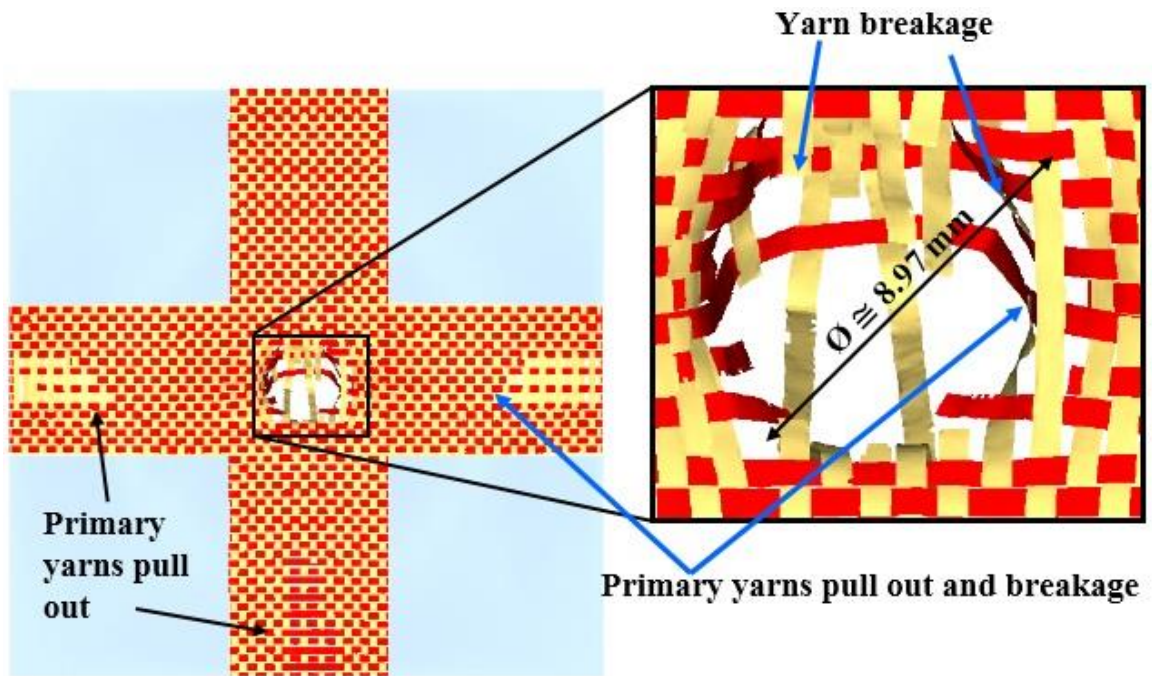
Figure 4.10: Sequential cross-sectional displacement profiles of the warp (left) and weft directions (right) in the impact point.

4.2.4 Damage patterns

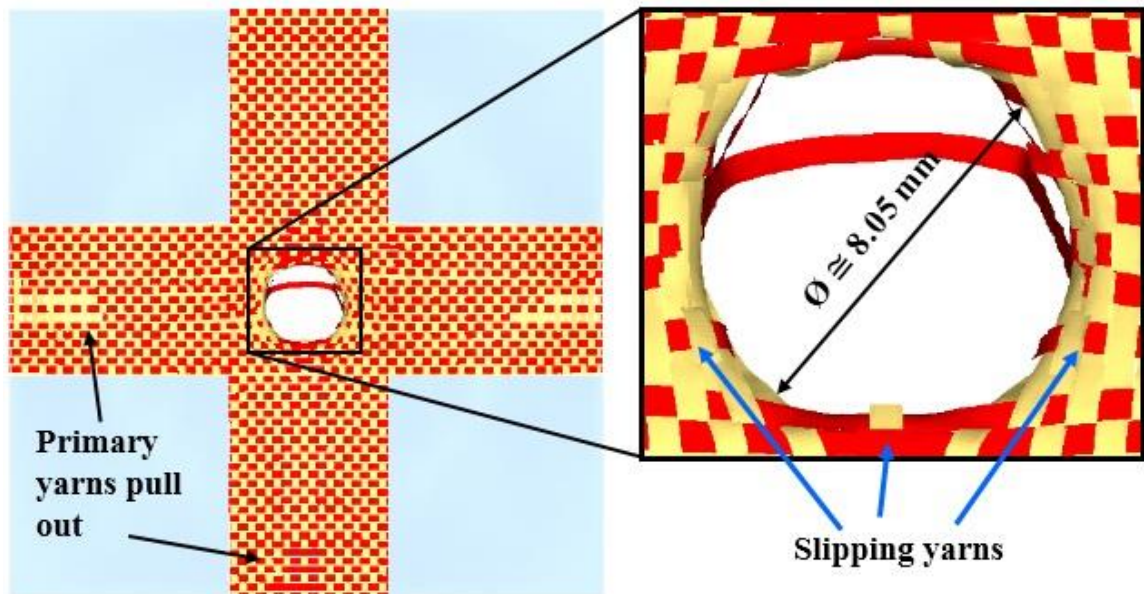
In this section, the damage severity of the four multi-ply fabric targets is examined and compared using the post-impact deformations on the first and last plies as shown in Figures 4.11 to 4.14. Comparing the damage on the first plies of the four targets, it was found that the 1P3T layer (i.e., first ply of the three-ply fabric target) had the largest damaged region among all the first plies of the four multi-ply fabric targets, and that the severity of damage was decreased with the increase of the total number of plies in the target. For the 1P3T and 1P5T layers shown in Figures 4.11a and 4.12a, primary yarn slippage and breakage occurred on both warp and weft yarns along the edges of the fabric in the impact area, forming a permanent, circular shaped penetration hole. This circular penetration pattern on the first ply in the impact area lost its form in the cases of 1P7T and 1P10T layers, as shown in Figures 4.13a and 4.14a. The 1P10T layer had only localized damage that was mainly caused by the primary yarn failures in the impact area. In short, the dominant failure mechanism of the first plies of the three- and five-ply fabric targets was found to be primary yarn breakage in the impact area along with yarn breakage and yarn pull-out in the fixed edges. Whereas for the seven- and ten-ply fabrics, the perforations of the first plies was only caused by localized primary yarn breakage in the impact areas.

The damage patterns of the last plies were found to be similar to each other among all the multi-ply fabric targets. In addition to the primary yarn breakage, yarn slippage was also found on the last plies of all targets. During impacts by the projectile, the middle primary yarns in the impact areas experienced the largest tensile stresses, and the tensile stresses were decreased in primary yarns at increased distances from the center of the impact center. While the primary yarns near the center of impact (i.e., middle primary

yarns) contacted the impacting face of the projectile, the surrounding primary yarns only contacted the side of the projectile. This interaction caused the surrounding primary yarns to slip towards to the fixed edges after penetration occurred. Regardless of the total number of plies, the permanent deformations in the impact area of the last plies resumed a circular pattern, with only the size of the deformed areas affected by the total number of plies in the target. As the total number of plies increased, the size of the damaged region decreased. It was also observed that yarn breakage and yarn pull-out near the fixed edges were not affected by the total number of plies of the target. Overall, for the three- and five-ply fabric targets, there was no considerable difference between the failure mechanisms of the first and the last plies. For the seven- and ten-ply fabric targets, however, significant difference (i.e., type of failure and magnitude of the damages) was found between the failure mechanisms of their first and last plies.



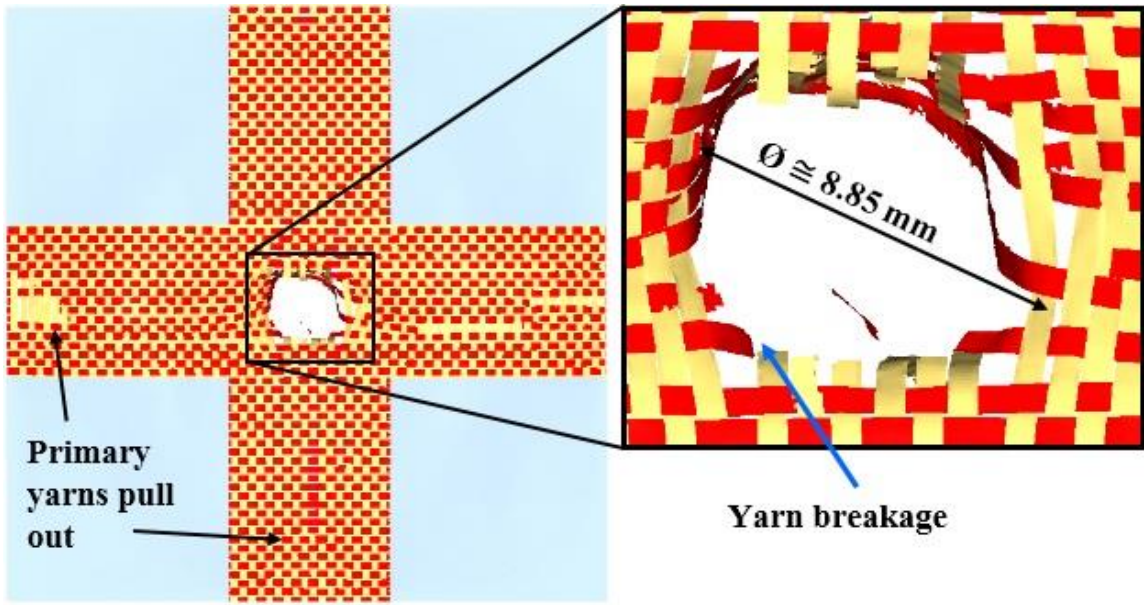
(a)



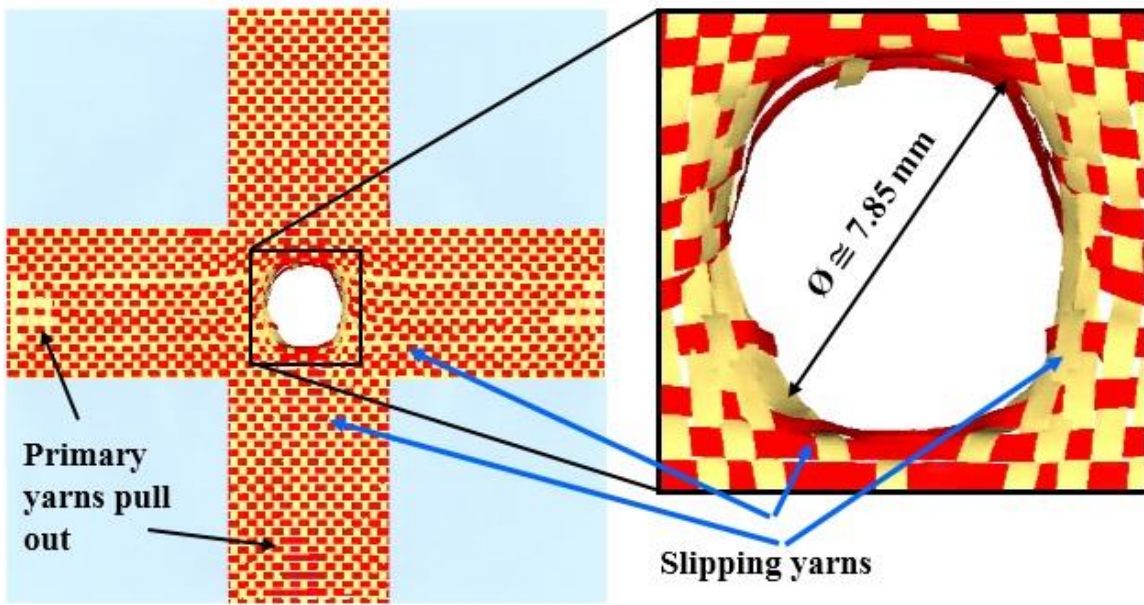
(b)

Figure 4.11: Post-impact damage patterns of the first and the last ply of the three-ply fabric.

a. the first ply and b. the third ply.

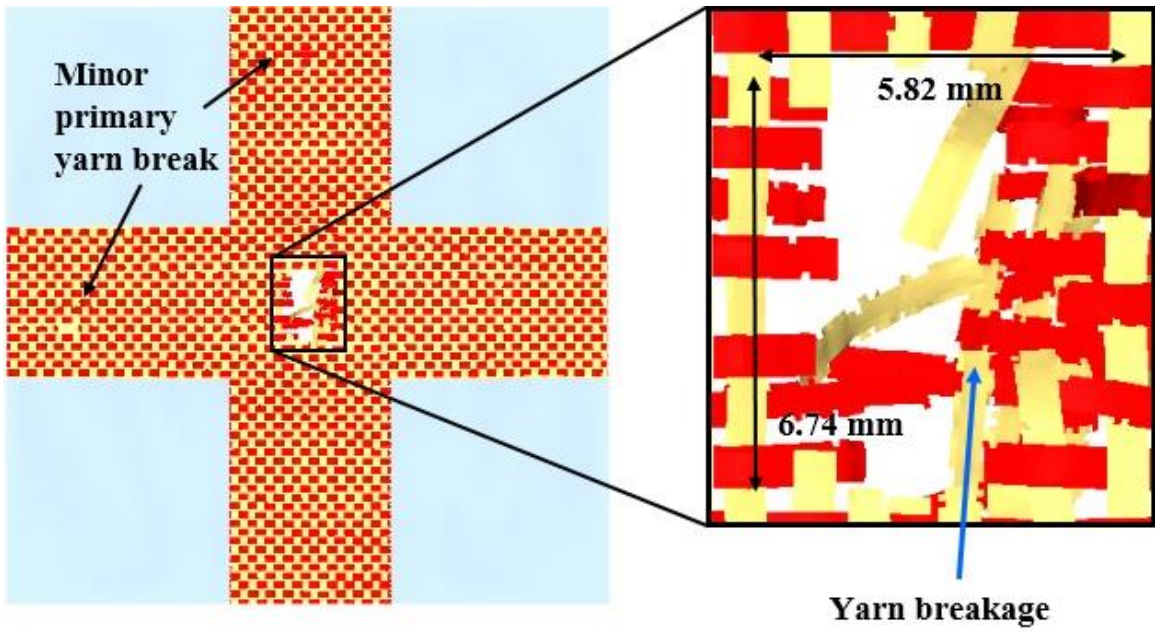


(a)

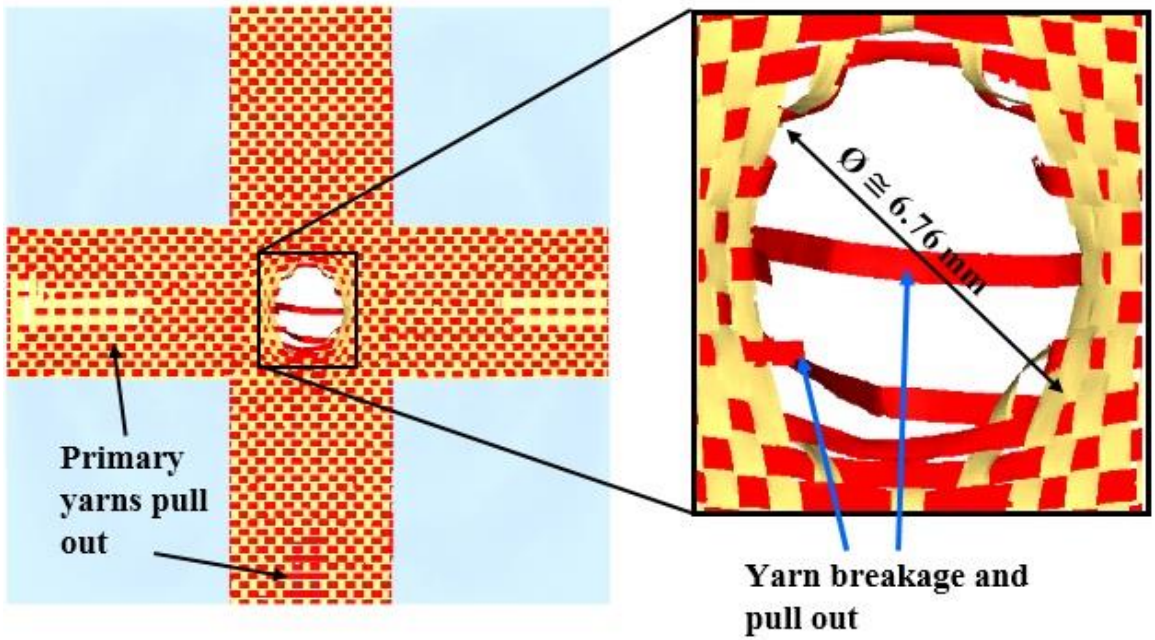


(b)

Figure 4.12: Post-impact damage patterns of the first and the last ply of the five-ply fabric.
 a. the first ply and b. the fifth ply.

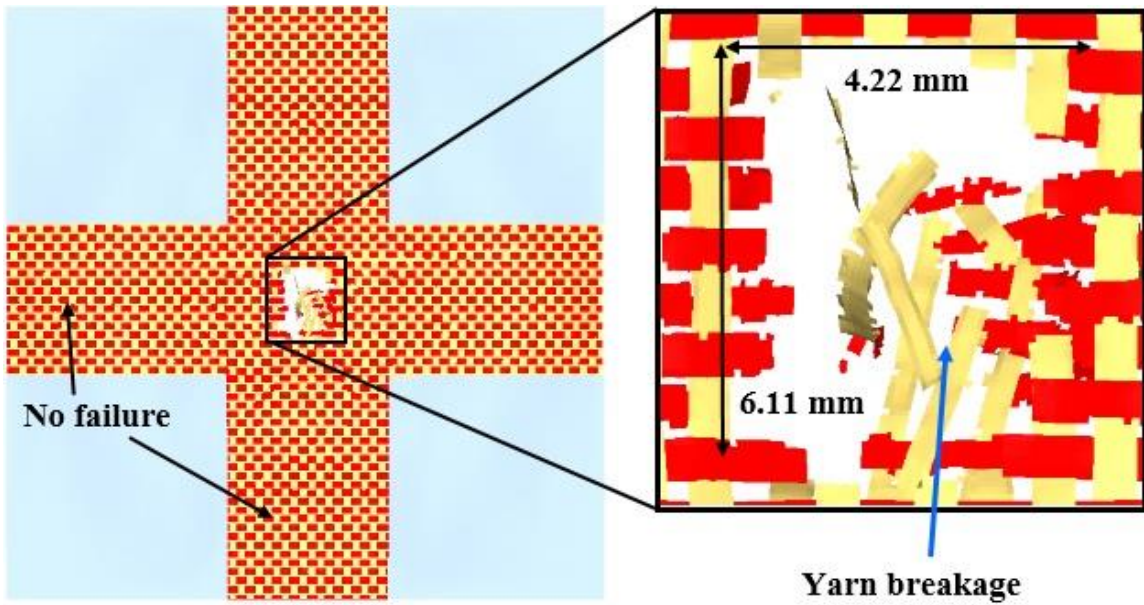


(a)

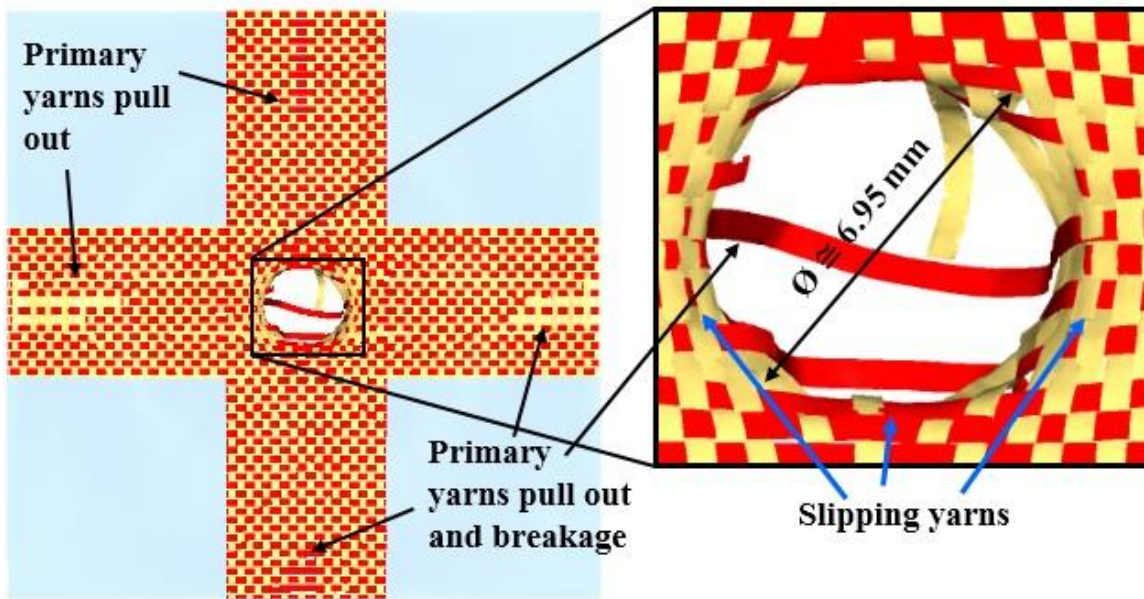


(b)

Figure 4.13: Post-impact damage patterns of the first and the last ply of the seven-ply fabric.
 a. the first ply and b. the seventh ply.



(a)



(b)

Figure 4.14: Post-impact damage patterns of the first and the last ply of the ten-ply fabric.

a. the first ply and b. the tenth ply.

Figure 4.15 illustrates a schematic classification of damage patterns of the last plies of multi-ply fabric targets based on the research findings. Five distinct regions were found on the fabric targets and numbered according to the damage severity, with R1 having the most severe damage and R5 having the least severe damage. The yarns within each region were shown in different colors for ease of viewing. The R1 region, i.e., the impact area, had the largest damage due to yarn breakage in all the four targets. The R2 region, which was located near the middle of the four edges and shown in green, was the second in damage severity with yarn pull-out as the dominant failure accompanied by yarn breakage. The damage in the R3 region (shown in blue) was dominated by yarn slippage. The damage in the R4 region was shown as local yarn breakage and yarn slippage as a continuation of the damage from R2 and R3, respectively. Lastly, yarns in the R5 region, which were referred to as secondary yarns, were the least affected and underwent only elastic deformations. It should be noted that these schematic damage patterns only apply to the last plies of the four multi-ply fabric targets under the impact of a 1.1-gr FSP at V_{100} ballistic limit.

The failure time of each ply is necessary to fully understand the ballistic behavior of multi-ply fabrics. As seen in Figure 4.16, the perforation times of the last two plies of all multi-ply fabrics are very close to each other. For three-ply fabric, there is no considerable time difference between the perforations of each ply; however, in the five-ply fabric, the 1P5T perforates approximately $5 \mu\text{s}$ sooner than the remaining four plies. The seven-ply fabric had four distinct penetration time frames, while the ten-ply fabric had five-time frames. The failure time increases as the number of plies increase as shown in Figure 4.16c-d.

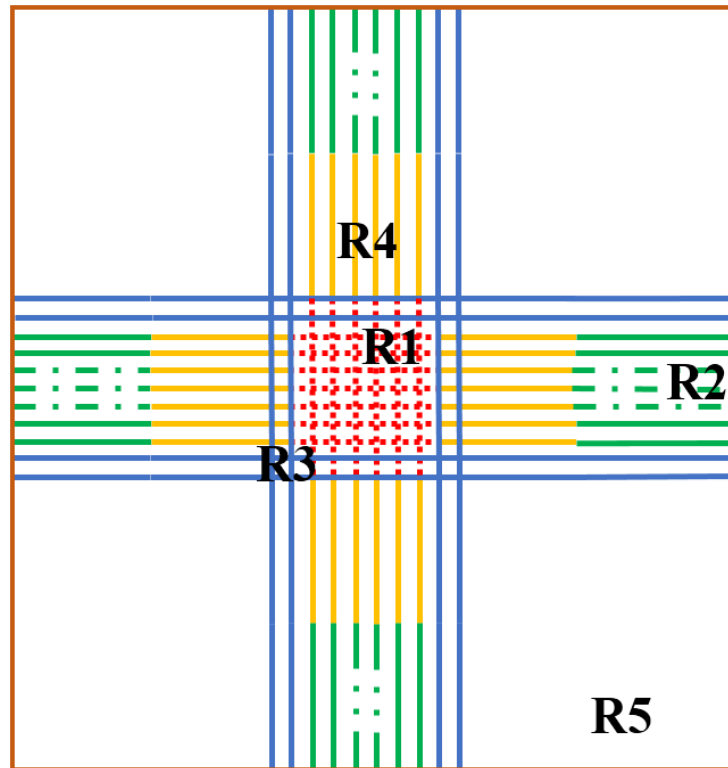


Figure 4.15: Schematic classification of damage patterns of the last plies of multi-ply fabrics under V_{100} impacts.

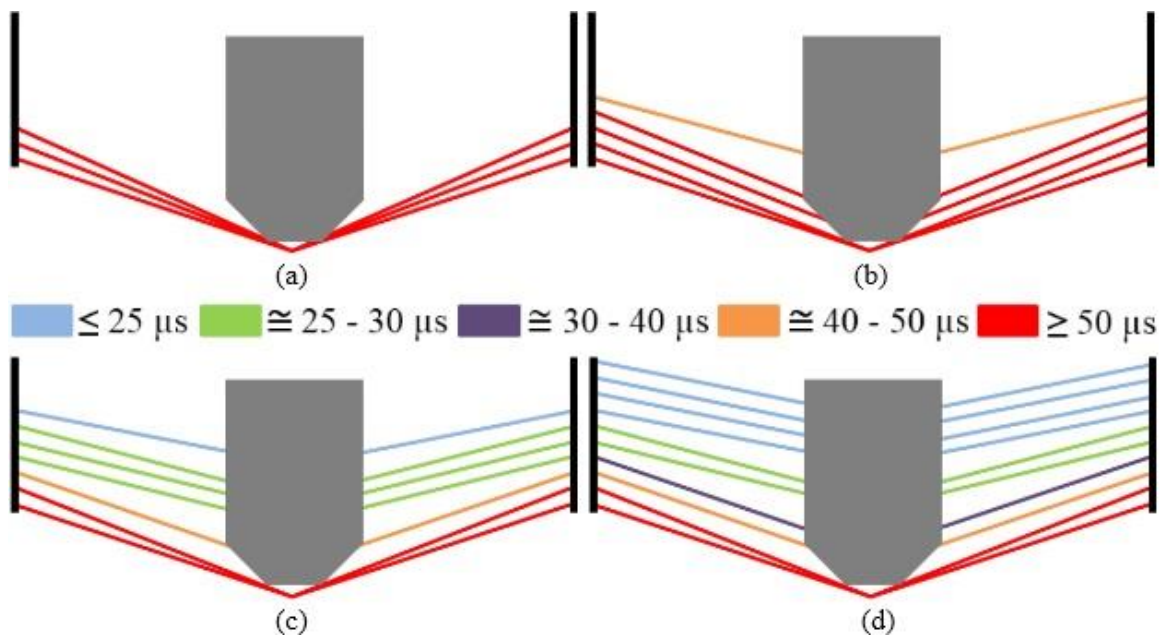


Figure 4.16: Failure time representation of the multiply fabrics.

a. 3-ply; b. 5-ply; c. 7-ply; and d. ten-ply.

CHAPTER 5: THE EFFECT OF PROJECTILE CHARACTERISTICS ON BALLISTIC PERFORMANCE OF MULTI-PLY WOVEN FABRICS

5.1 Problem Description

In this Chapter, the effect of a projectile's size and shape along with impact velocities on the ballistic performance of multi-ply woven fabrics is presented. A ten-ply Kevlar woven fabric was used in the simulations of ballistic impacts by six different projectiles. It was found in the work presented in Chapter 4 that, the overall ballistic behavior of multi-ply woven fabrics resembled each other for those with seven or more plies. In other words, the ballistic resistance mechanism (e.g., energy transitions, damage patterns, etc.) of the seven-ply fabric was similar to the ten-ply fabric; hence, the findings from ten-ply fabric could be applied to fabrics with more than ten plies. In addition, the ten-ply fabric was selected as the target because soft body armor equipment is made of at least ten-ply fabrics [71].

The projectiles used in this Chapter had two different diameters and three different nose shapes. Since the .22 caliber (e.g., .22 LR and .223 rifle bullet) and the .30 caliber (e.g., the bullet used in AK-47 rifle) are the most commonly used projectile calibers, the projectiles were created in .22 cal. (i.e., 5.58 mm) and .30 cal. (i.e., 7.62 mm) sizes. The projectiles had three different nose shapes, flat, pointed and spherical named as right circular cylinder (RCC), conical and spherical, respectively. For each nose shape, two projectiles were created in .22 cal. and .30 cal., resulting in a total of six different projectiles. It should be noted that the edges of the RCC projectiles were rounded by a

small fillet for the sole purpose of promoting tensile failure only, since the yarn's transverse shear strength was unavailable [44]. Moreover, to eliminate the effect of the nose angle, both the .22 and .30 cal. conical projectiles were created with the same cone angle (i.e., 45°). To have consistent initial kinetic energy of the projectile, all six projectiles were assigned the same mass, 1.1 gr., which was the mass of the fragment simulation projectile (FSP) required by the U.S. Army testing standard. The density was adjusted for each projectile based on its volume to reach a mass of 1.1 gr. The materials of the projectiles were assumed to be steel with a Young's Modulus of 210 GPa and Poisson's ratio of 0.3. The projectiles were assumed to be elastic, and 3D solid elements were used to create the FE models of the projectiles shown in Figure 5.1.

The ten-ply woven fabric target, boundary conditions, and impact conditions were the same as those used in Chapter 4: the ten-ply fabric was constrained along the four edges and impacted by the projectiles at the center of the target. For impacts by the conical projectiles, the projectiles were set to initially hit the gap between two adjacent yarns at the center of the target to avoid numerical difficulties caused by the sharp tips of the projectiles. To assist the discussion, each ply was assigned a number in ascending order starting from the one at the impact side, i.e., the ply closest to the projectiles. The ballistic limits were first determined for the impact by each projectile and the impact mechanism of the ten-ply woven fabric under the impacts of six projectiles were analyzed in detail.

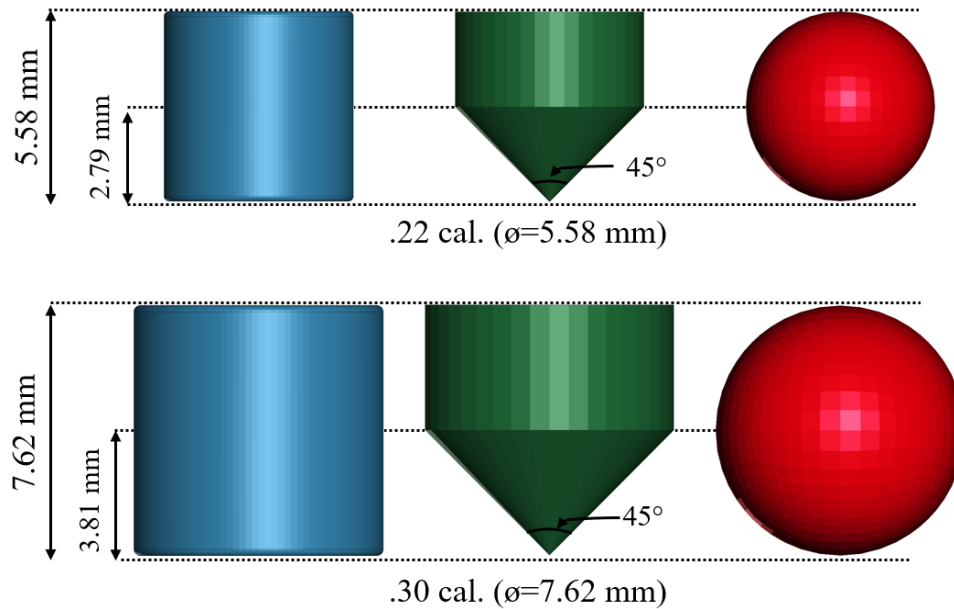


Figure 5.1: FE models of the six projectiles: RCC, conical and spherical (from left to right).

5.2 Results and Discussion

5.2.1 Ballistic limit velocities

Numerical simulations were conducted on impacts of the ten-ply woven fabric target by the six projectiles at different impact velocities ranging from 150 to 550 m/s and the residual velocities of the projectiles were recorded from the simulations. The Recht-Ipson model, which was presented and discussed in Chapter 3, was utilized to curve fit the impact-residual velocity data points, as shown in Figure 5.2. The ballistic limit, V_{bl} , was defined as the smallest impact velocity at which the projectile made a full penetration (or perforation) on the target.

Figure 5.3 shows a comparison of the ballistic limits for the six projectiles, with the target having the largest ballistic limit, i.e., 378 m/s, when impacted by the .30 cal. RCC projectile. The smallest ballistic limit, i.e., 174 m/s, occurred when the target was impacted by the .22 cal. conical projectile. The second largest and smallest ballistic limits occurred

under impacts of the .22 cal. RCC and .30 cal. conical projectiles, respectively. It can be seen from the comparison that it would require the largest impact velocity (or initial kinetic energies) for the RCC projectiles (i.e., with flat noses) to perforate the ten-ply Kevlar woven fabric, while it would require the smallest impact velocities (or initial kinetic energies) for the conical projectiles (i.e., with pointed tips) to perforate the same target.

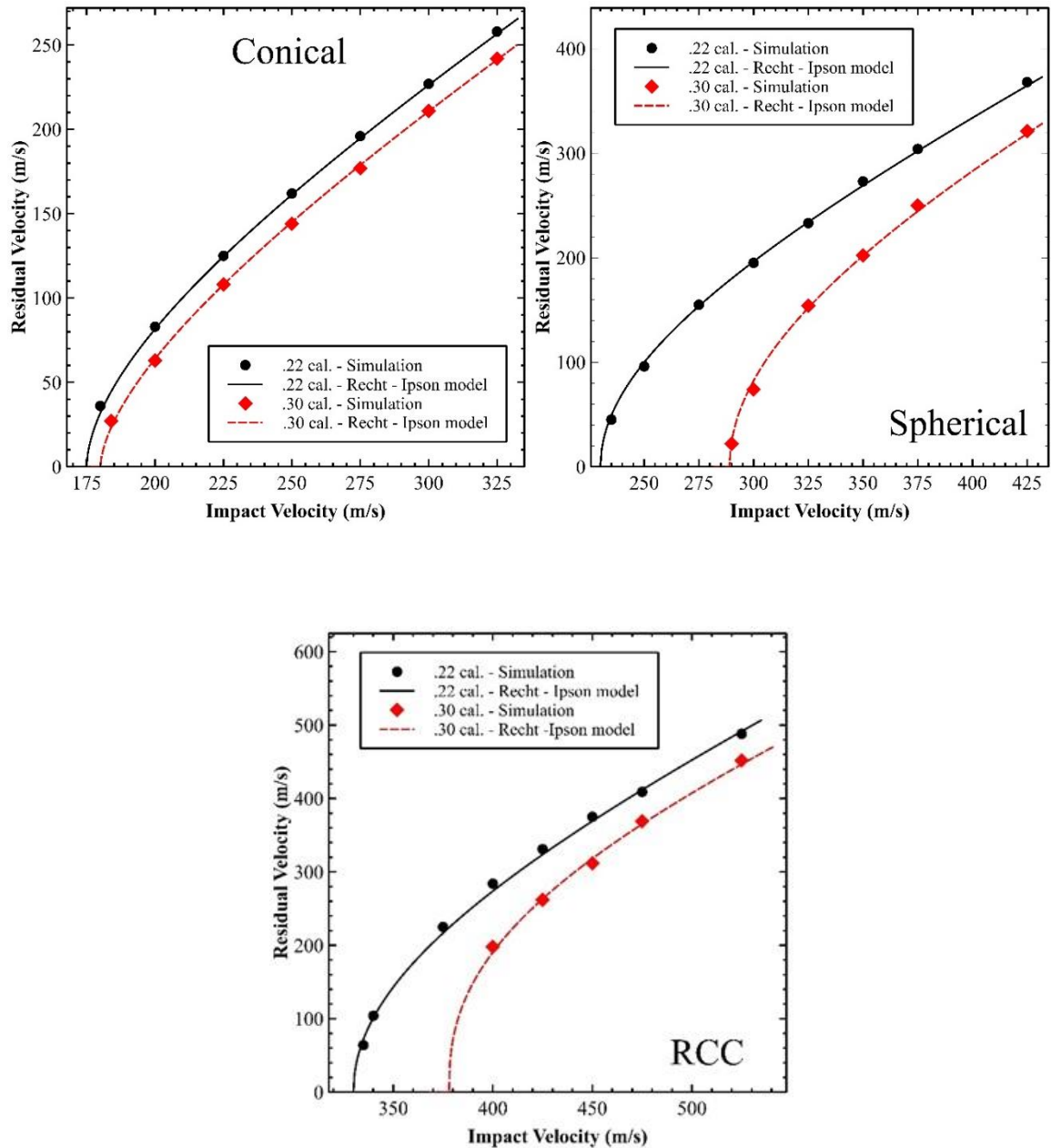


Figure 5.2: Residual velocities of the projectiles.

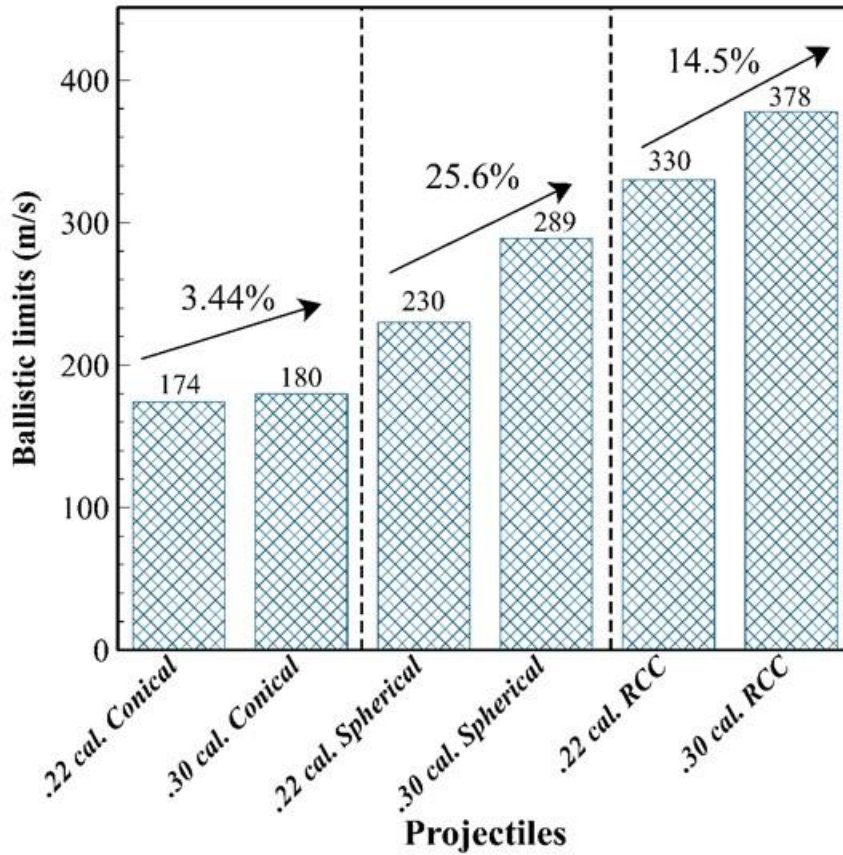


Figure 5.3: Comparison of the ballistic limits for the projectiles.

It is also observed from Figure 5.3 that among all the projectiles, the change in projectile size affected the spherical projectiles the most (a 25.6% increase in ballistic limit from .22 to .30 cal.), and the conical projectile the least (only 3.44% increase in ballistic limit from .22 to .30 cal.). The six projectiles were also compared, as shown in Figure 5.4, using normalized residual velocity (NRV) and normalized absorbed kinetic energy (NAKE) by the initial impact velocities and initial kinetic energies, respectively. The NRVs are calculated by

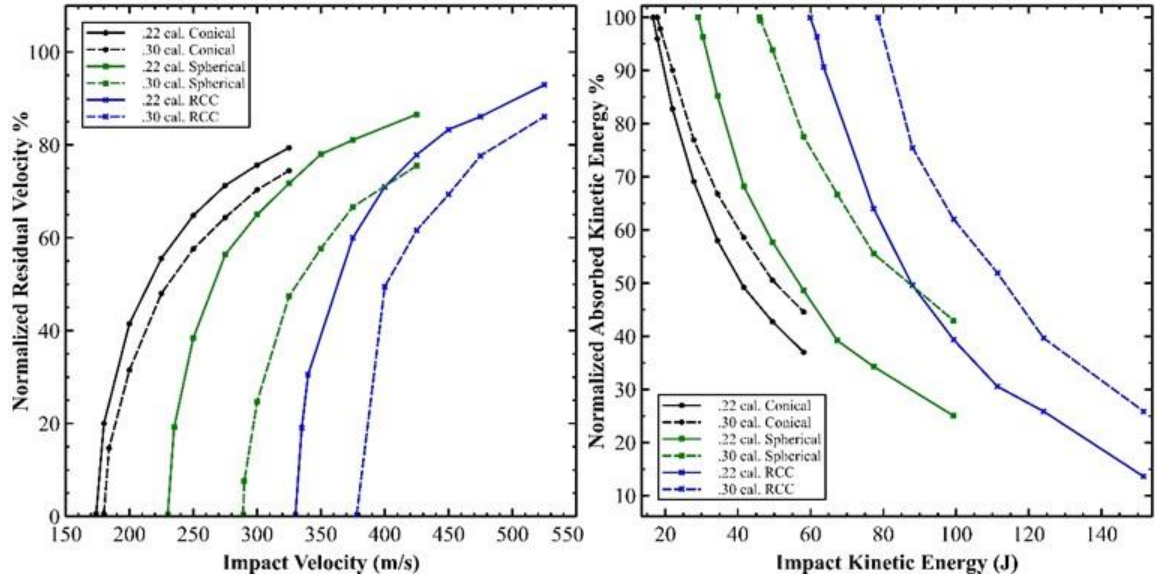
$$NRV = \frac{v_i - v_r}{v_i} \times 100\% \quad (10)$$

where V_i and V_r are the initial impact velocity and residual velocity, respectively. Similarly, the NAKEs for all impact case are given by

$$NAKE = \frac{0.5 m (V_i^2 - V_r^2)}{0.5 m V_i^2} \times 100\% \quad (11)$$

where m is the mass (i.e., 1.1 gr) of the projectile. It should be noted that the initial kinetic energy was calculated as $(0.5 m V_i^2)/1000$ in Joule.

It can be seen in Figure 5.4 that all the projectiles follow a similar trend: the rapid increase in normalized residual velocities, which corresponds to the rapid decrease in normalized absorbed energies, until the impact velocities are 40-45% larger than the ballistic limits. When the impact velocities reach the highest values, which are 50% more than the ballistic limits, the rate of increase in normalized residual velocities becomes smaller, as seen in the change of slopes in the graphs of Figure 5.4. Moreover, when the projectiles hit the target at velocities up to 45% higher than the ballistic limits, the target absorbs up to 50% of the projectiles' initial kinetic energies. However, when the impact velocities reach the highest impact velocities, i.e., 50% more than the ballistic limits, the target can only absorb 10 to 30% of the projectiles' initial kinetic energies. Finally, corresponding to the findings from results in Figure 5.2, the .30 cal. RCC needs the largest initial kinetic energy, 78.58 J, to perforate the ten-ply Kevlar woven fabrics, while the .22 cal. conical projectile needs the smallest initial kinetic energy, 16.65 J, to perforate this same target.



Normalized residual velocities

Normalized absorbed kinetic energies.

Figure 5.4: Comparison of the projectiles.

5.2.2 Energy transitions

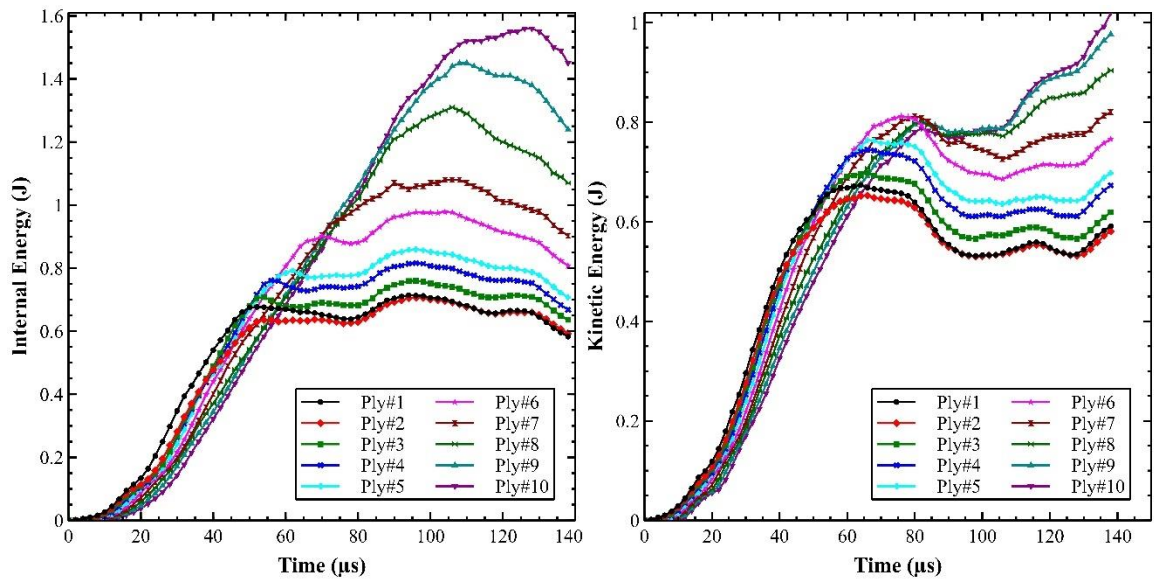
When a projectile hits the woven fabric at ballistic limit velocity, part of the projectile's kinetic energy is transmitted to the internal and kinetic energy of the fabric, and the frictional energy between the fabric and projectile. The internal energy of the fabric is seen from the stress waves propagating along the longitudinal axis of the yarn. The kinetic energy of the fabric is seen from the transverse waves that create the transverse (i.e., out-of-plane) displacements in the fabric. The frictional energy is typically very small compared to the internal and kinetic energy of the fabric. Hence, only the internal and kinetic energy of the fabric are discussed here.

Figures 5.5 to 5.7 show the energy absorption of each ply under impacts by the six projectiles at the ballistic limit velocities. It can be seen from Figures 5.5 to 5.7 that the energy absorbed as the total internal energy of the fabric was larger than the kinetic energy of the fabric for all types of projectiles. This indicated that the internal energy of the fabric

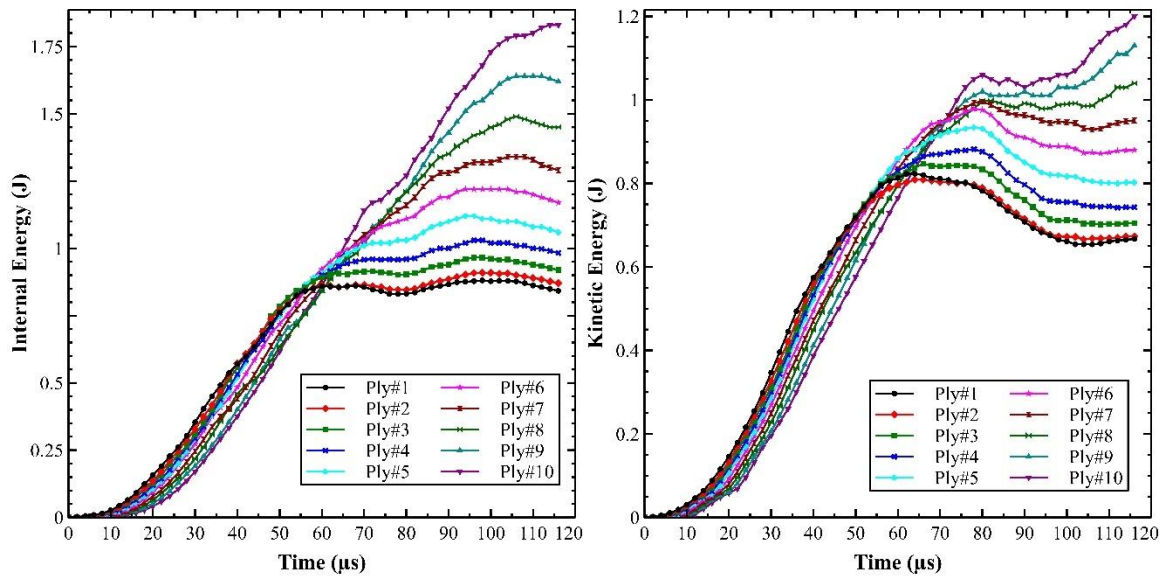
was the dominant form of energy absorption for all type projectiles in all impact cases. For energy absorption by the individual plies, it was observed that plies towards the backside of the target generally absorbed more energy than those towards the impact side. This was true for both internal energy and kinetic energy of the fabric. Among all the plies, the tenth ply had the largest internal energy for all types of projectiles. Table 5.1 gives a comparison of the internal energies absorbed by the first and last plies for the six projectiles. It can be seen that the difference between internal energies of the tenth and first ply was the smallest for impacts by the conical projectiles and the largest under impacts of the RCC projectiles, approximately two times and four times, respectively. Under impacts of the same projectiles, the difference between the internal energies of the tenth and first ply was larger for the .30 cal. projectiles than the respective .22 cal. projectiles. Furthermore, under impacts of the same projectiles, both the first and tenth plies had larger internal energies for the .30 cal. projectiles than the respective .22 cal. projectiles.

Table 5.1: Comparison of internal energy of the first and last plies for each projectile.

Projectile Type	Internal Energy		
	First Ply	Tenth Ply	Difference
.22 cal. Conical	.65 J	1.45 J	223%
.30 cal. Conical	.77 J	1.8	235%
.22 cal. Spherical	1.05 J	2.6 J	247%
.30 cal. Spherical	1.5 J	4.2 J	280%
.22 cal. RCC	1.05 J	4.25 J	404%
.30 cal. RCC	1.25 J	5.5 J	440%

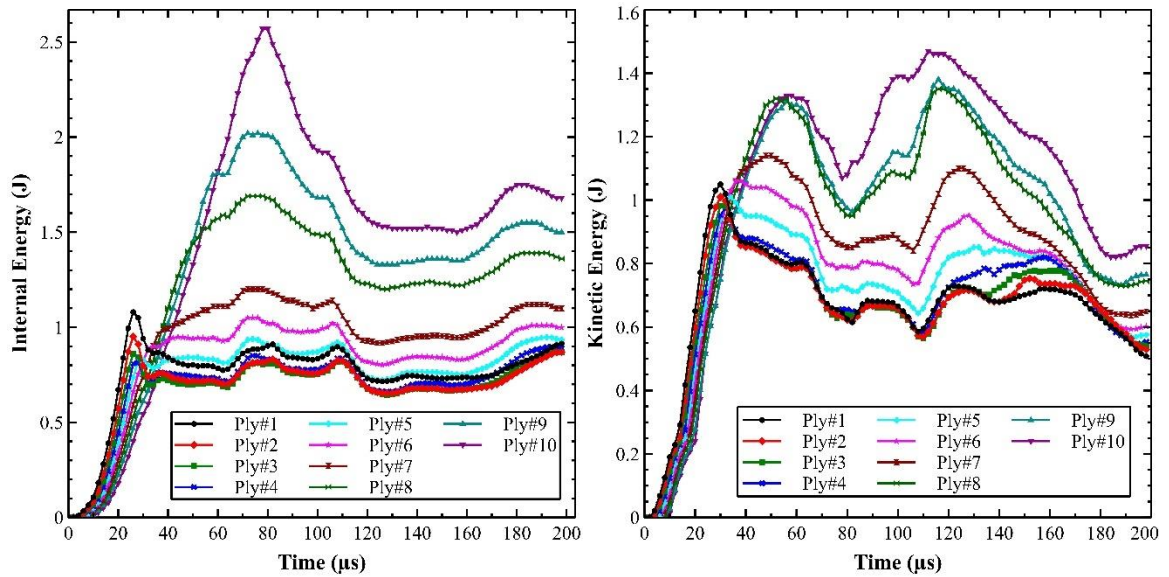


.22 cal.

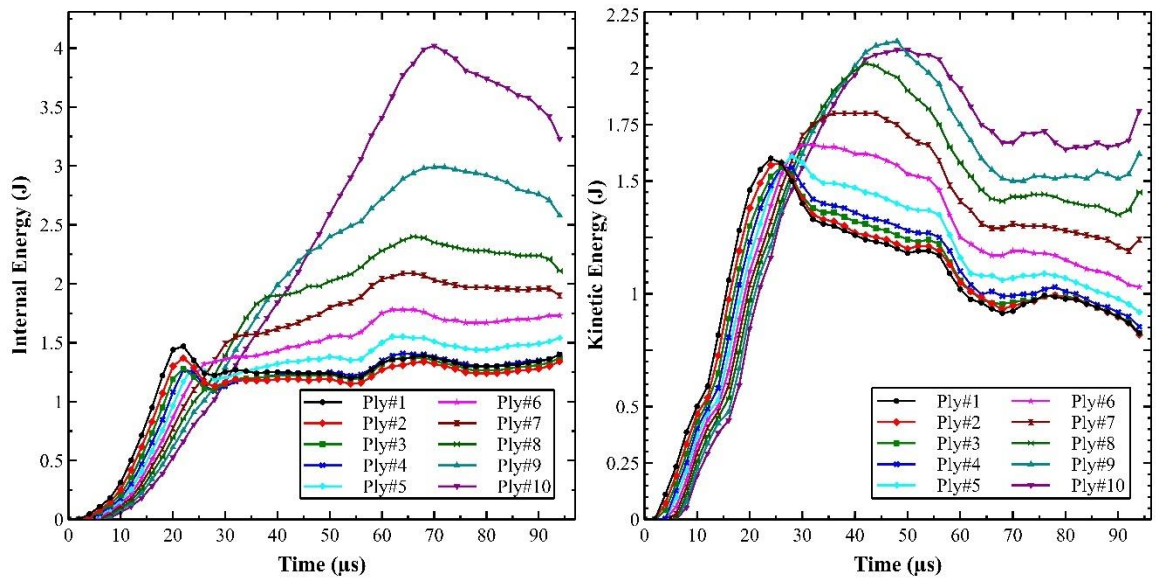


.30 cal.

Figure 5.5: Energy absorption of the fabric for conical projectiles at ballistic limits.

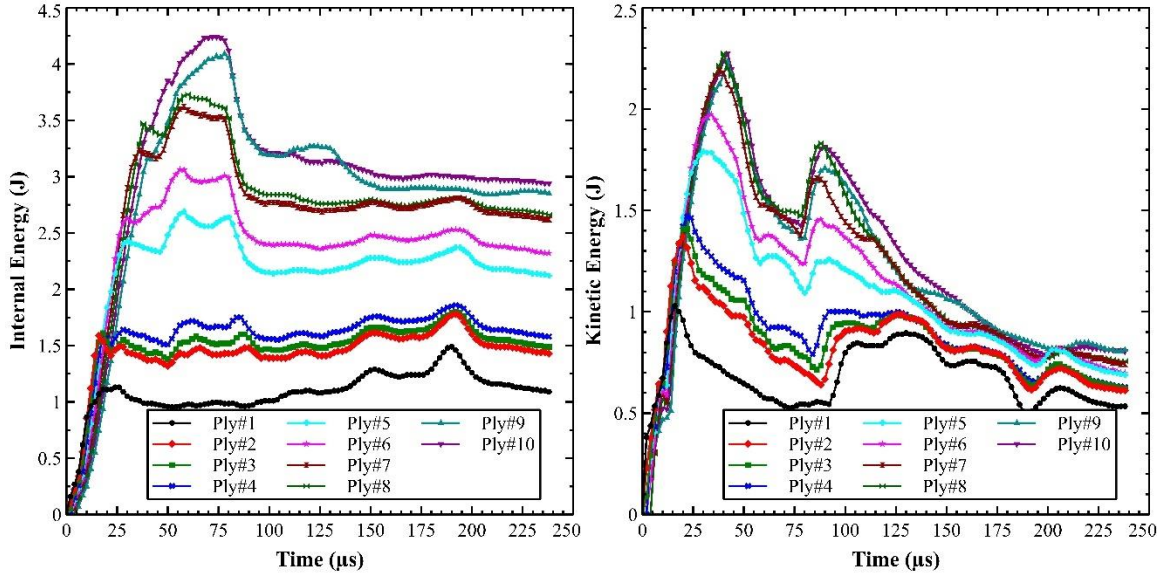


.22 cal.

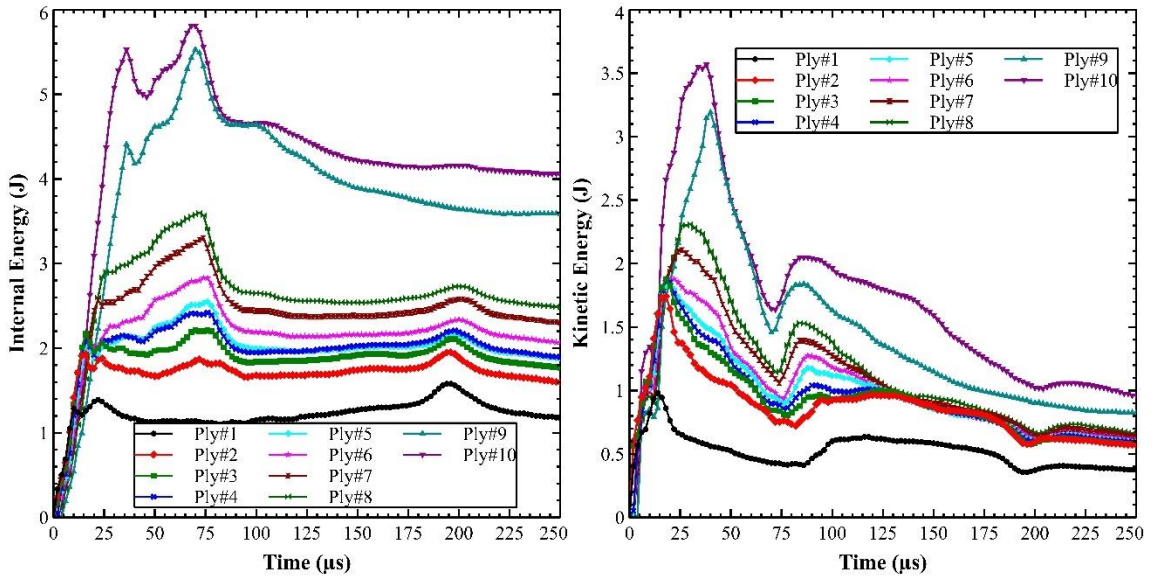


.30 cal.

Figure 5.6: Energy absorption of the fabric for spherical projectiles at ballistic limits.



.22 cal.



.30 cal.

Figure 5.7: Energy absorption of the fabric for RCC projectiles at ballistic limits.

For all six projectiles, the internal energy of each of the first five plies (i.e., the first to the fifth ply) was nearly the same as its kinetic energy. For the last five plies (i.e., the sixth to the tenth ply), the internal energy was always larger than the respective kinetic energy of the fabric. In other words, the energy absorption of the first five plies was composed of equal amount of internal and kinetic energy, while the energy absorption of the last five plies was dominated by the internal energy.

However, projectile characteristics (i.e., size and nose shape) affected the loading rate of each ply as shown in Figures 5.5 - 5.7. Loading rate can be defined as the period starting from the initial impact to the yarns break. For example, the first plies of the fabric under the impact of .22 cal. conical projectile at ballistic limit were subjected to tensile loading until approximately 50 μ s; however, the same plies under the .22 cal. spherical projectile at the ballistic limit were subjected to tensile loading until 30 μ s. So, the first five plies loaded faster under the impact of spherical projectiles. As seen in Figures 5.5 – 5.7. the loading rate increased as the projectile size increased, and the most rapid tensile load occurred during the impact of the .30 cal. RCC projectile while the slowest tensile loading happened during the impact of .22 cal. conical projectile. This impact phenomenon can be explained through the impact mechanisms of each projectile which were explained in the following section.

Overall, for impacts at the ballistic limit velocities, the energy absorbed by the fabric was mainly in the form of internal and kinetic energy. While the total internal energy of the fabric was always larger than the total kinetic energy regardless of the projectile type, the internal and kinetic energy of each individual ply depended on its position as well as the projectile characteristics (i.e., size and nose shape).

5.2.3 Out-of-plane displacements

Figures 5.8 and 5.9 show the cross-sectional views of out-of-plane displacements of the warp and weft yarns in the last ply at the impact point for impacts by the .22 cal. and .30 cal. projectiles, respectively. For consistency in the comparison, the out-of-plane displacements were compared at the instant when the yarns on the last plies started to break. Since the projectiles were symmetrical with respect to both the x - and y -axis, there was no considerable difference in the displaced cross-sectional profiles between the warp and weft yarns. The largest out-of-plane displacements occurred under impacts by the spherical projectiles while the smallest out-of-plane displacements were under impacts by the conical projectiles. It was also observed that the magnitude of out-of-plane displacements were mainly affected by the nose shape of the projectile (i.e., flat, tip, spherical). Although the magnitudes of the displacements by the .30 cal. projectiles were slightly larger than those by the .22 cal. projectiles, the differences were small and negligible. For example, the out-of-plane displacement was 7.12 mm under the impact of a .22 cal. spherical projectile, while it was 7.25 mm under the impact of a .30 cal. spherical projectile, indicating a difference of less than 2% between the two projectiles with the same nose shape but different calibers.

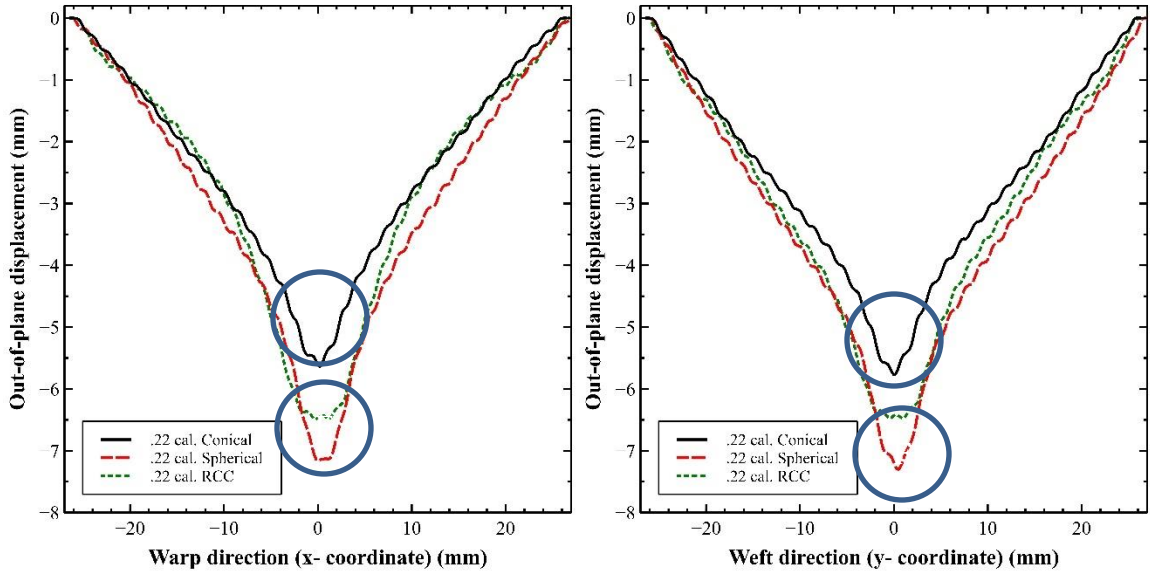


Figure 5.8: Cross-sectional views of out-of-plane displacements of the warp and weft yarns at the impact point for impacts by the .22 cal. projectile.

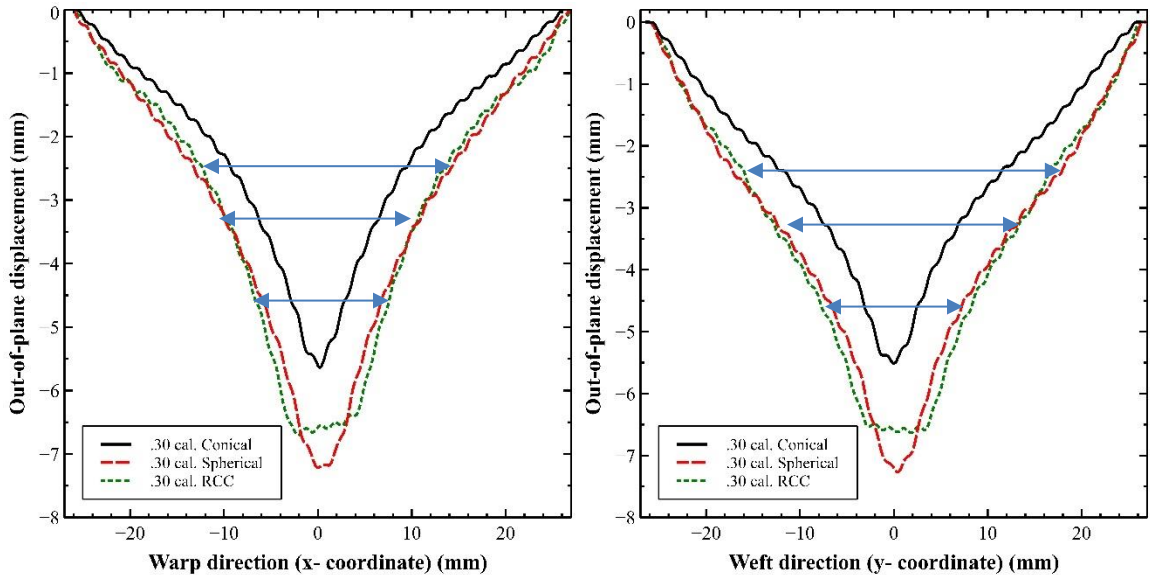


Figure 5.9: Cross-sectional views of out-of-plane displacements of the warp and weft yarns at the impact point for impacts by the .30 cal. projectile.

For impacts by the conical projectiles, the sharp noses of the projectiles pierced between yarns at the impact points and the cone sides pushed the primary yarns aside, allowing the conical projectiles to go through the fabric, which had only minimal out-of-

plane displacements. When impacted by the flat-nose (i.e., RCC) projectiles, the primary yarns at the impact location were engaged with the projectiles' flat noses, and the yarns were pushed and stretched (i.e., under tensile loading) until the yarns reached the failure strain. For impacts by the spherical projectiles, the impact mechanism can be viewed as a combination of the conical and RCC projectiles. For impacts by the spherical projectiles, only the middle primary yarns at the impact location were engaged with the projectiles while the rest of the primary yarns were pushed aside by the curved noses of the projectiles. Since fewer primary yarns were engaged with the spherical projectiles than those engaged with the RCC projectile, the fabric had larger out-of-plane displacements under impacts by the spherical projectiles than by the RCC projectiles. Since both the spherical and conical projectiles pushed the yarns aside, the displaced cross-sectional profiles of the fabric resembled each other for the two projectile types at the impact point, as indicated by the circles in Figure 5.8. In addition, the widths of the displaced profiles for the spherical and RCC projectiles were similar to each other, as shown in Figure 5.9.

5.2.4 Damage patterns

In this section, the post-impact damage patterns of the first and last plies of the fabric are examined and compared for impacts by the six projectiles at the ballistic limit velocities, as shown in Figures 5.10 to 5.15. It was observed that the damage in the first plies were due to fiber breakage and localized at the impact location regardless of the type of projectile. The shape and severity of the damage on the first ply was dependent on the projectile characteristics. For example, the shape of the perforated holes on the first plies were circular for impacts by the spherical and conical projectiles; however, the perforated

holes by the RCC projectiles were in rectangular shapes. The sizes of the perforations on the first plies were smaller than the diameters of the projectiles for impacts by the conical and spherical projectiles, but larger for impacts by the RCC projectiles. For example, the diameter of the perforated holes caused by the .22 cal. conical and spherical projectiles were approximately 4.9 and 4.6 mm, respectively, which were smaller than the diameter of the projectile, i.e., 5.56 mm. In contrast, the size of the perforated hole by the .30 cal. RCC projectile was approximately 8.6 x 8.9 mm in a rectangular shape.

The deformed area on the last ply of the fabric was found to be larger than that of the first ply for all types of projectiles. This was anticipated since it was observed that the last ply of the fabric absorbed the largest amount of energy among all the plies (see Section 5.2.2). Unlike damage in the first ply, the damage in the last ply was not localized to the impact locations. The shapes of the deformation on the last ply at the impact point were similar to those on the first ply. For example, the damages on the last ply were circular for both the conical and spherical projectiles and were rectangular for the RCC projectiles. The sizes of perforations on the last ply were smaller than the diameter of the projectiles for impacts by the .22 cal. projectiles, but larger than the diameter of the projectile for impacts by the .30 cal. projectiles.

In addition to fiber breakage, yarn sliding (or yarn slippage) was the other dominant failure mode on the last ply of the fabric under impacts by the conical and spherical projectiles. Under the impact by the .22 cal. conical projectile (see Figure 5.10), the deformed area of the last ply resembled a star shape due to extensive yarn slippage of the fabric. Under the impact by the .30 cal. conical projectile, the deformation area was an 8.7-mm circular shape, which was different from that by the .22 cal. conical projectile. For

impacts by the spherical projectiles, there was no considerable difference between the damage patterns by the .22 cal. and .30 cal. projectiles. In addition to yarn slippage, yarn pullout was an additional failure mode on the last ply of the fabric in the impact by the .30 cal. spherical projectile, as shown in Figure 5.14. Under impacts by the RCC projectiles, the fabric had the largest post-impact damages on the last ply, with the .30 cal. RCC projectile causing larger damage than the .22 cal. RCC projectile. Unlike the impacts by the spherical and conical projectiles, the yarn slippage failure mode was negligible for impacts by the RCC projectiles. Instead, yarn pullout was the dominant failure mode along with yarn breakage as shown in Figures 5.14 and 5.15.

Figure 5.16 shows the projections of the .22 cal. and .30 cal. projectiles onto the fabric to determine the maximum numbers of primary yarns for impacts by these two sized projectiles. There were 16 and 22 primary yarns underneath the .22 cal. and .30 cal. projectiles, respectively. Table 5.2 gives the total number of broken yarns for each ply of the fabric impacted by the six projectiles at their ballistic limits. As seen in Table 5.2, the plies towards the impact side of the fabric generally had more broken yarns than those towards the backside of the fabric. For projectiles with the same nose shape, the biggest difference in the number of broken yarns on each ply occurred for the conical projectiles. This was due to the increased diameter of the conical projectile, which reduced the projectile's capability for yarn sliding and caused more yarn breakage. In agreement with and support of the above statement, the .30 cal. RCC projectile, which had the least capability for yarn sliding, had the most broken yarns on each ply of the fabric among all six projectiles. It should be also noted that the total number of broken yarns in impacts by both the conical and spherical projectiles were less than the number of primary yarns

underneath the projectile (i.e., 16 for .22 cal. and 22 for .30 cal.), due to yarn sliding along the projectiles' nose. The damage modes in study had similarities with the experimental study [16] in terms of damage mechanism of the woven fabrics under impacts of different nose shape projectiles.

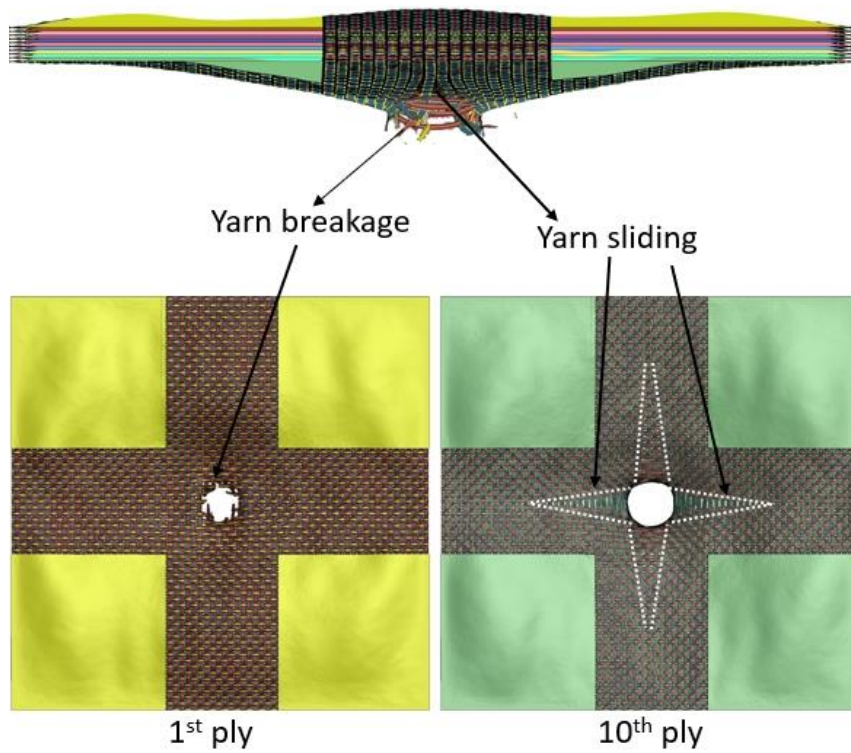


Figure 5.10: Post-impact damage patterns of the fabric impacted by a .22 cal. conical projectile at ballistic limit velocity.

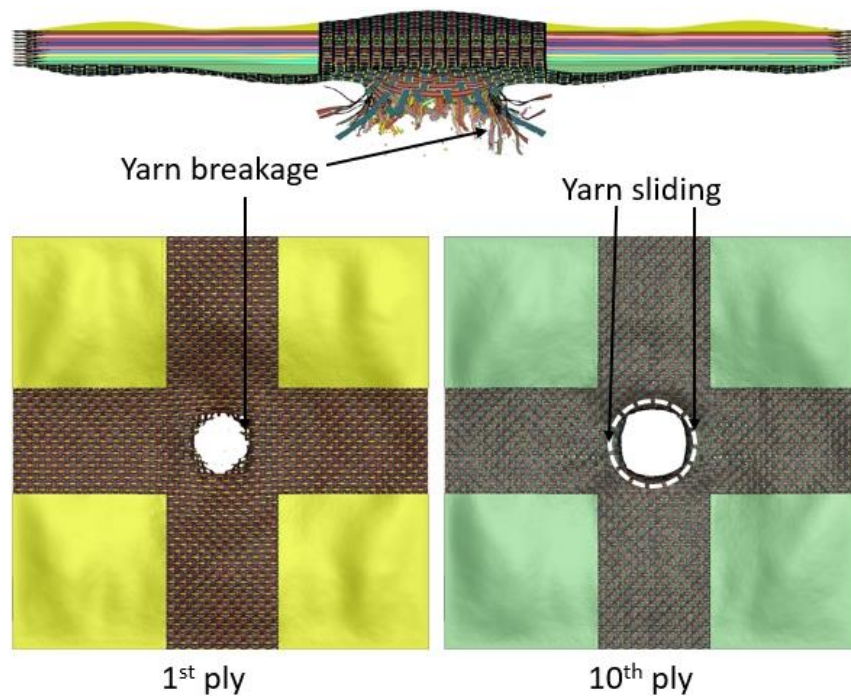


Figure 5.11: Post-impact damage patterns of the fabric impacted by a .30 cal. conical projectile at ballistic limit velocity.

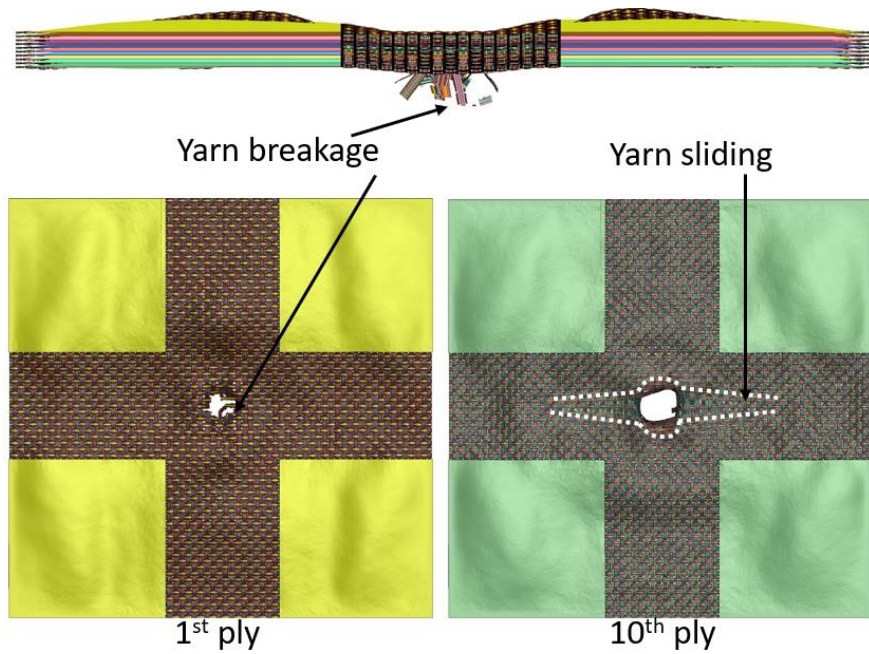


Figure 5.12: Post-impact damage patterns of the fabric impacted by a .22 cal. spherical projectile at ballistic limit velocity.

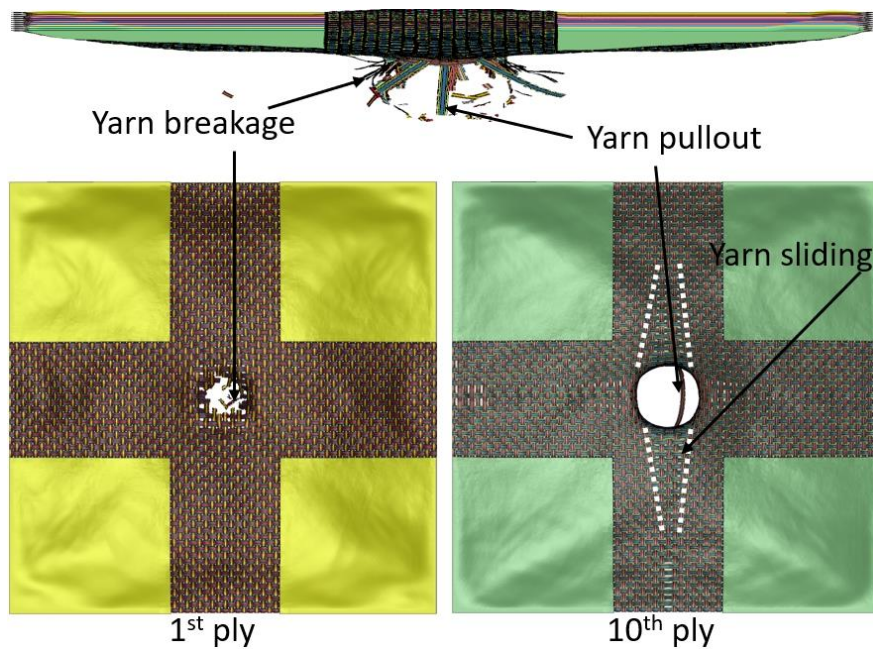


Figure 5.13: Post-impact damage patterns of the fabric impacted by a .30 cal. spherical projectile at ballistic limit velocity.

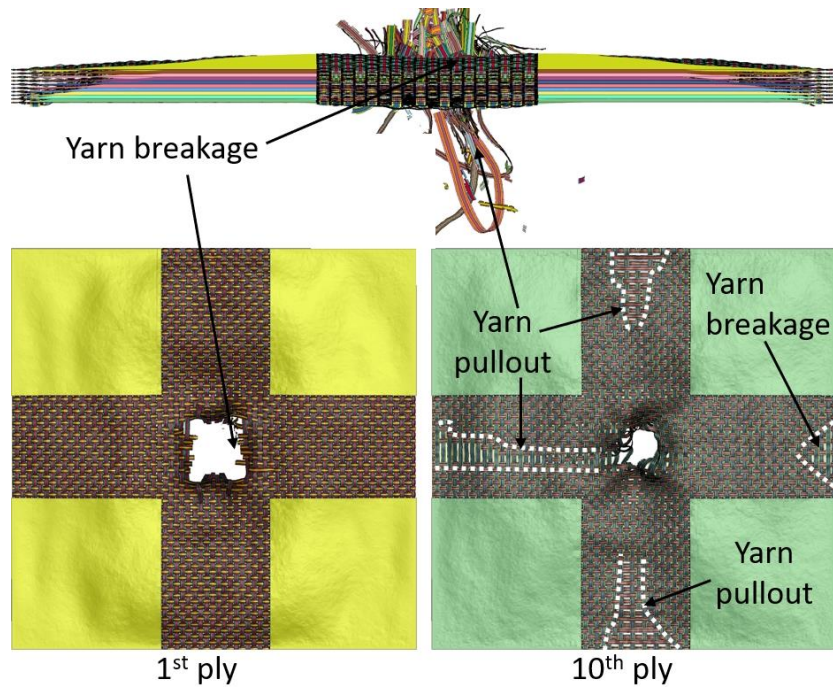


Figure 5.14: Post-impact damage patterns of the fabric impacted by a .22 cal. RCC projectile at ballistic limit velocity.

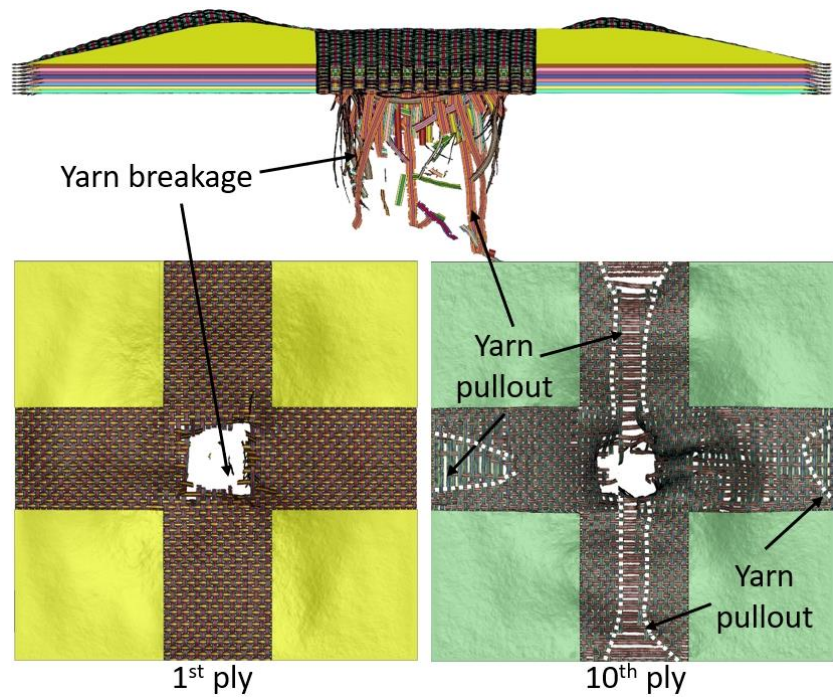


Figure 5.15: Post-impact damage patterns of the fabric impacted by a .30 cal. RCC projectile at ballistic limit velocity.

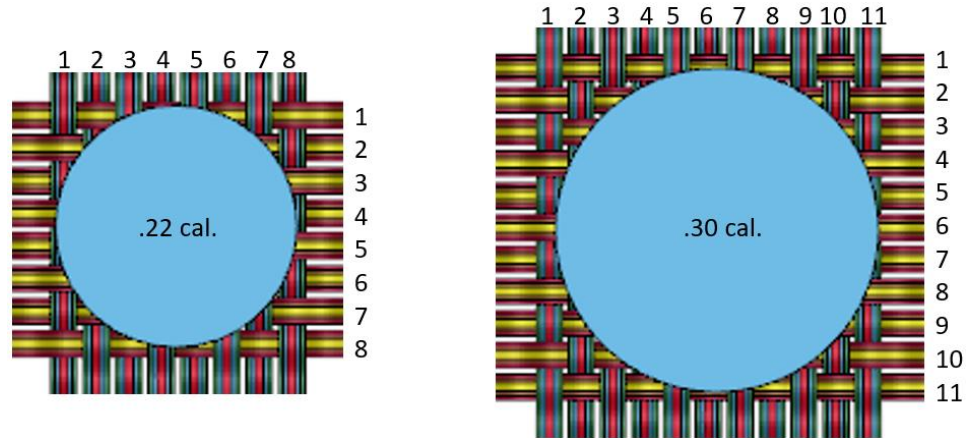


Figure 5.16: The primary yarns underneath the projectiles.

Table 5.2: Total number of broken yarns on the fabric under impacts by the six projectiles at their ballistic limits.

Ply	Total number of broken yarns					
	Conical		Spherical		RCC	
	.22 cal.	.30 cal.	.22 cal.	.30 cal.	.22 cal.	.30 cal.
1 st	9	16	10	14	16	21
2 nd	8	14	10	13	16	21
3 rd	8	14	10	12	16	19
4 th	8	12	8	11	16	19
5 th	8	12	8	10	16	19
6 th	8	12	7	10	14	17
7 th	7	12	7	10	16	18
8 th	7	12	7	10	13	18
9 th	5	12	5	7	12	18
10 th	4	11	4	6	12	17

CHAPTER 6: CONCLUSIONS AND FUTURE WORK

6.1 Conclusions

In this dissertation, an improved multi-scale FE modeling technique for woven fabrics was developed and used to study the ballistic impact resistance mechanism of multi-ply woven fabrics. The improved multi-scale model, which was composed of a meso- and a macro-scale component, was first created along with a full meso-scale model. Both the meso-scale and multi-scale numerical models were validated against experiment data. It was found that the improved multi-scale model was computationally efficient and capable of predicting, with good accuracy, the responses of Kevlar woven fabrics under ballistic impacts. Compared to the existing multi-scale models in literature, the multi-scale model of this study had enhanced accuracy in simulating wave propagation between meso- and macro-scale regions without using contact definitions at the interface of the two distinct regions. Another improvement of the multi-scale model in this study was the significantly increased computational efficiency without sacrificing the numerical accuracy and robustness.

To study the effect of the total number of plies on the ballistic performance of multi-ply woven fabrics, the multi-scale FE models were created for four different multi-ply fabric targets, with three, five, seven, and ten plies, respectively. The ballistic impact responses of the four targets were investigated, using NATO specified ballistic impacts, on the ballistic limit velocities, dynamic displacements, and damage patterns at the V_{100} impact velocities. It was found that the ballistic limit velocity was increased as the increase

of the total number of plies in the fabrics, as seen by the V_{100} values of 190, 255, 280, and 310 m/s for the three-, five-, seven-, and ten-ply fabrics, respectively. However, the efficiency of the target in terms of the ratio of ballistic limit to the number of plies was decreased as the increase of total number of plies.

The ballistic responses of the four multi-ply fabric targets, when impacted at their ballistic limit velocities, exhibited two distinct stages in all the ballistic impacts. In the first stage, the projectile lost 90-95% of its initial kinetic energy when the fabrics reaching their maximum dynamic displacements without full penetrations. In the second stage, the yarns exceeded their failure stress values as the projectile continued to deform the fabrics and eventually caused a complete perforation.

The initial kinetic energy of the projectile was found to convert primarily to the internal and kinetic energy of the fabrics. Since the projectile did not have permanent deformation and its residual velocity was approximately zero. The the internal energy and kinetic energy of the projectile after perforation were negligible compared to those of the fabrics. In the three-ply fabrics, the first ply had more internal energy than the other two plies, while in the other multi-ply fabrics, the plies towards the backsides had larger internal energies than those towards the front-sides. In addition, the three- and five-ply fabrics had similar trends of absorbed kinetic energy, while the internal and kinetic energies of the seven- and ten-ply fabrics followed similar trends and differed from those of the third- and five-ply fabrics.

The displacement profiles of the warp and weft yarns of the last ply differed in the four multi-ply fabrics. This difference was caused by the projectile's impacting surface configuration, which consisted of a flat region spanning the diameter of the projectile,

surrounded by two chamfered edges. Due to the initial orientation of the projectile, the flat region was aligned in such a way to initially contact the weft yarns, while the warp yarns subsequently interacted with the chamfered edges. This indicated that angled nose or head of the projectile could affect the responses of the targets.

It was observed from the four multi-ply fabrics that the damage severity on the last plies exhibited five different levels at five distinct regions, denoted as R1 to R5 with R1 having the most severe damage and R5 the least severe damage. It was also found that yarn breakage was the dominant failure mode in R1, R2 and R4, whereas yarn slippage was the dominant in R3. The yarns in R5 were called secondary yarns since there was no permanent deformation on these yarns.

To study the effect of projectile characteristics (i.e., the projectile's size and nose shape) on the ballistic impact performance of multi-ply woven fabrics, six projectiles were created in two different sizes (i.e., .22 cal. and 30 cal.) with three different nose shapes (i.e., flat or RCC, conical, and spherical). Since the overall ballistic responses of the multi-ply fabrics were similar with seven or more plies, the ten-ply fabric was selected as the target. The ballistic limit velocities of the target under impacts by the six projectiles were found to be the smallest for conical projectiles and largest for the RCC or flat projectiles. It was also found that for projectiles with the same nose shape, the ballistic limit velocities were increased from the .22 cal. to the .30 cal. projectile.

The ballistic impact responses of the multi-ply woven fabric were found to be dependent on the projectile's nose shape. Projectiles with pointed noses (i.e., the conical projectiles) tended to push the yarns aside at the impact location and caused yarns to slip with only the minimal out-of-plane displacements of the fabric. In contrast, projectiles with

flat noses (i.e., the RCC projectiles) engaged more yarns at the impact location and stretched the yarns until reaching the failure strain, resulting in larger out-of-plane displacements of the fabric than those by the pointed projectiles. For projectiles in between the pointed and flat nose ones (i.e., the spherical projectiles), fewer yarns were engaged with the projectiles and more yarns were pushed aside than in the cases of flat nose projectiles. Due to the reduced number of yarns engaged with the projectiles, the spherical projectiles caused the largest out-of-plane displacements among projectiles with the three nose shapes.

It was observed that the internal energy of the fabric was the largest energy absorption from the kinetic energy of the projectile, and the last ply of the fabric absorbed the largest amount of initial kinetic energy of the projectile among all plies regardless of the projectile characteristics. It was also found that yarn breakage was the only failure mode on the first ply of the fabric under the impacts of all types of projectiles. Yarn slippage (or yarn sliding) was the dominant failure mode in addition to the yarn breakage on the last ply of the fabric impacted by the spherical and conical projectiles, and yarn pullout and yarn breakage were the dominant failure modes on the last ply of the fabric when impacted by the RCC projectiles.

6.2 Future Work

Future work should be conducted to improve the accuracy and details of the multi-scale model created in this dissertation research. The multi-scale model of this dissertation was the combination of the meso- and macro- FE model of the fabric. Modeling the yarn at the fiber level, i.e., at micro-scale, could provide more accurate results by modeling fiber interactions within the yarns. Since modeling the entire fabric at the micro-scale (i.e., at

fiber level) is significantly computational expensive, the primary yarns underneath the projectile can be modeled at micro-scale while the rest of the primary yarns are modeled at meso-scale, and the secondary yarns can be modeled at the macro-scale as created in this study. This multi-scale modeling technique, which combines all three length scales (i.e., micro-, meso- and macro-scales), will provide more insights into the ballistic responses of multi-ply fabrics than the current multi-scale model.

The main objective of ballistic impact studies on the woven fabric is to understand the ballistic responses of the fabric and consequently improve the fabric's ballistic resistance without increasing its weight, if it all possible. To this end, hybrid fabric designs can be achieved by combining different types of fibers so as to utilize the strength of each type and overcome the drawbacks of each. For example, there exist fibers with less areal density and higher tensile strength than the Kevlar fibers used to create the fabric in this study. However, those fibers have some drawbacks, for example, the HPPE (e.g., Dyneema) fibers could have larger back-face deformation than the Kevlar fiber under the same level of impacts. Creating a hybrid fabric by combining these two fibers may lead to stronger and lighter woven fabrics, with assist from the multi-scale FE modeling technique of this study and design optimization methodologies.

REFERENCES

- [1] Sockalingam, S., Gillespie, J. W., & Keefe, M. (2014). On the transverse compression response of Kevlar KM2 using fiber-level finite element model. *International Journal of Solids and Structures*, 51(13), 2504–2517. <https://doi.org/10.1016/j.ijsolstr.2014.03.020>
- [2] Hearle, J. W. S. (2001). *High-performance fibres. High-performance fibres*. <https://doi.org/10.1533/9781855737549>
- [3] Smith, J. C., Mccrackin, F. L., & Schiefer, H. F. (1958). Stress-Strain Relationships in Yarns Subjected. *Textile Research Journal*, 288–302. <https://doi.org/10.1177/004051755802800402>
- [4] Smith, J. C., Blandford, J. M., & Schiefer, H. F. (1960). Stress-Strain Relationships. in Yarns Subjected to Rapid Impact Loading: Part VI: Velocities of Strain Waves Resulting from Impact. *Textile Research Journal*, 30(10), 752–760. <https://doi.org/10.1177/004051756003001002>
- [5] Smith, J. C., McCrackin, F. L., & Schiefer, H. F. (1958). Stress-strain relationships in yarns subjected to rapid impact loading Part V: wave propagation in long textile yarns impacted transversely. *Textile Research Journal*, 28(4), 288–302.
- [6] Cheeseman, B. a., & Bogetti, T. a. (2003). Ballistic impact into fabric and compliant composite laminates. *Composite Structures*, 61(1–2), 161–173. [https://doi.org/10.1016/S0263-8223\(03\)00029-1](https://doi.org/10.1016/S0263-8223(03)00029-1)
- [7] Dimeski, D., Srebrenkoska, V., & Mirceska, N. (2015). Ballistic Impact Resistance Mechanism of Woven Fabrics and their Composites. *International Journal of Engineering Research and Technology*, 4(12), 107–111.
- [8] Roylance, D. K., Wilde, A. F., Tocc, G. C., & Materials, A. (1973). Impact of Textile Structures, (February).
- [9] Wilde, A. F., Roylance, D. K., & Rogers, M. (1973). Photographic Investigation of High-Speed in Fabric, 753–761.
- [10] Roy, C. Laible, M. R. D. (1975). Laminates for ballistic protection. *US Army Natick Lab, Natick, Massachusetts*.
- [11] Montgomery, T. G., Grady, P. L., & Tomasino, C. (1982). The Effects of Projectile Geometry on the Performance of Ballistic Fabrics. *Textile Research Journal*, 52(7), 442–450. <https://doi.org/10.1177/004051758205200703>

- [12] Taylor, W. J., & Vinson, J. R. (1990). Modeling Ballistic Impact Into Flexible Materials. *Aiaa Journal*, 28(12), 2098–2103. <https://doi.org/10.2514/3.10527>
- [13] Sun, Q., & Field, J. E. (1991). High-speed photographic study of impact on fibers and woven fabrics. *19th Intl Congress on High-Speed Photography and Photonics*, (April 1991), 20. <https://doi.org/10.1117/12.23993>
- [14] Briscoe, B. J., & Motamedi, F. (1992). The ballistic impact characteristics of aramid fabrics: The influence of interface friction. *Wear*, 158(1–2), 229–247. [https://doi.org/10.1016/0043-1648\(92\)90041-6](https://doi.org/10.1016/0043-1648(92)90041-6)
- [15] Shim, V. P. W., Tan, V. B. C., & Tay, T. E. (1995). Modelling deformation and damage characteristics of woven fabric under small projectile impact. *International Journal of Impact Engineering*, 16(4), 585–605. [https://doi.org/10.1016/0734-743X\(94\)00063-3](https://doi.org/10.1016/0734-743X(94)00063-3)
- [16] Tan, V. B. C., Lim, C. T., & Cheong, C. H. (2003). Perforation of high-strength fabric by projectiles of different geometry. *International Journal of Impact Engineering*, 28(2), 207–222. [https://doi.org/10.1016/S0734-743X\(02\)00055-6](https://doi.org/10.1016/S0734-743X(02)00055-6)
- [17] Lim, C. T., Tan, V. B. C., & Cheong, C. H. (2002). Perforation of high-strength double-ply fabric system by varying shaped projectiles. *International Journal of Impact Engineering*, 27(6), 577–591. [https://doi.org/10.1016/S0734-743X\(02\)00004-0](https://doi.org/10.1016/S0734-743X(02)00004-0)
- [18] Rabb, R. J. (2007). A Mesomechanical Particle-Element Model of Impact Dynamics in Neat and Shear Thickening Fluid Kevlar, 213.
- [19] Yu, J. H., Dehmer, P. G., & Yen, C. (2010). High-speed Photogrammetric Analysis on the Ballistic Behavior of Kevlar Fabrics Impacted by Various Projectiles, (September).
- [20] Vinson, J. R., & Zukas, J. A. (1975). On the Ballistic Impact of Textile Body Armor. *Journal of Applied Mechanics*, 42(2), 263. <https://doi.org/10.1115/1.3423564>
- [21] Leech, C.; Hearle, J.W.S.; Mansell, J. (1979). A variational Model for the Arrest of Projectiles by Woven Cloth and Nets. *Journal of The Textile Institute*, 70(11), 469–478. <https://doi.org/http://dx.doi.org/10.1080/00405007908658888>
- [22] Parga-Landa, B., & Hernández-Olivares, F. (1995). An analytical model to predict impact behaviour of soft armours. *International Journal of Impact Engineering*, 16(3), 455–466. [https://doi.org/10.1016/0734-743X\(94\)00054-Z](https://doi.org/10.1016/0734-743X(94)00054-Z)
- [23] Billon, H. H., & Robinson, D. J. (2001). Models for the ballistic impact of fabric armour. *International Journal of Impact Engineering*, 25(4), 411–422. [https://doi.org/10.1016/S0734-743X\(00\)00049-X](https://doi.org/10.1016/S0734-743X(00)00049-X)

- [24] Gu, B. (2003). Analytical modeling for the ballistic perforation of planar plain-woven fabric target by projectile. *Composites Part B: Engineering*, 34(4), 361–371. [https://doi.org/10.1016/S1359-8368\(02\)00137-3](https://doi.org/10.1016/S1359-8368(02)00137-3)
- [25] Mamivand, M., & Liaghat, G. H. (2010). A model for ballistic impact on multi-layer fabric targets. *International Journal of Impact Engineering*, 37(7), 806–812. <https://doi.org/10.1016/j.ijimpeng.2010.01.003>
- [26] Ha-Minh, C., Imad, A., Boussu, F., & Kanit, T. (2013). On analytical modelling to predict of the ballistic impact behaviour of textile multi-layer woven fabric. *Composite Structures*, 99, 462–476. <https://doi.org/10.1016/j.compstruct.2012.10.011>
- [27] Roylance, D. (1973). Wave propagation in a viscoelastic fiber subjected to transverse impact. *Journal of Applied Mechanics*, 143-148.
- [28] Roylance, D., Chammas, P., & Ting, J. (1995). Numerical modeling of fabric impact. Proceeding of the National Meeting of the American Society of Mechanical Engineers. San Francisco.
- [29] Roylance, D., & Wang, S. S. (1980). Penetration mechanics of textile structures. *Ballistic Materials and Penetration Mechanics*, 272-292.
- [30] Cunniff, P., Ting, C., Ting, J., & Roylance, D. (1998). Numerical characterization of the effects of transverse yarn interaction on textile ballistic response. *30th International SAMPE Technical Conference*, 1–13. <https://doi.org/10.1007/s00542-004-0389-0>
- [31] Shockey, D. A., Erlich, D. C., & Simons, J. W. (2001). Improved barriers to turbine engine fragments: interim report III. Office of Aviation Research. Washington, DC.
- [32] Shockey, D. A., Erlich, D. C., & Simons, J. W. (2002). Improved barriers to turbine engine fragments: final annual report. Office of Aviation Research. Washington, DC.
- [33] Shockey, D. A., Erlich, D. C., Simons, J. W., & Shin, H. (2002). Improved barriers to turbine engine fragments: interim report IV. Office of Aviation Research. Washington, DC.
- [34] Lim, C. T., Shim., V. P. W., & Ng, Y. H. (2003). Finite-element modeling of the ballistic impact of fabric armor. *International Journal of Impact Engineering*, 28, 13-31.
- [35] Ivanov, I. & Tabiei, A. (2004). Loosely woven fabric model with viscoelastic crimped fibres for ballistic impact simulations. *International Journal for Numerical Methods in Engineering*, 61, 1565-1583.

- [36] Duan, Y., Keefe, M., Bogetti, T. A., & Cheeseman, B. A. (2005). Modeling the role of friction during ballistic impact of a high-strength plain-weave fabric. *Composite Structures*, 68, 331-337.
- [37] Duan, Y., Keefe, M., Bogetti, T. A., & Powers, B. (2006a). A numerical investigation of the influence of friction on energy absorption by a high-strength fabric subjected to ballistic impact. *International Journal of Impact Engineering*, 32, 1299-1312.
- [38] Duan, Y., Keefe, M., Bogetti, T. A., & Powers, B. (2006b). Finite element modeling of transverse impact on a ballistic fabric. *International Journal of Mechanical Sciences*, 48, 33-43.
- [39] Rao, M. P., Duan, Y., Keefe, M., Powers, B. M., & Bogetti, T. a. (2009). Modeling the effects of yarn material properties and friction on the ballistic impact of a plain-weave fabric. *Composite Structures*, 89(4), 556-566.
<https://doi.org/10.1016/j.compstruct.2008.11.012>
- [40] Talebi, H., Wong, S. V., & Hamouda, A. M. S. (2009). Finite element evaluation of projectile nose angle effects in ballistic perforation of high strength fabric. *Composite Structures*, 87(4), 314-320.
<https://doi.org/10.1016/j.compstruct.2008.02.009>
- [41] Wang, Y., Miao, Y., Swenson, D., Cheeseman, B. A., Yen, C. F., & LaMattina, B. (2010). Digital element approach for simulating impact and penetration of textiles. *International Journal of Impact Engineering*, 37(5), 552-560.
<https://doi.org/10.1016/j.ijimpeng.2009.10.009>
- [42] Ha-Minh, C., Imad, A., Boussu, F., Kanit, T., & Crepin, D. (2012). Numerical study on the effects of yarn mechanical transverse properties on the ballistic impact behaviour of textile fabric. *Journal of Strain Analysis for Engineering Design*, 47(7), 524-534. <https://doi.org/10.1177/0309324712457901>
- [43] Ha-Minh, C., Imad, A., Kanit, T., & Boussu, F. (2013). Numerical analysis of a ballistic impact on textile fabric. *International Journal of Mechanical Sciences*, 69, 32-39. <https://doi.org/10.1016/j.ijmecsci.2013.01.014>
- [44] Nilakantan, G., Wetzel, E. D., Bogetti, T. A., & Gillespie, J. W. (2012). Finite element analysis of projectile size and shape effects on the probabilistic penetration response of high strength fabrics. *Composite Structures*, 94(5), 1846-1854.
<https://doi.org/10.1016/j.compstruct.2011.12.028>
- [45] Nilakantan, G., & Nutt, S. (2014). Effects of clamping design on the ballistic impact response of soft body armor. *Composite Structures*, 108(1), 13-150.
<https://doi.org/10.1016/j.compstruct.2013.09.017>

- [46] Yang, C.-C., Ngo, T., & Tran, P. (2015). Influences of weaving architectures on the impact resistance of multi-layer fabrics. *Materials & Design*, 85, 282–295. <https://doi.org/10.1016/j.matdes.2015.07.014>
- [47] Zhou, Y., & Chen, X. (2015). A numerical investigation into the influence of fabric construction on ballistic performance. *Composites Part B: Engineering*, 76, 209–217. <https://doi.org/10.1016/j.compositesb.2015.02.008>
- [48] Chu, Y., & Chen, X. (2018). Finite element modelling effects of inter-yarn friction on the single-layer high-performance fabrics subject to ballistic impact. *Mechanics of Materials*, 126(August), 99–110. <https://doi.org/10.1016/j.mechmat.2018.08.003>
- [49] Palta, E., Fang, H., & Weggel, D. C. (2018). Finite element analysis of the Advanced Combat Helmet under various ballistic impacts. *International Journal of Impact Engineering*, 112, 125–143. <https://doi.org/10.1016/j.ijimpeng.2017.10.010>
- [50] Palta, E., Gutowski, M., & Fang, H. (2018). A numerical study of steel and hybrid armor plates under ballistic impacts. *International Journal of Solids and Structures*, 136–137, 279–294. <https://doi.org/10.1016/j.ijsolstr.2017.12.021>
- [51] Fang, H., Palta, E., & Gutowski, M., (2018). Numerical simulation of high-speed impacts involving metallic and non-metallic materials. *International Journal of Computational Methods and Experimental Measurements*, 6-3, 463-475. 10.2495/CMEM-V6-N3-463-475
- [52] Palta, E., & Fang, H. (2019). On a multi-scale finite element model for evaluating ballistic performance of multi-ply woven fabrics. *Composite Structures*, 207(September), 488–508. <https://doi.org/10.1016/j.compstruct.2018.09.080>
- [53] Fang, H., Gutowski, M., Disogra, M., & Wang, Q. (2016). A numerical and experimental study of woven fabric material under ballistic impacts. *Advances in Engineering Software*, 96, 14–28. <https://doi.org/10.1016/j.advengsoft.2015.12.008>
- [54] Chocron, S., Figueroa, E., King, N., Kirchdoerfer, T., Nicholls, A. E., Sagebiel, E., ... Freitas, C. J. (2010). Modeling and validation of full fabric targets under ballistic impact. *Composites Science and Technology*, 70(13), 2012–2022. <https://doi.org/10.1016/j.compscitech.2010.07.025>
- [55] Park, Y., Kim, Y., Baluch, A. H., & Kim, C. G. (2015). Numerical simulation and empirical comparison of the high velocity impact of STF impregnated Kevlar fabric using friction effects. *Composite Structures*, 125, 520–529. <https://doi.org/10.1016/j.compstruct.2015.02.041>
- [56] Verberne, C. W. (2010). Mechanical modelling of textiles Literature Survey. *University of Technology, Eindhoven Department of Mechanical Engineering, Report number MT10.15.*

- [57] Cheng, M., Chen, W., & Weerasooriya, T. (2005). Mechanical Properties of Kevlar® KM2 Single Fiber. *Journal of Engineering Materials and Technology*, 127(2), 197. <https://doi.org/10.1115/1.1857937>
- [58] Grujicic, M., Hariharan, a., Pandurangan, B., Yen, C. F., Cheeseman, B. a., Wang, Y., ... Zheng, J. Q. (2012). Fiber-level modeling of dynamic strength of kevlar® KM2 ballistic fabric. *Journal of Materials Engineering and Performance*, 21(7), 1107–1119. <https://doi.org/10.1007/s11665-011-0006-1>
- [59] Nilakantan, G. (2013). Filament-level modeling of Kevlar KM2 yarns for ballistic impact studies. *Composite Structures*, 104, 1–13. <https://doi.org/10.1016/j.compstruct.2013.04.001>
- [60] Erol, G. O. (2017). Multi Length Scale Finite Element Design Framework for Advanced Woven Fabrics. *University of Delaware, Dissertation*.
- [61] Boresi A, Chong K. Elasticity in engineering mechanics. 2nd ed.: John Wiley & Sons, Inc
- [62] Stahlecker, Z., Mobasher, B., Rajan, S. D., & Pereira, J. M. (2009). Development of reliable modeling methodologies for engine fan blade out containment analysis. Part II: Finite element analysis. *International Journal of Impact Engineering*, 36(3), 447–459. <https://doi.org/10.1016/j.ijimpeng.2008.08.004>
- [63] Sockalingam, S., Chowdhury, S. C., Gillespie, J. W., & Keefe, M. (2016). Recent advances in modeling and experiments of Kevlar ballistic fibrils, fibers, yarns and flexible woven textile fabrics - a review. *Textile Research Journal*. <https://doi.org/10.1177/0040517516646039>
- [64] Barauskas, R., Abraitiene, A., & Vilkauskas, A. (2005). Simulation of a ballistic impact of a deformable bullet upon a multilayer fabric package. *WIT Transactions on Modelling and Simulation*, 40, 41–51.
- [65] Rao, M. P., Nilakantan, G., Keefe, M., Powers, B. M., & Bogetti, T. a. (2009). Global/Local Modeling of Ballistic Impact onto Woven Fabrics. *Journal of Composite Materials*, 43(5), 445–467. <https://doi.org/10.1177/0021998308097684>
- [66] Nilakantan, G., Keefe, M., Gillespie, J. W., & Bogetti, T. A. (2008). Novel Multi-scale Modeling of Woven Fabric. *10th International LS-DYNA® Users Conference*, (1984), 19–38.
- [67] Nilakantan, G., Keefe, M., Bogetti, T. a., Adkinson, R., & Gillespie, J. W. (2010). On the finite element analysis of woven fabric impact using multiscale modeling techniques. *International Journal of Solids and Structures*, 47(17), 2300–2315. <https://doi.org/10.1016/j.ijsolstr.2010.04.029>

- [68] Bresciani, L. M., Manes, A., Ruggiero, A., Iannitti, G., & Giglio, M. (2016). Experimental tests and numerical modelling of ballistic impacts against Kevlar 29 plain-woven fabrics with an epoxy matrix: Macro-homogeneous and Meso-heterogeneous approaches. *Composites Part B: Engineering*, 88, 114–130. <https://doi.org/10.1016/j.compositesb.2015.10.039>
- [69] Hallquist JO, LS-DYNA theory manual. Livermore Software Technology Corporation. 01/05/17 (r:8102).
- [70] Recht, R. F., & Ipson, T. W. (1963). Ballistic Perforation Dynamics. *Journal of Applied Mechanics*, 30(3), 384. <https://doi.org/10.1115/1.3636566>
- [71] Yuan, Z. (2017). Study on the Ballistic Performance of Quasi-isotropic (QI) Panels Made from Woven and Unidirectional (UD) Structures.